Max Planck Institute of Colloids and Interfaces

Universität Potsdam

Mechanical stimulation of *in-vitro* tissue growth using magnetic beads

Max-Planck-Institut für Kolloid- und Grenzflächenforschung

Abteilung Biomaterialien

Univ.-Diss.

zur Erlangung des akademischen Grades

"doctor rerum naturalium"

(Dr. rer. nat.)

in der Wissenschaftsdisziplin Biologische Physik

eingereicht an der

Mathematisch-Naturwissenschaftlichen Fakultät

der Universität Potsdam

von

Livnat Landau

Juli 2, 2019

Table of contents

Abstract

Cells and tissues are sensitive to mechanical forces applied to them. In particular, bone forming cells and connective tissues, composed of cells embedded in fibrous extracellular matrix (ECM), are continuously remodeled in response to the loads they bear. The mechanoresponses of cells embedded in tissue include proliferation, differentiation, apoptosis, internal signaling between cells, and formation and resorption of tissue.

Experimental *in-vitro* systems of various designs have demonstrated that forces affect tissue growth, maturation and mineralization. However, the results depended on different parameters such as the type and magnitude of the force applied in each study. Some experiments demonstrated that applied forces increase cell proliferation and inhibit cell maturation rate, while other studies found the opposite effect. When the effect of different magnitudes of forces was compared, some studies showed that higher forces resulted in a cell proliferation increase or differentiation decrease, while other studies observed the opposite trend or no trend at all.

In this study, MC3T3-E1 cells, a cell line of pre-osteoblasts (bone forming cells), was used. In this cell line, cell differentiation is known to accelerate after cells stop proliferating, typically at confluency. This makes this cell line an interesting subject for studying the influence of forces on the switch between the proliferation stage of the precursor cell and the differentiation to the mature osteoblasts.

A new experimental system was designed to perform systematic investigations of the influence of the type and magnitude of forces on tissue growth. A single well plate contained an array of 80 rectangular pores. Each pore was seeded with MC3T3-E1 cells. The culture medium contained magnetic beads (MBs) of 4.5 µm in diameter that were incorporated into the pre-osteoblast cells. Using an N52 neodymium magnet, forces ranging over three orders of magnitude were applied to MBs incorporated in cells at 10 different distances from the magnet. The amount of formed tissue was assessed after 24 days of culture. The experimental design allowed to obtain data concerning (i) the influence of the type of the force (static, oscillating, no force) on tissue growth; (ii) the influence of the magnitude of force (pN-nN range); (iii) the effect of functionalizing the magnetic beads with the tripeptide Arg-Gly-Asp (RGD). To learn about cell differentiation state, in the final state of the tissue

growth experiments, an analysis for the expression of alkaline phosphatase (ALP), a well-known marker of osteoblast differentiation, was performed.

The experiments showed that the application of static magnetic forces increased tissue growth compared to control, while oscillating forces resulted in tissue growth reduction. A statistically significant positive correlation was found between the amount of tissue grown and the magnitude of the oscillating magnetic force. A positive but non-significant correlation of the amount of tissue with the magnitude of forces was obtained when static forces were applied. Functionalizing the MBs with RGD peptides and applying oscillating forces resulted in an increase of tissue growth relative to tissues incubated with "plain" epoxy MBs. ALP expression decreased as a function of the magnitude of force both when static and oscillating forces were applied. ALP stain intensity was reduced relative to control when oscillating forces were applied and was not significantly different than control for static forces.

The suggested interpretation of the experimental findings is that larger mechanical forces delay cell maturation and keep the pre-osteoblasts in a more proliferative stage characterized by more tissue formed and lower expression of ALP. While the influence of the force magnitude can be well explained by an effect of the force on the switch between proliferation and differentiation, the influence of force type (static or oscillating) is less clear. In particular, it is challenging to reconcile the reduction of tissue formed under oscillating forces as compared to controls with the simultaneous reduction of ALP expression. To better understand this, it may be necessary to refine the staining protocol of the scaffolds and to include the amount and structure of ECM as well as other factors that were not monitored in the experiment and which may influence tissue growth and maturation.

The developed experimental system proved well suited for a systematic and efficient study of the mechanoresponsiveness of tissue growth, it allowed a study of the dependence of tissue growth on force magnitude ranging over three orders of magnitude, and a comparison between the effect of static and oscillating forces. Future experiments can explore the multiple parameters that affect tissue growth as a function of the magnitude of the force: by applying different time-dependent forces; by extending the force range studied; or by using different cell lines and manipulating the mechanotransduction in the cells biochemically.

Mechanische Stimulation des in-vitro-Gewebewachstums mit Magnetkügelchen

Zellen und Gewebe sind empfindlich gegenüber mechanischen Kräften, die auf sie einwirken. Die Reaktion von Zellen, die in Gewebe eingebettet sind, umfasst die Zellproduktion, die Spezialisierung Knochenzellen zu reifen, den kontrollierten Zelltod, die interne Signalübertragung zwischen Zellen sowie die Bildung und Resorption von Gewebe. Experimentelle Systeme unterschiedlicher Bauart haben gezeigt, dass Kräfte das Wachstum und die Reifung des Gewebes beeinflussen. Einige Experimente zeigten jedoch, dass angewandte Kräfte die Zellproduktion erhöhen und die Zellreifungsrate hemmen, während andere Studien den gegenteiligen Effekt vertreten. Bei einem Vergleich der Wirkung unterschiedlicher Kraftgrößen zeigten einige Studien, dass höhere Kräfte zu einer Zunahme oder Abnahme der Zellproduktion führten, während andere Studien den entgegengesetzten oder gar keine Veränderung beobachteten.

In dieser Studie wurde ein neues experimentelles System entwickelt, um systematisch den Einfluss von statischen oder oszillierenden Kräften über drei Größenordnungen auf das Gewebewachstum zu untersuchen. Eine einzelne Testplatte enthielt eine Anordnung von 8 mal 10 rechteckigen Poren. Jede Pore wurde mit knochenbildenden Zellen besät. Das Kulturmedium enthielt Magnetkügelchen mit einem Durchmesser von 4,5 um, die in die Prä-Osteoblastenzellen eingebaut waren. Unter Verwendung eines N52-Neodym-Magneten wurden Kräfte unterschiedlicher Größenordnung auf MBs in den Zellen aufgebracht, die sich in Poren in 10 verschiedenen Abständen vom Magneten befanden. Die Menge des gebildeten Gewebes wurde nach 24 Tagen Kultur abgebildet und der Zellreifungszustand der Zellschicht zwischen den Geweben wurde bewertet.

Die Interpretation der experimentellen Ergebnisse zeigt, dass größere mechanische Kräfte die Zellproduktion erhöhen im Vergleich zum verzögertem Zellwachstum durch oszillierende Kräfte. Es wurde eine statistisch signifikante positive Korrelation zwischen der gewachsenen Gewebemenge und der Größe der oszillierenden Magnetkraft gefunden. Eine positive, aber nicht signifikante Korrelation der Gewebemenge mit der Größe der Kräfte wurde erhalten, wenn statische Kräfte angewendet wurden. Die Zellreifung nahm in Abhängigkeit von der Stärke der Kraft sowohl bei statischen als auch bei oszillierenden Kräften ab

Das neu entwickelte experimentelle System erwies sich als gut geeignet für eine systematische und effiziente Untersuchung der mechanischen Reaktionsfähigkeit von Zellkulturen in definiert Geometrien. Zukünftige Experimente können die vielfältigen Parameter untersuchen, die das Gewebewachstum in definiert Geometrien als Funktion der Größe der mechanischen Kraft beeinflussen: indem verschiedene zeitabhängige Kräfte angewendet werden und der untersuchte Kraftbereich erweitert wird; durch Ändern der Geometrie der Poren; und indem zusätzliche Aspekte der mechanischen Reaktion von Geweben untersucht werden.

List of figures

List of abbreviations

Abbreviation	Full form
MB	Magnetic Beads
ALP	Alkaline phosphatase
ECM	Extracellular matrix
MSC	Mesenchymal stem cell
FAC	Focal adhesion complex
RGD	The tripeptide Arg-Gly-Asp
PDMS	Polydimethylsiloxane
HA	Hydroxyapatite
PTA	Projected tissue area
BMP-2	Bone morphogenetic protein 2
HUVEC	Human umbilical vein endothelial cells
MB	Magnetic Beads
MSC	Mesenchymal stem cell
hMSC	Human mesenchymal stem cells
hBMSC	Human bone mesenchymal stem cells
PBS	Phosphate buffer saline
BSA	bovine serum albumin
MPICI	Max Planck Institute of Colloids and Interfaces
S	Standard error of regression
SD	Standard deviation

1 Introduction

Forces are major influencers on function, mechanical and chemical properties, and fate of single cells, tissues and entire organisms (Klein-Nulend, Bacabac et al. 2005, Huang, Kwon et al. 2012). Tissue growth and maturation as a function of mechanical stimulation is studied as a part of the broader research field of mechanobiology, which focuses on understanding the effect of the mechanical environment on biological response (Mullender, El Haj et al. 2004, Wang and Thampatty 2006).

In this thesis, the focus is on the effects of *in-vitro* mechanical stimulation on a particular type of mechanosensitive cell: the bone forming cell called osteoblast. Osteoblasts play a key role in the ability of bones to create new bone matrix as a response to the alterations in the loads they bear (Klein-Nulend, Bacabac et al. 2005). They secrete molecules that self-assemble into bundles of protein consisting mainly of type I collagen and mineralize by incorporating bone apatite (carbonated hydroxyapatite) (Wang and Thampatty 2006). The application of mechanical forces during tissue growth is an integral step in the process leading to properly formed bone tissue (Klein-Nulend, Bacabac et al. 2005).

In-vitro studies are used in this context to enable the study of an isolated system of interest, often a system model such as the MC3T3-E1 cell line used in this study. In this cell line, cell differentiation is known to accelerate after cells stop proliferating, typically at confluency. This makes the cell line an interesting subject for studying the influence of forces on the switch between the proliferation stage of the precursor cell and the differentiation to the mature osteoblasts (Quarles, Yohay et al. 1992).

A broad set of studies found that bone forming cells are extremely mechanosensitive and can react to a wide range of forces. However, while many studies of tissues grown under the influence of mechanical forces report cell proliferation upon force application (Neidlinger-Wilke, Wilke et al. 1994, Kaspar, Seidl et al. 2000, Sikavitsas, Bancroft et al. 2003, Li, Batra et al. 2004, Kim, Song et al. 2010), others report cell apoptosis and mitotic halt or an increase in differentiation associated with the end of the proliferative stage (Neidlinger-Wilke, Wilke et al. 1994, Cartmell, Dobson et al. 2002, Tanakaa, Lib et al. 2003, Dobson, Cartmell et al. 2006, Kanczler, Sura et al. 2010, Henstock, Rotherham et al. 2014). Some comparative studies

found that moderate forces result in an increase in cell number while stronger forces cause a mitotic halt (Neidlinger-Wilke, Wilke et al. 1994, Kaspar, Seidl et al. 2000, Rosenberg, Levy et al. 2002), other studies found no dependency of cell proliferation on the magnitude of force (Sikavitsas, Bancroft et al. 2003), or an increased cell differentiation when forces of only a few pN were applied (Hughes, Dobson et al. 2007, Kanczler, Sura et al. 2010, Henstock, Rotherham et al. 2014). The discrepancies in experimental results emphasize the need for a single experimental system able to examine trends of tissue growth and maturation as a function of the type and magnitude of force.

Growing tissues in multiple pores with defined geometries in a single well plate, has been used to study the effect of pore geometry on tissue growth in a 3D environment (Rumpler, Woesz et al. 2008, Kommareddy, Lange et al. 2010, Bidan, Kommareddy et al. 2013). Employment of magnetic beads (MB) for introducing defined mechanical loads on cells and tissues has been used as a tool to investigate the mechanosensitivity of the cells and tissues (Cartmell, Dobson et al. 2002, Kollmannsberger and Fabry 2007, Dobson 2008, Kanczler, Sura et al. 2010, Henstock, Rotherham et al. 2014). Here these approaches are extended to seek trends in tissue growth in a 3D environment as a function of the type and magnitude of force applied.

In this thesis, a new experimental setup which allows a systematic study of how forces, ranging over three orders of magnitude, oscillating and static, affect pre-osteoblast tissue growth and maturation *in vitro* is established. In the experimental apparatus, magnetic beads were used as actuators of cells in an array of 8x10 tissue cultures per scaffold, allowing 8 repeats with 10 different distances from the magnet in one well plate. The setup was pre-characterized by simulating and calculating the forces applied to MBs under magnetic fields applied, and a measurement area, where the forces are relatively homogenous in the direction perpendicular to the force while decaying as a function of the distance from the force source, was determined. Magnetic beads were introduced to the MC3T3-E1 cell culture in scaffolds, where they are demonstrated to have been taken up by the cells and are firmly anchored within the tissue. Magnetic forces were then applied to growing tissues with magnetic beads. Application of magnetic fields resulted in mechanical forces on the cell layer and tissues in the measurement area. Finally, 3D tissue growth was imaged and the expression of Alklaine Phosphatase (ALP), a well-known marker of osteoblast

differentiation was measured (Rumpler, Woesz et al. 2007) in the cell layer on top of scaffolds.

The effect of forces on the *in-vitro* model system of pre-osteoblast tissues was therefore studied by varying four key parameters in the set of experiments:

- Ten distinct mechanical forces on magnetic beads in the pN-nN range
- Two types of force application: static or oscillating forces
- Varying orientation of the rectangular pores relative to the direction of the force vector
- Different kinds of magnetic bead functionalization

2 Background and literature review

2.1 Biological background

2.1.1 The mechanosensitivity of individual cells

Cells and bone forming cells in particular, are extremely sensitive to mechanical cues from their environment and actively respond to forces applied on their membrane by performing migration, opening of ion channels and protein activation and morphological or destiny alteration (Mack, Kaazempur-Mofrad et al. 2004, Ringer, Colo et al. 2017). Cells' proliferation, differentiation and apoptosis were shown to be significantly affected by external forces acting on cells (section 2.4) as well as by mechanical properties of their environment such as substrate rigidity and roughness (Schoen, Pruitt et al. 2013), and confining geometry (section 2.2). Biological mechanisms proposed to be cell related force sensors (Bonnet and Ferrari 2010), will be described in the following paragraphs.

A leading theory describing how cells absorb and transmit forces takes into account cells' filament network structure. According to this model, mechanical signals are transferred across the cell via the cytoskeleton (Regul 1988). The cytoskeleton – a network of actin filaments, microtubules and intermediate filaments, extending throughout the cytoplasm between the nucleus and the cell's membrane, is responsible for maintaining the overall structure of the cell. The cytoskeleton's own rigidity and structure is largely influenced by mechanical and chemical perturbations from cell-cell and cell-matrix interactions (Bao and Suresh 2003). Mechanical force within cells translates to reorganization of cell structure to maintain structural homeostasis (Huang, Dong et al. 2002). It can induce cytoskeleton conformational modifications such as unfolding of filaments and crosslinking proteins (Fig. 2f) and thereby change its components' affinity to intracellular signaling molecules. The cytoskeleton is therefore primarily responsible for the cell's ability to respond to external mechanical stimulation (Ringer, Colo et al. 2017)(Fig. 1e).

Mechanical loads and signals are sensed by focal adhesion complexes (FACs), the points of mechanical linkage between the cytoskeleton and the ECM which then transmit the signals

through interconnected cell elements within the cell's matrix. FACs transmit both mechanical stimulation and chemical signals from the ECM to the cell's interior, and take part in cells' mechanotransduction mechanism, the mechanism which translates mechanical signals to electrochemical signals (Wang, Tytell et al. 2009, Bao and Suresh 2003)(Fig. 1d).

FACs consist of three vertical layers: the inner layer which is integrated in the cytoskeleton; an intermediate layer containing hundreds of proteins processing mechanical and chemical signals; and an outer layer where the FAC-based adhesion of cells to the ECM takes place. This layer contains integrin receptors, transmembrane proteins which are integrated into ECM proteins such as fibronectin (Ringer, Colo et al. 2017). Cell adhesion is accomplished when integrins adhere to the tripeptide Arginine-Glycine-Aspartate (RGD) in the adjacent ECM. RGD is therefore useful for attaching mechanical probes and stimulators to cells in mechanobiological studies (Wang, Butler et al. 1993, Mack, Kaazempur-Mofrad et al. 2004, Geiger, Spatz et al. 2009).

Other proposed force sensors include the following components of the cell: the mechanosensitive ion-channels anchored in the cell's membrane that open in response to cells' membrane tension, thereby controlling the influx and efflux of ions (Fig. 1a)(Ringer, Colo et al. 2017); The glycocalix, a layer on the outer side of the cell membrane, takes part in mechanotransduction due to shear flow and cell-cell adhesion or communication (Fig. 1b); Cell-cell adhesion complexes, the points of linkage between the cytoskeleton of one cell to its neighbor, transmit chemical and mechanical stimulations between cells (Ringer, Colo et al. 2017) (Fig. 1c).

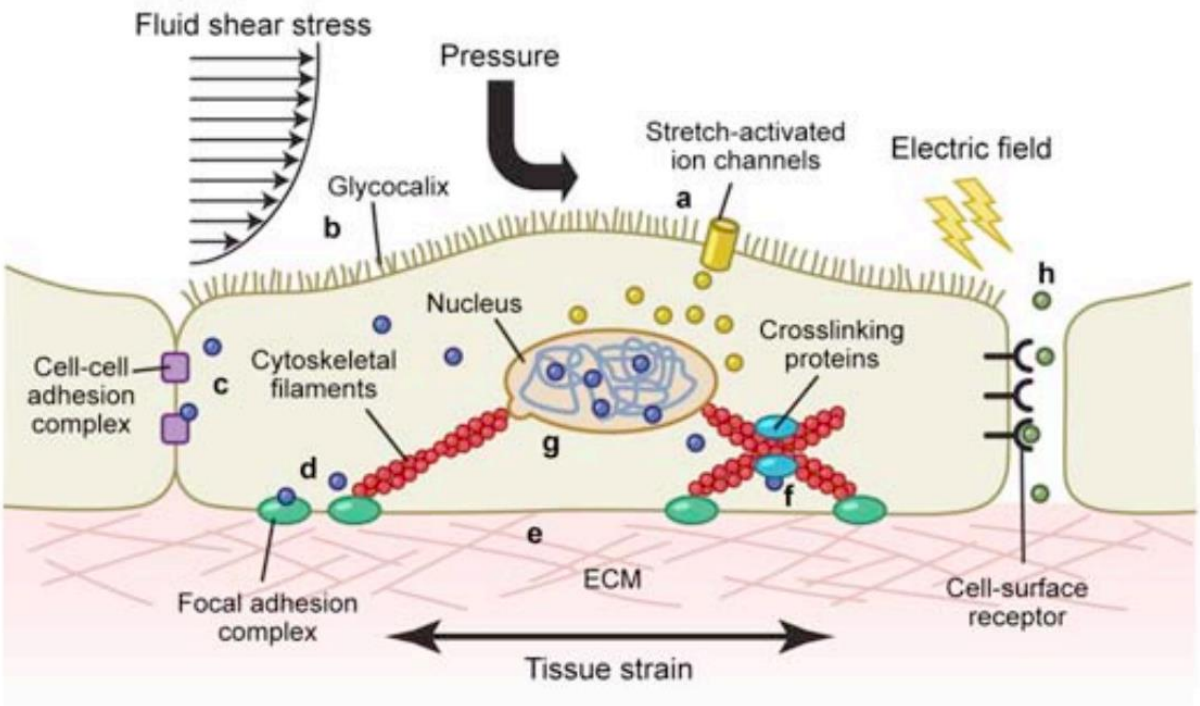

1. An illustration of a cell along with relevant biological components taking part in the mechanosensing mechanism. Mechanical stimulation due to shear flow, changes in membrane potential, cell-cell and cell-ECM interaction are sensed via the following components (details in text): a) Stretch-activated ion channels b) Glycocalix c) Cell-cell adhesion complex d) Focal adhesion complex e) ECM f) Crosslinking proteins g) Nucleus h) Cell surface receptor. Reprinted by permission from Springer Nature (Bonnet and Ferrari 2010).

2.1.2 The mechanosensitivity of bone tissue

Osteoblasts, bone-forming cells, osteoclasts, bone-resorbing cells and osteocytes, which are embedded in the bone matrix, are all different types of bone cells. As a response to forces applied to bone tissues, a multicellular unit consisting of osteoblasts and osteoclasts is constantly remodeling the structure of the bone extracellular matrix (ECM) by applying two different mechanisms: osteoclasts resorb the bone matrix, and osteoblasts produce the bone tissue by depositing an un-mineralized collagen matrix called osteoid, which mineralizes to form the bone matrix. Upon mechanical overloading resulting in local damage and cell apoptosis, osteoclasts dissolve the mineral out of the damaged bone and then

resorb ECM to allow a formation of new bone and attainment of structural homeostasis with the mechanical environment (bone remodeling). When osteoblasts stop producing bone matrix they either differentiate to become osteocytes, embedded in the matrix they produced, or enter a resting state as bone lining cells covering bone's surface (Fig. 2) (Klein-Nulend, Bacabac et al. 2005)(Burger and Klein-Nulend 1999).

Osteocytes, the majority of bone cells, are embedded in the mineralized bone matrix in pores called lacunae and are connected to other bone cells via small channels in the bone matrix called canaliculi. These cell-cell connections facilitate the transfer of nutrients and biochemical signals through the bone matrix, and enable cells embedded in the matrix to communicate with other cells. Osteocytes are considered to be responsible to sense the mechanical stimulation and, therefore, to coordinate bone remodeling (Klein-Nulend, Van der Plas et al. 1995, Bonnet and Ferrari 2010).

One hypothesis of bone mechanosensing mechanism is that damage of the bone material results in osteocyte apoptosis followed by bone remodeling as described above. Alternatively, load-induced flow of interstitial fluid through the network of lacunae and canaliculi and the resulting shear forces on the cell membrane may provide mechanical stimulus for bone remodeling (Klein-Nulend, Van der Plas et al. 1995).

Structural adaptation is enabled in the highly organized extracellular matrix (ECM), containing functional and structural proteins, by aligning ECM's stress fibers in the direction of applied force. This allows tissues to regulate forces and cope with large loads (Burger and Klein-Nulend 1999, Wang and Thampatty 2006).

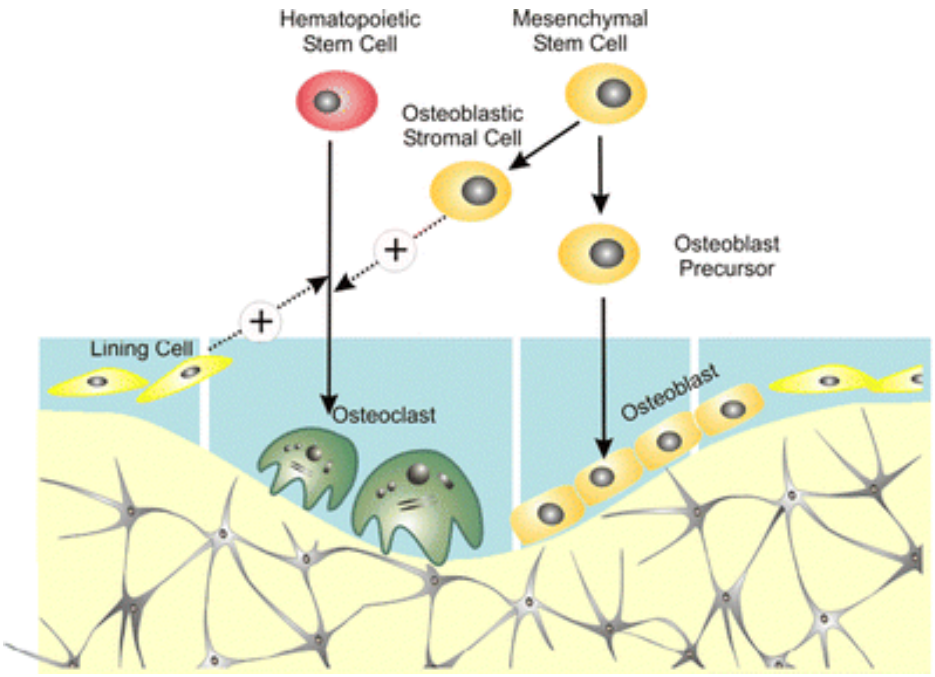

2. Types of cells found in bones: osteoblasts, bone-forming cells derived from mesenchymal stem cells (MSCs); osteoclasts, bone resorbing cells, derived from hematopoietic stem cells; osteocytes, mature osteoblasts that got embedded in the mineralized bone matrix (gray star like cells) that play a key role in bone mechanosensing mechanism; and bone lining cells, located on inactive bone surfaces. Reprinted by permission from Springer Nature (Proff and Römer 2009).

2.1.3 The MC3T3-E1 cell line

The widely studied MC3T3-E1 cell line is a derivation of the immortalized precursor pre-osteoblast cell line MC3T3 derived from mouse calvaria (Kodama, Amagai et al. 1981). In a similar way to the developmental sequence of osteoblasts in bone tissue, the proliferative stage of the pre-cursor and the mature, ready to mineralize state of this cell line were found to be sequential (Quarles, Yohay et al. 1992). This makes this cell line a good subject for studying the variables affecting the switch between these stages.

The first days of MC3T3-E1 pre-osteoblast cell culture are defined by proliferation in which cells in the undifferentiated precursor state replicate mitotically. During the proliferative stage: the synthesis of collagen type I, the most abundant collagen type in the human body and in bone forming tissue in particular, peaks; collagen starts to accumulate into the extracellular matrix; and they do not secrete alkaline phosphatase (ALP) (Fig. 3a) or produce mineralized matrix components. When cells become confluent, the culture's growth is arrested and cells mature to differentiate to the osteoblast cell line. This stage may be identified by the beginning of production of ALP that is secreted mostly just before matrix mineralization (Fig. 3b). Finally, the mineralization of the extracellular matrix marks the final stage of osteoblast development (Quarles, Yohay et al. 1992).

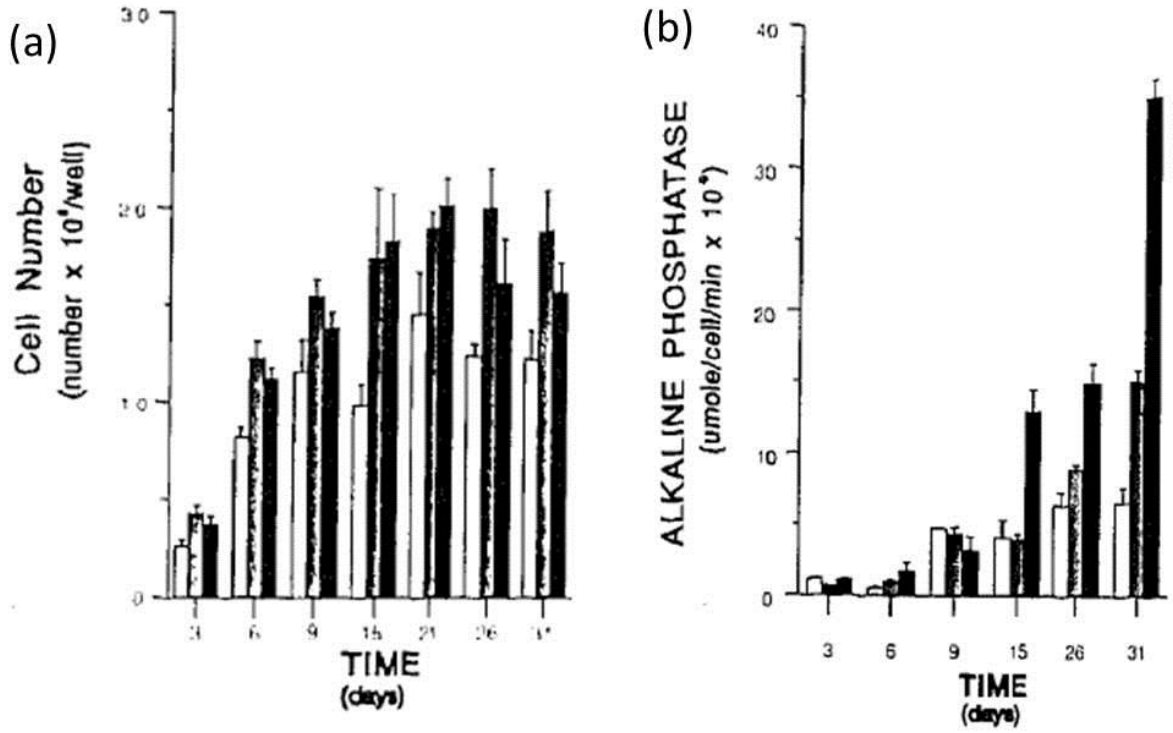

3. MC3T3-E1 cell proliferation and ALP expression: a) Measurements of MC3T3-E1 cell number as a function of time in culture. By day 9 the culture is confluent and experience growth arrest. Reprinted by permission from John Wiley and Sons (Quarles, Yohay et al. 1992) b) ALP expression of cell layer increased after 9 days concomitant with the downregulation of cell number growth rate, marking the transition to mature osteoblasts. Reprinted by permission from John Wiley and Sons (Quarles, Yohay et al. 1992).

2.2 Tissue growth in porous scaffolds *in-vitro*

2.2.1 Scaffolds used for 3D tissue growth

Scaffolds designed for tissue growth in pores provide a porous 3D environment for cells to adhere, proliferate and differentiate. The scaffolds' architecture defines the shape of the resultant tissue and can be controlled to a high extent (Kommareddy, Lange et al. 2010, Bidan, Kommareddy et al. 2012)(Fig. 4). Different materials have been used for scaffolds dedicated to tissue growth including: hydrogel forming bio-polymers such as collagen, the main protein of the ECM (Drury and Mooney 2003); polydimethylsiloxane (PDMS), an organosilicon easily fabricated and functionalized to create a substrate for cell adherence and tissue formation (Fig. 4c-d) (Herklotz, Prewitz et al. 2015, Ehrig 2017); and hydroxyapatite (HA), the calcium phosphate mineral found in bones (Bidan, Kommareddy et al. 2012)(Fig. 4a-b and d are examples of different scaffolds used for tissue growth).

2.2.2 Tissue formation as a function of geometrical constraints

Growing tissue in pores with defined geometries has been successfully used in the past to examine the influence of pore geometry on tissue formation in a 3D environment (Rumpler, Woesz et al. 2008, Kommareddy, Lange et al. 2010, Bidan, Kommareddy et al. 2012, Bidan, Kommareddy et al. 2013). In these experiments cells are seeded on top of a porous scaffold. Initially the cells adhere to the scaffold and proliferate on top of it. Over the following few weeks the cells migrate inside the pores, continue proliferating and form a tissue inside the pores (Fig. 4e is an illustration of a cross section of a tissue formed on top of scaffold and inside a pore).

Tissue grown in pores was shown by Rumpler *et al* to be created first in areas within pores with a high curvatures of the pore surface (an example can be seen at the right side of Figure 4a), and tissue growth rate was proportional to the curvature of its substrate (Rumpler, Woesz et al. 2008). As the tissue grows, the area of the interface between medium and

tissue is decreases (Fig. 4a shows different stages of tissue growth in pores). Another, more complex shape of pore, demonstrating the organized manner in which tissue is growing in curved surfaces, can be seen in Fig. 4b. ECM and cells were found to be highly organized with a higher percentage of actin presence closer to the tissue-medium interface where the tissue is younger (Bidan, Kommareddy et al. 2013, Bidan, Kollmannsberger et al. 2016) (Fig. 4b).

To understand how cells organize to form tissues Bidan *et al* developed a chord model. By this model, tissue is formed in a very organized manner with cells stretched and ECM formed in the direction parallel to the interface with the medium in which the tissues are cultured. Cells first adhere to the curved substrate and then contract their cytoskeleton until they reach a tensile stable state (Bidan, Kommareddy et al. 2012). When the substrate is covered with tensile cells a new layer of cells stretch upon it, increasing tissue volume and decreasing tissue-medium interface area. Tissue growth is arrested when tissue-medium interface area reached a minimal surface structure, much like a liquid would do (Ehrig 2017). Simulations based on this model predict experimental tissue growth in defined geometries (Bidan, Kommareddy et al. 2013).

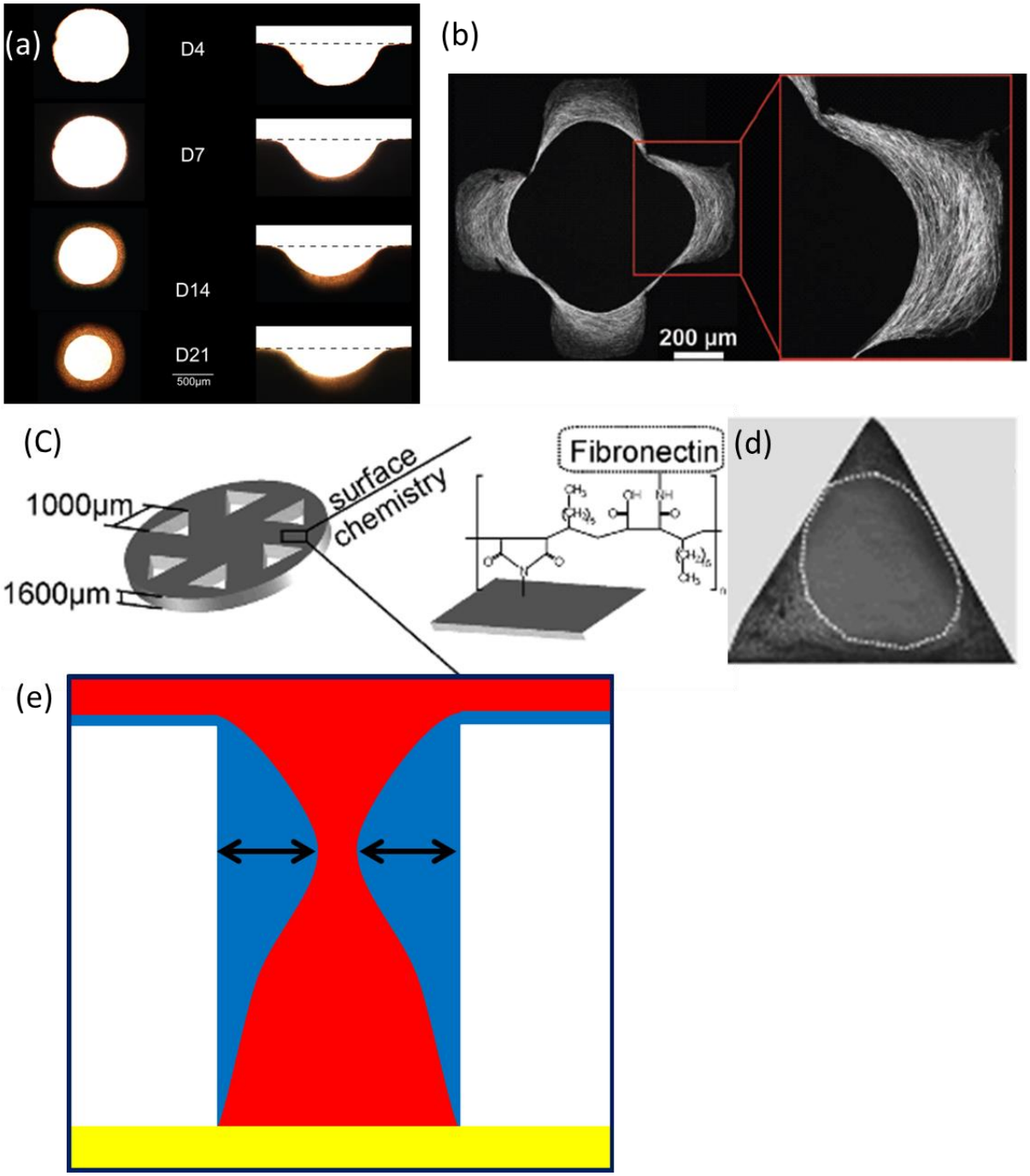

4. Tissue growth in different types of porous scaffolds; examples and illustration: a) Phase contrast images of osteoblast tissue growing on curved surfaces (right side) and pores (left side). Tissue-medium interface is decreasing with time indicating tissue (light brown in pores and on top of curved surfaces) volume increase. Tissue growth on curved surface starts in areas where the surface curvature is highest. Reprinted by permission from Bidan et al. (Bidan, Kommareddy et al. 2012). b) Confocal microscopy image of tissue growing in pore: actin fibers can be seen organized in the direction parallel to the tissue-medium interface. Reprinted by permission from John Wiley and Sons (Bidan, Kommareddy et al. 2013). c)

Computer aided design of PDMS scaffold for triangular tissue growth. 6 pores are located in one scaffold to allow for 6 tissues to be formed. After scaffolds production, scaffold is functionalized with fibronectin to enable cells to adhere to PDMS surface. Reprinted by permission from Elsevier (Herklotz, Prewitz et al. 2015). d) Osteoblast tissue growing in a triangular PDMS scaffold. Tissue is thickest near the edges of the triangular pore, where curvature is highest. Reprinted by permission from Elsevier (Herklotz, Prewitz et al. 2015). e) An illustration of a cross section of a tissue (blue) growing inside a pore and on top of a scaffold (white). Growth medium is red, the well plate on which the scaffold is placed is yellow, arrows represent the area in which tissue is thickest. Tissue growth is often evaluated at this height of the pore and is referred to as "projected tissue area" (PTA).

2.3 Magnetic beads used to apply loads on cells and tissue

Many commercially available magnetic particles, used to apply mechanical loads on cells, are composed of a combination of magnetite and polystyrene (Thermo Fischer Scientific, Spherotec, Bang Laboratories etc.). Magnetite, an oxide of iron, Fe_3O_4, is a naturally occurring magnetic mineral in the human body and is biocompatible (Kirschvink, Kobayashi-Kirschvink et al. 1992, Gieré 2016). Polystyrene is a widely used inexpensive plastic that can be used to form uniform spherical micro-beads (Thermo Fisher Scientific, Waltham, MA). It is made from the monomer styrene (C_8H_8), and has been tested in long term tissue cultures to demonstrate good biocompatibility (van Midwoud, Janse et al. 2012, Pandey, Srivastava et al. 2016). MBs consisting of different composites of polymers and magnetite have been cleared for clinical use by the United States Food and Drug Administration and have been employed in studying how forces affect cells and tissues (Cartmell, Dobson et al. 2002, Dobson, Cartmell et al. 2006, Hughes, Dobson et al. 2007, Kanczler, Sura et al. 2010, Henstock, Rotherham et al. 2014).

Different kinds of polystyrene-magnetite beads are commercially available with sizes ranging from tens of nm to hundreds of µm (Thermo Fischer Scientific, Spherotec, Bang Laboratories etc.). Magnetic susceptibility and form of magnetism of beads (superparamagnetic, ferromagnetic or paramagnetic) vary and, therefore, allow the application of different types

of forces on cells and tissues. Ferromagnetic beads are usually composed of a polymeric core with ferromagnetic coating. The relative stability of the magnetization direction in ferromagnetic particles, consisting of multiple domains stabilizing each other in the easy axis of the magnetization direction (Fig. 5a), has been exploited to physically twist beads attached to cell membrane receptors by using magnetic forces too weak to reverse the particles' magnetization direction relative to their axes (Wang, Butler et al. 1993, Chen, Fabry et al. 2001).

To reverse the magnetization direction of ferromagnetic particles, fields stronger than the coercive field (H_c in Fig. 5a) are required and often, only very strong fields align these materials' magnetization entirely in the magnetic field's direction(Coey 2010). To provide a more defined magnitude of force in a defined direction to be applied to cells and tissues, superparamagnetic beads are used in mechanobiological studies (Hughes, Dobson et al. 2007, Dobson 2008, Henstock, Rotherham et al. 2014). Superparamagnetic micro-spheres (or magnetic beads) are colloids composed of polystyrene spheres, with superparamagnetic magnetite nucleations (Thermo Fisher Scientific, Waltham, MA). Superparamagnetic particles are very small magnetic materials, usually few nm to tens of nm in diameter. Their small size allows for the entire particles' region to have a uniform magnetization direction, which is very sensitive to thermal fluctuations. Due to their small size, these particles constantly change the magnetization direction when no external magnetic field is applied. This instability of magnetization allows for very small fields to reverse particles' magnetization direction entirely in the direction of the magnetic fields applied (Coey 2010) (Fig. 5b).

Many short term studies employing magnetic bead-based actuation of cells take into account beads' attachment to membrane receptors (Wang, Butler et al. 1993, Cartmell, Dobson et al. 2002, Mack, Kaazempur-Mofrad et al. 2004, Henstock, Rotherham et al. 2014). However, in long term studies of tissue cultured with MB, beads were found to be internalized in cells. These studies showed that more than 50% of MBs were internalized into cells after 24 hours and almost all beads were internalized after 48 hours. Cell internalization had no effect on cell viability even when a large number of beads were internalized (Heinemann, Lohmann et al. 2000, Hughes, Dobson et al. 2007). In another study, using 4.5

µm ferromagnetic beads coated by RGD, scanning electron microscopy revealed beads' internalization 1 hour after incubation with cells (Chen, Fabry et al. 2001).

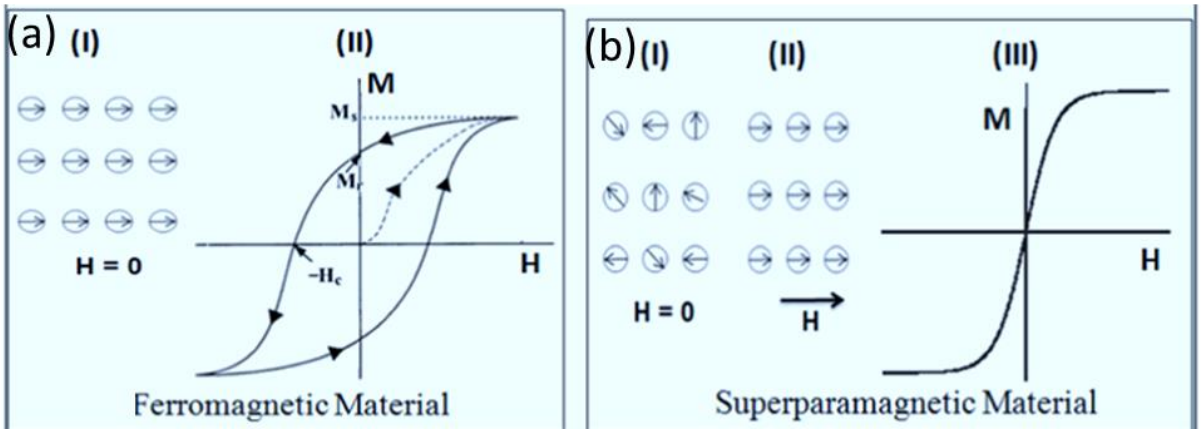

5. Magnetic moments M of magnetic materials and response to magnetic field H: a) Domain structure (I) and magnetization curve due to external magnetic field (hysteresis loop) of ferromagnetic materials (II). In ferromagnetic materials, magnetic moments, indicated by circles with arrows, are aligned and exert a remanent magnetization (M_r) even after the magnetic field was removed. Magnetic field greater than the coercive field (H_c) is required to reverse the magnetization direction. b) Superparamagnetic nucleations, composed of a single domain each, align instantaneously in the direction of magnetic field. Superparamagnetic particles' magnetic moment when there is no magnetic field (I) and when magnetic field is applied (II) and M-H curve (III). Reprinted by permission from Elsevier (Sodipo and Aziz 2016).

2.4 Instruments used to apply loads on cells and tissues to study cell proliferation and differentiation into the osteoblast lineage

Many techniques have been employed to probe cellular and tissue response to external forces. Among them are stretchable substrates, well plate shakers, and forces applied to tissue directly using tools such as magnetic tweezers, micro-pipettes, optical tweezers, atomic force microscope and shear flow (Vogel and Sheetz 2006). While mechano-biological studies have been performed on many cell types such as fibroblasts, chondrocytes,

endothelial cells and muscle cells (Wang and Thampatty 2006), here the focus will be on instruments used to apply loads on mesenchymal stem cells (MSCs) differentiating into the osteoblast lineage, pre-osteoblasts and osteoblast cells.

In addition to being a well-known marker of cell differentiation into the osteoblast lineage, alkaline phosphatase (ALP) expression is a predictor of tissue mineralization (Golub and Boesze-Battaglia 2007). Osteoblasts, much like pre-osteoblasts, secrete ALP after they become confluent, and before mineralization and it was previously suggested that the proliferative stage, and mature, ready to mineralize state, are sequential in human osteoblasts as well (Fedarko, Bianco et al. 1990, Neidlinger-Wilke, Wilke et al. 1994). Since ALP expression is a late marker of osteoblast differentiation, it is a marker of cell maturation to both pre-osteoblasts and osteoblast cells. In addition, MC3T3-E1 cells display a developmental sequence comparable to osteoblasts cells in bone tissues (Quarles, Yohay et al. 1992). Therefore, when comparing this study to other studies (discussion in section 6.1) where forces were applied to osteoblast cells and markers of proliferation, number of cells and cell maturation were examined, it may be also of interest to review papers where osteoblast cells and not only pre-osteoblasts or MSCs differentiating into the osteoblast lineage were studied.

First, studies where application of stretch forces resulted in cell proliferation increase and/or cell differentiation decrease are reviewed. Studies where proliferation increased and differentiation decreased are reviewed together in the same group since the differentiation stage was found to be sequential to the proliferation stage (Quarles, Yohay et al. 1992). Therefore, prolongation of the proliferative stage may be associated with a delay in differentiation and in the same manner; early differentiation may accompany early halt of proliferation. Then, studies where opposite trends were observed will be presented. Finally, studies where cell proliferation or differentiation trends were studied as a function of the magnitude of force applied will be reviewed.

2.4.1 Studies where forces applied resulted in cell proliferation increase and/or differentiation decrease

- Significant increase in proliferation was demonstrated on human derived osteoblast cells subjected to 1 Hz oscillatory strain of 0.1% strain applied to their silicone substrate. Cell proliferation increased as a function of number of stretch cycles until it reached a maximum at 1800 cycles. Different frequencies including 0.1, 1, 10 and 30 Hz were tested for 5 minutes of oscillations each. 1 Hz frequency showed to be most efficient in increasing proliferation rate relative to control. High frequency of 30 Hz and 9000 cycles reduced proliferation to control level (Kaspar, Seidl et al. 2002).
- A similar system also demonstrated in addition to an increase in proliferation, also an increase in collagen type I peptide presence, an early osteoblast activity related to matrix production. However, later markers of osteoblast differentiation including ALP activity and osteocalcin release indicating mineralization were reduced relative to controls (Kaspar, Seidl et al. 2000).
- Osteoblast precursor cells were cultured in type I collagen gel inside stretchable silicone dishes. Dishes were subjected to 1%, 1Hz cyclic strain, 30 minutes a day for 21 days. Cell proliferation increased and cell osteogenic markers such as ALP expression only slightly increased. Cells and tissue stress fibers were oriented in the direction of applied stress (Ignatius, Blessing et al. 2004, Rauh, Milan et al. 2011).

2.4.2 Studies where forces applied resulted in cell proliferation decrease and/or differentiation increase

- In a 2003 study by Tanakaa et al., piezo electric compressors were used to apply loads to tissue cultured in collagen gels. A comparison between oscillating forces and sinusoidal forces acting on tissue showed that application of low amplitude high frequency forces (vibrations) resulted in a lower cell number and stronger indication of tissue matrix remodeling than moderate 1 Hz sinusoidal forces. In both cases cell number was lower than control upon force application, suggesting vibrations are of more disruptive nature to tissue (Tanakaa, Lib et al. 2003).

- In another study, 1 Hz oscillating mechanical tension was applied to collagen scaffolds incubated with osteoblast precursor cells. This together with an addition of bone morphogenetic protein 2 (BMP-2, a growth factor) yielded immediate substantial expression of differentiation markers (Kopf, Petersen et al. 2012).
- hMSCs were seeded on flexible silicone well plates and allowed to adhere and proliferate for 48 hours. A sinusoidal 0.5 Hz force was then applied to cells to create either a 3-5% elongation for 2 hours per day with 8, 15 minutes strain periods. Mechanical strain increased differentiation towards osteogenic lineage and matrix mineralization (Ward Jr, Salasznyk et al. 2007, Assanah and Khan 2018)
- hMSCs seeded on well plates with flexible bottoms and allowed to adhere for 24 hours, were subjected to 0.1 Hz oscillating force with 3% surface elongation for 1, 3, or 5 days. An increase in ALP expression and mineralization was observed (Huang, Dong et al. 2002, Assanah and Khan 2018).
- A custom bioreactor was designed by Jon Dobson and colleagues to allow introduction of oscillating magnetic forces to incubated bone tissue cultures labelled with MBs (Fig. 6a). A 2D stem cell monolayer was studied under an oscillating field of 1 Hz for one hour a day during 21 days. Significant upregulation of bone matrix proteins and mineralization (Fig. 6b) was demonstrated (Cartmell, Dobson et al. 2002).
- Another magnetic bio-reactor was designed by Dobson and colleagues to apply forces of 10-30 pN on growing tissues. This setup was the inspiration for designing the magnet actuator described in this thesis (section 3.2). 2D tissue cultures were cultured for 21 days and 3D tissue cultures were cultured for 1 week, both with RGD MBs. Both types of cultures were tested under the application of oscillating forces of 1 Hz for 1 hour a day. Significant upregulation of specific bone matrix proteins (osteocalcin and osteopontin) and mineralization was found. ALP level increased as well, but not significantly (Dobson, Cartmell et al. 2006).
- In another study along these lines, this time on ex-vivo whole bones, Henstock and colleagues labeled magnetic beads with RGD and injected them into a chick fetal femur. They then applied a 1 Hz magnetic force of 4pN for 1 hour daily for 14 days. This resulted in a significant increase of differentiation and mineralization markers relative to both control and to actuated non-labeled beads. A similar effect was

demonstrated in 3D collagen scaffolds cultured with magnetic beads and the growth factor BMP-2 for 21 days (Henstock, Rotherham et al. 2014).

- A 1 Hz oscillating magnetic force of 1-100 pN was applied three times a week for 21 days to 250 nm magnetic particles cultured *in vitro* with a monolayer of hMSCs or encapsulated into microcapsules. The same kind of microcapsules with hMSCs and MBs were also cultured *in-vivo* as implants in mice. 1Hz magnetic field was applied *in-vivo* using a magnetic box in which the mice experienced the periodic magnetic field application. Despite the relatively long incubation times (21 days) and the rather small size of the particles, they were assumed to be externally attached to cell membrane receptors and ion channels rather than internalized by cells. It was concluded that mechanical activation of cells using MB can induce hMSC differentiation toward an osteogenic linage (Kanczler, Sura et al. 2010).

2.4.3 Studies where forces of different magnitudes were compared

- A 1 Hz uniaxial force was applied for 15 minutes a day to silicone substrates cultured with human osteoblast cells. Four different strains were applied in addition to control. While an increase of cell proliferation was found in the lowest strain of 1% cyclic strain, higher strains of 2.5, 5.3 and 8.8% had no significant effect on cell proliferation or reduced cell proliferation. ALP levels did not alter significantly due to applied forces (Neidlinger-Wilke, Wilke et al. 1994).
- Differentiation of MSCs into the osteoblast lineage was investigated under 1Hz stretch of 0.8%-15% of well plates with flexible bottoms for two days. Cell proliferation increased after 48 hours when 5%, 10% and 15% strains were applied. ALP expression increased at the lower strain magnitudes of 0.8% but decreased relative to control at higher strains of 10% and 15% elongation (Koike, Shimokawa et al. 2005).
- Rat bone marrow MSCs were stretched in 1 Hz oscillatory forces on their substrate, for 15, 30 and 60 minutes with 2%, 4% and 8% strains. Proliferation increased both as a function of number of cycles and as a function of strain, and increased relative to control (Song, Ju et al. 2007)

- In one example involving static forces, stretch loads were applied to monolayers of progenitor cells cultivated on flexible cell culture plates (Kim, Song et al. 2009). Moderate stretch forces, which resulted in a cell elongation of 0.01% to 0.04%, yielded an increase in cell number. A larger elongation of 1.67% resulted in cell apoptosis and decrease in cell number. While stretch alone did not increase the differentiation to the osteoblast lineage significantly, when applied together with the growth factor BMP-2 a significant increase in ALP was found on top of the monolayer indicating cell differentiation into the osteoblast lineage (Kim, Song et al. 2009).
- hBMSCs (human bone MSCs) were incubated for 3 days in flexible silicone dishes containing culture medium with osteogenic supplements to induce differentiation to the osteogenic lineage. Dishes were stretched for either 2% or 8% with 1 Hz for 3 days, 2-3 times on each day in a total of 2 hours per day. Osteogenic differentiation markers increased respectively to the force application (Haasper, Jagodzinski et al. 2008, Assanah and Khan 2018).
- Osteoblast cells were seeded on collagen I coated flexible well plates and subjected to 0.5 Hz oscillating stretch forces of 0.4- 2.5%. Force application resulted in a decrease in cell number on day 7 and in an increase in cell number on day 14. This suggests force application effect on these cells depend on their differentiation stage. No dependency on the magnitude of force was found (Weyts, Bosmans et al. 2003).

In summary, in most cases, when stretch forces were applied either externally on tissue substrate, scaffold or well plate or internally via MBs, an increase of cell differentiation accompanied either by a decrease in proliferation or in non-significant proliferation increase was observed (Tanakaa, Lib et al. 2003, Dobson, Cartmell et al. 2006, Ward Jr, Salasznyk et al. 2007, Huang, Chen et al. 2009, Kanczler, Sura et al. 2010, Kopf, Petersen et al. 2012, Henstock, Rotherham et al. 2014). Oscillatory forces caused a decrease in cell differentiation and a higher proliferation rate in other system studied (Kaspar, Seidl et al. 2000, Kaspar, Seidl et al. 2002, Ignatius, Blessing et al. 2004, Li, Batra et al. 2004, Song, Ju et al. 2007). An oscillation frequency of 1 Hz was usually used, and lower frequencies rather than higher frequencies were found to increase proliferation more significantly, when comparative studies investigating different frequencies were performed (Kaspar, Seidl et al. 2002, Rosenberg, Levy et al. 2002). When the magnitude of force was compared, in some cases lower strains resulted in an increased proliferation (Neidlinger-

Wilke, Wilke et al. 1994, Kim, Song et al. 2010) and higher forces resulted in an increase of osteogenic differentiation markers (Haasper, Jagodzinski et al. 2008), while in other cases an opposite trend was found (Koike, Shimokawa et al. 2005), or no dependency on the magnitude of force was found (Weyts, Bosmans et al. 2003).

(a)

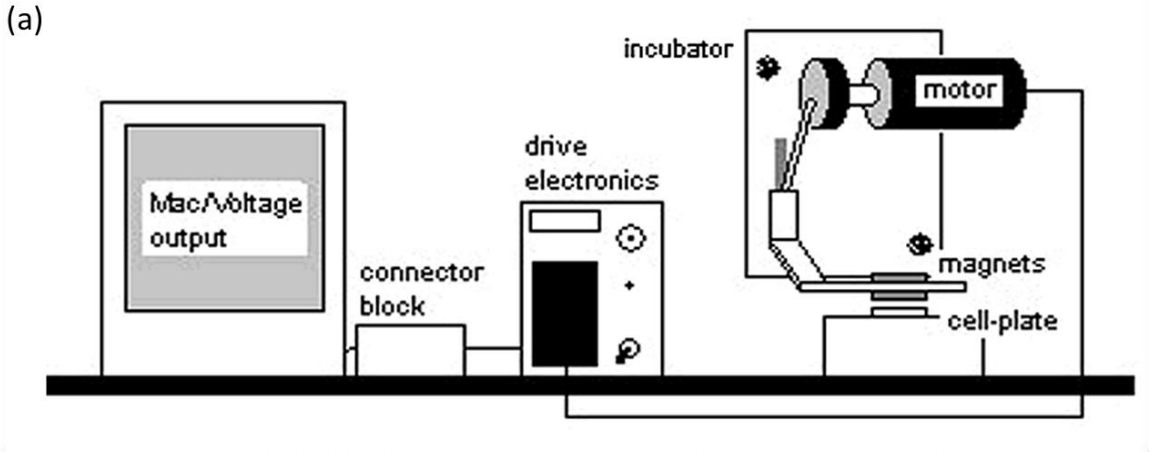
incubator
motor
drive
electronics
Mac/Voltage
output
connector
block
magnets
cell-plate

(b)

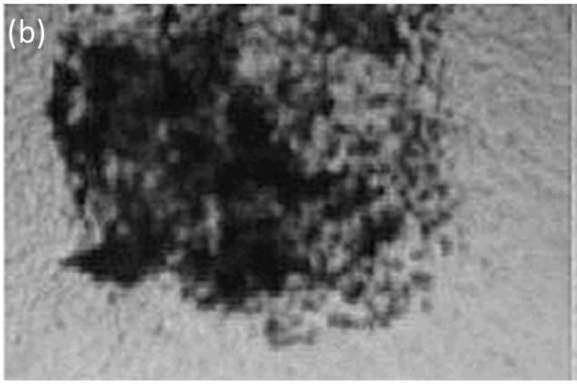

(c)

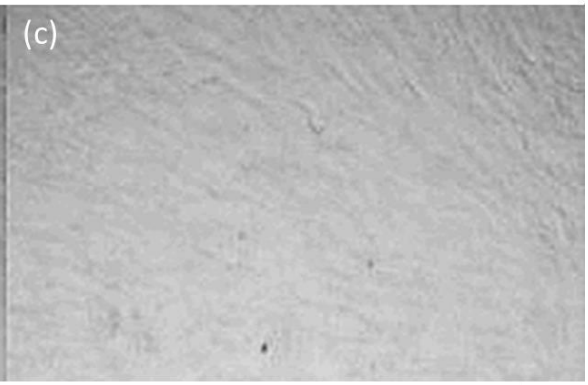

(d)

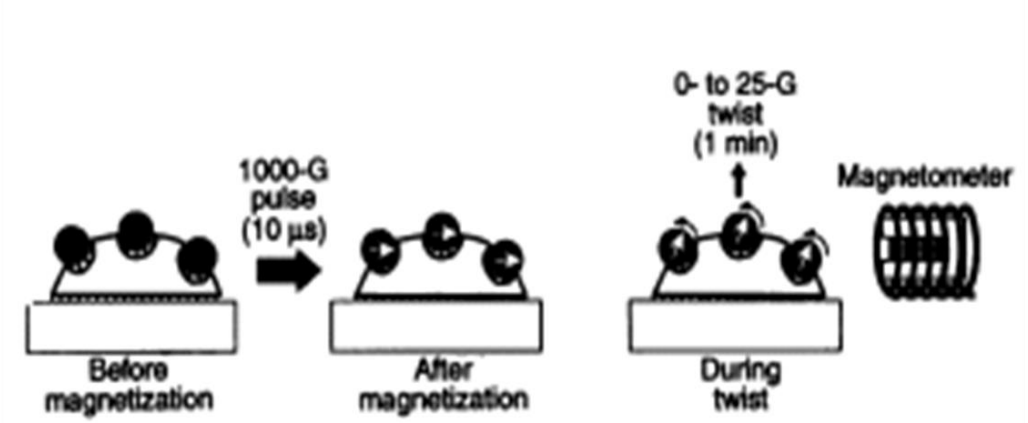
0- to 25-G
twist
(1 min)
1000-G
pulse
(10 μs)
Magnetometer
Before
magnetization
After
magnetization
During
twist

(e)

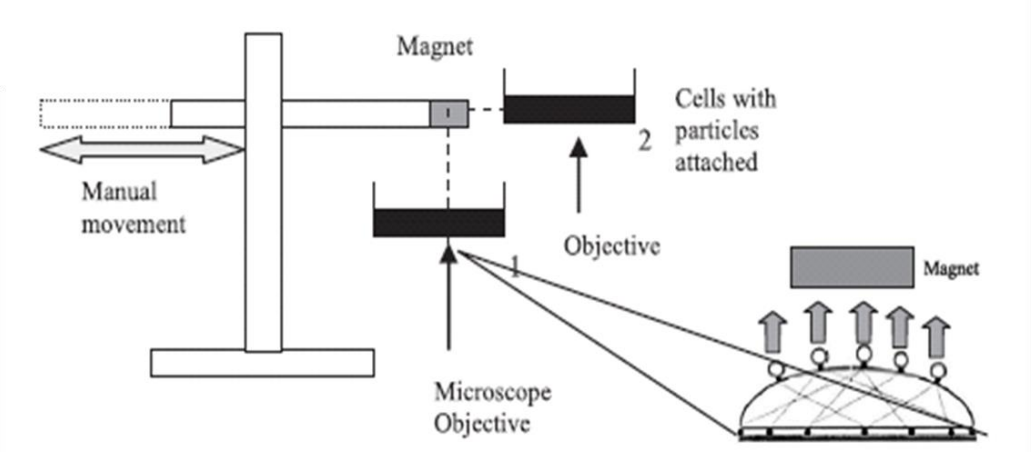
Magnet
Cells with
particles
attached
2
Manual
movement
Objective
1
Magnet
Microscope
Objective

6. Example of instrumentation used to apply loads on cells and tissues: a) Schematic of experimental setup designed by Cartmell et al. to apply oscillating magnetic forces on well plates cultured with cells and MBs. A 21 day old cell layer cultured with MBs and subjected to 1 Hz oscillating forces (b) and control (c) was tested for mineralization. Reprinted by permission from IEEE. (Cartmell, Dobson et al. 2002) d) Ferromagnetic beads functionalized with RGD were bound to cells' membrane. A magnetic field strong enough to reverse the beads' magnetization direction (about 0.1 T) was applied on beads followed by a weaker static magnetic field to the perpendicular direction able to rotate the magnetized beads to an extent confined by the beads' mechanical environment. Reprinted by permission from The American Association for the Advancement of Science (Wang, Butler et al. 1993) e) Schematics of a permanent magnet manipulator setup which enabled the application of magnetic forces to cells. Forces were applied in parallel or perpendicular to the cell layer. Reprinted by permission from Elsevier (Hughes, Dobson et al. 2007).

2.5 Examples of other uses of magnetic beads in biology

Uses of magnetic beads in biology other than exerting mechanical forces on them to study cell proliferation and differentiation inspired and motivated some of the work done in this thesis.

Magnetic beads have been widely used for various types of force measurements of mechanical properties of cells (Wang, Butler et al. 1993, Bausch, Ziemann et al. 1998, Alenghat, Fabry et al. 2000, Kollmannsberger and Fabry 2007). Typically, for these types of measurements a magnetic setup is composed of a permanent magnet or magnetic tweezers pulling on MBs functionalized with fibronectin or RGD peptides and either attached to the cells' membrane or incorporated in cells. Tracking the beads' movement due to applied force and analyzing the trajectories has provided insight on cells' mechanical properties. A work by Galy et al incorporating MBs inside biofilms to study biofilms' mechanical properties (Galy, Latour-Lambert et al. 2012) motivated the inconclusive experiment described in section 5.1, where an attempt to probe mechanical properties of tissues using MBs was performed.

Ning Wang and colleagues studied how forces induced by MBs are transferred to the cytoskeleton through the surface of the membrane and specifically membrane receptors such as integrins. The cytoskeleton of cells is seen as a network that remodels itself constantly to reach structural homeostasis with the forces applied on it. To quantify how transmembrane forces affect cytoskeleton reorganization and thereby cell stiffness, ferromagnetic particles labeled with RGD were bound to cell membranes and shear forces were applied to them in the following manner: first a strong magnetic field aligned the particles' magnetization in one direction; this was followed by a weaker magnetic force applied for one minute in the perpendicular direction resulting in a spatial rotation of the particles (Fig. 6d). The researchers observed that the particles' rotation became increasingly confined the longer the magnetic forces had been applied. They concluded that the longer duration of magnetic forces had resulted in higher stiffness of cells – indicating that the forces applied to the cells had induced cell structure changes to maintain structural homeostasis with forces from the surrounding (Wang, Butler et al. 1993).

Another example of magnetic beads used to study cell behavior due to forces is a 2015 study by Rotherham *et al* where 1 Hz oscillating magnetic fields were used to stimulate 250 nm magnetic particles functionalized with an antibody tagging the Frizzled protein that serves as a receptor in the Wnt signaling pathway which regulates gene transcription and affects cell shape, calcium levels and cell-cell communication. Magnetic particles were labeled and incubated with human mesenchymal stem cells (hMSCs), and they were then placed in a magnetic bio-reactor with an array of Neodymium magnets exerting low magnetic fields for 1-3 hour sessions. 1 hour sessions were shown to be effective in activating the Wnt signaling via Frizzled receptors relative to controls (Rotherham and El Haj 2015).

In another example by Steven Hughes et al., 3pN forces were applied vertically or horizontally to magnetic beads internalized within osteoblast cells or attached to membrane integrin (Fig. 6e). Static force application resulted in a significant increase of calcium levels within cells both when particles were on the outside of the membrane and when they were internalized (Hughes, Dobson et al. 2007).

Another use of magnetic beads is to alter cell migration patterns. Low mechanical forces induced by magnetic beads have been shown to induce directional movement of single cells

in a direction opposing the magnetic force (Rivière, Marion et al. 2007). This work inspired the performance of the inconclusive experiments described in section 5.3 and 5.4.

3 Methods

To address the research aims of this thesis a novel experimental system was designed that offers a tool for examining the effect of oscillating and static mechanical forces with force magnitudes ranging between pN and nN within a single well plate. Magnetic beads (MBs) with two kinds of functionalization were introduced to the cells and the geometry of the tissue culture pores relative to the force vector was investigated. The details of this experimental setup are described in the following sections.

3.1 Cell and tissue culture with magnetic beads

3.1.1 Handling and functionalizing magnetic beads (MBs)

Commercially available Dynabeads M-450 (Thermo Fisher Scientific, Waltham, Massachusetts) are spherical polystyrene beads with a diameter of 4.5 µm containing superparamagnetic magnetite colloidal nanoparticles distributed over the entire bead. Their magnetic susceptibility is 1.63 and they have displayed good force-to-volume ratio in previous studies (Kollmannsberger and Fabry 2007). Beads were ordered with an epoxy functionalization and then handled and functionalized in three different ways to achieve three types of magnetic beads (2 for the tissue growth experiment and 1 for a preparatory investigation).

“Plain” epoxy functionalized MBs (epoxy MBs) were handled according to the manufacturer’s instructions as follows: beads were first transferred to a falcon tube, and supernatant was discarded by approaching the tube with a permanent magnet (Fig. 7b) and aspirating the supernatant. Beads were then sterilized using 70% ethanol for 5 minutes followed by ethanol aspiration. Finally, the falcon tube was filled with growth medium before introduction to cells (Thermo Fischer Scientific protocols).

Functionalizing MBs with arginylglycylaspartic acid (RGD), a sequence within ECM fibronectin responsible for cell adhesion, was performed to improve the adhesion of MBs to cells’ integrin. The rationale of this functionalization was to test whether this specific binding

between MBs and cells will result in alterations of the tissues grown. Epoxy MBs functionalized with RGD peptides (RGD MBs) were prepared as follows: MBs were first transferred to a falcon tube and sterilized as described above for epoxy MBs. The falcon tube was then filled with 0.1 M sodium phosphate buffer, pH 7.4-8.0 and RGD peptide to fill half of the falcon tube. The tube was mixed for 30 minutes followed by introduction of phosphate buffer saline (PBS) with 0.1% bovine serum albumin (BSA), to reach the initial volume of beads' supernatant. BSA is a standard ligand often used in blocking solutions because of its moderately non-reactive and stable nature. PBS is a salt solution commonly used for cell culture applications. The falcon tube was then incubated overnight while tilting and rotating. Finally, beads were re-suspended in culture medium before introduction to cells (Thermo Fisher Scientific's protocols). Fig. 7a is an illustration of epoxy superparamagnetic micro-sphere coated with RGD peptides.

Bovine serum albumin (BSA) was also used as a third functionalization of MBs for preparatory investigations of beads' adhesion to cells. As BSA binds in a non-specific manner to cells and tissues, it is used in mechanobiological studies as a control of the use of functionalization resulting in more specific binding (for example with RGD) (Wang, Butler et al. 1993). Binding to BSA was performed as follows: 1 ml of washed Dynabeads were transferred to a falcon tube. A permanent magnet was then placed next to the tube (Fig. 7b) for 1 minute after which the supernatant was discarded. 6% BSA-PBS (sterilized using a filter) was added to reach a total coupling volume of 1 ml. The tube was incubated overnight at room temperature with gentle tilting and rotation. Beads were then washed 3 times by placing the tube next to a magnet for 1 minute and discarding the supernatant. Finally, 1 ml PBS was added, and the tube was incubated with gentle tilting and rotation for 5 minutes. Finally, before incubation with cells, the tube was taken away from the magnet and MBs were suspended in culture medium (Thermo Fisher Scientific protocols).

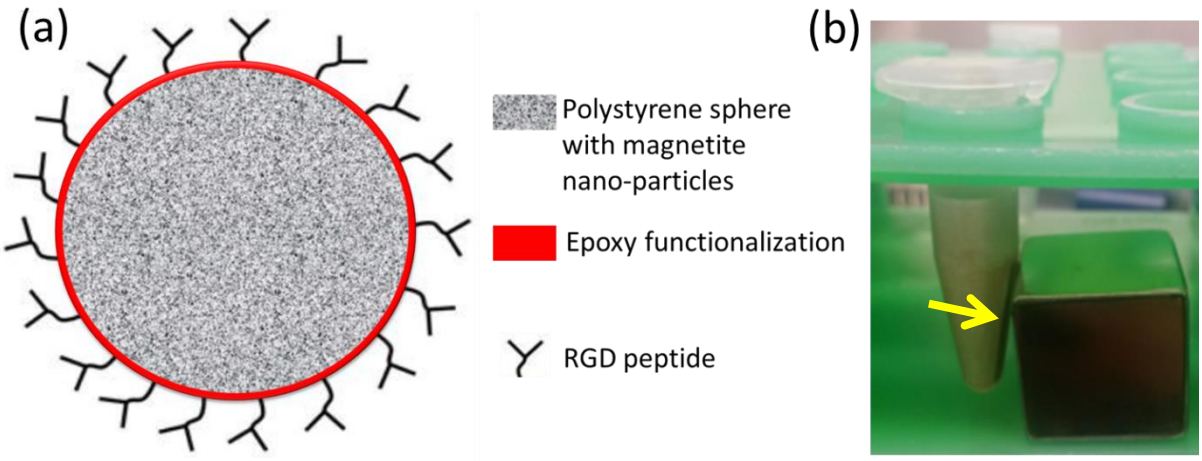

7. Handling and functionalization of magnetic beads (MBs): a) Schematics of epoxy polystyrene microsphere functionalized with RGD peptides. Adapted with permission from the Optical Society of America (Kim, Ahmad et al. 2013). b) Falcon tube with MB suspension. MBs are washed and separated using a permanent magnet (cube to the right of the falcon tube). The dark line that can be seen inside the falcon tube on its edge and close to the magnet (marked with a yellow arrow) is the MBs attracted to the magnet.

3.1.2 Scaffolds used for tissue growth

3.1.2.1 PDMS Scaffolds for mechanical stimulation of tissue growth using MBs

Aluminum mold for Polydimethylsiloxane (PDMS) casting (Fig. 8b) was designed to allow for PDMS casting of scaffold for tissue growth in an array of rectangular pores, resembling a previous design by Kommareddy et al where a 3x4 array of rectangular pores were used to study tissue growth dependence on pore size (Kommareddy, Lange et al. 2010). On top of the baseplate of the mold an array of cuboids is put on in an 8x10 array of cuboids to allow for 8 different tissues to grow in 10 different distances from the magnet, each cuboid of a size of 1x0.5x1.5 mm^3. Cuboids had two different orientations relative to the mold: one with the long face in the direction of the magnetic force, the other were oriented perpendicular (with the short face in the direction of the magnetic force) (Fig. 8a). The aluminum mold had specific dimensions such that the resulting scaffold can fit inside a commercial rectangular well plate (Nunc rectangular 8 well plate, Pharmaceutical online), with a thickness of 1.5 mm

to allow introduction of both scaffold and sufficient growth medium to the well plate. Molds were then manufactured by the mechanical workshop of the Max Planck Institute for Colloids and Interfaces (MPICI) where the designed geometry was etched into an aluminum plate. The design was performed using Rhinoceros software with the Grasshopper add-on.

Using a standard Polydimethylsiloxane (PDMS) casting procedure the produced aluminum mold was then casted with PDMS, cured and peeled off to result in a PDMS scaffold with well-defined pores (Herklotz, Prewitz et al. 2015). When casting PDMS scaffolds in molds, manufacturer instructions were followed. A two parts silicone elastomer kit (Sylgrad 184, Dow corning) was used where the elastomer was combined with its curing agent at a ratio of 10:1 and mixed well. To obtain a smooth solution that will flow into all parts of the mold, the mixture of elastomer and curing agent was evaporated in a vacuum chamber to remove all bubbles trapped in the mixing process. The mixture was then poured into the aluminum mold and was allowed to cover its surface with excess material removed using a glass slide. Finally, the mold was baked at 80^0 for two hours, and the cured PDMS scaffold (Fig. 8c) was removed from its mold using a curved tweezer with a fine tip (Ehrig 2017).

Fibronectin is a glycoprotein of the ECM that binds to integrins on the cells' membrane. In the experimental setup fibronection is used to improve the adhesion properties of the PDMS scaffolds so that cells can firmly adhere to it and proliferate. Functionalizing the scaffolds with fibronectin was performed in the following way (Tan and Desai 2004, Ehrig 2017): first, scaffolds were thoroughly washed with distilled water followed by 70% ethanol, dried and placed in rectangular cell culture plates. The scaffolds were then inserted into a plasma cleaner (Harrick Plasma) with pressure of 0.36 mbar and the maximal power available on the radiofrequency coil for one minute. After exposure to air plasma, scaffold was immediately treated with 3 ml of 3% aminopropyltriethoxysilane for 15 minutes and thoroughly washed with double-distilled water (ddH_2O). Scaffolds were then treated with 3 ml 1% glutaraldehyde for 30 minutes, washed thoroughly with ddH_2O and dried. Finally, scaffolds were incubated with 3 ml phosphate buffered saline (PBS) containing 75µg fibronectin for 1 hour at room temperature and then washed extensively with PBS (Bidan, Kollmannsberger et al. 2016, Ehrig 2017).

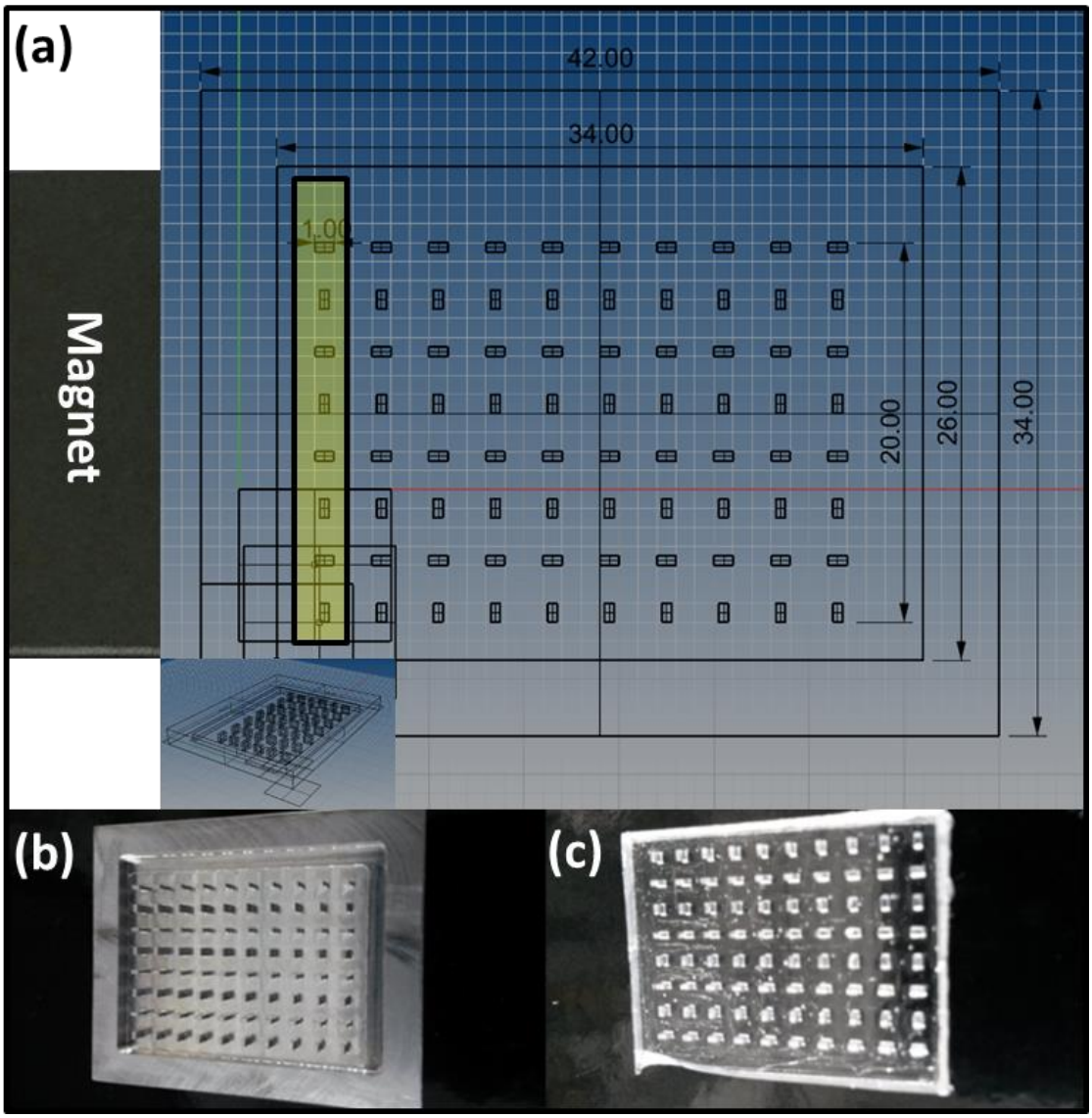

8. Design and production of scaffolds for tissue growth within an array of pores and under the influence of magnetic fields: a) A design of a mold for scaffold casting, consists of an array of 1x0.5x1.5 mm cuboids. The gray area to the left denotes the position of the magnet. The first row of pores in the vicinity of the magnet is highlighted in yellow. There are 10 rows in the array corresponding to 10 different distances from the magnet; each row consists of 8 pores of the same dimension with two different orientations relative to the magnetic force direction. Units specified in figure are in mm. b) Aluminum mold for PDMS casting. c) Casted PDMS scaffold for culturing tissue in an array of pores with defined geometry.

3.1.2.2 Hydroxyapatite scaffolds used for preparatory experiments

Hydroxyapatite scaffolds with triangular pores were produced for previous experiments by Cecile Bidan (Bidan, Kommareddy et al. 2013). These scaffolds could be recycled and used for preparatory investigations of movement of MBs within tissue due to force application (section 3.3.4 and section 4.1.4). The scaffolds comprised three triangular pores each, in which tissues with MBs could grow.

Scaffolds were recycled as was previously described (Ehrig 2017): scaffolds were first soaked in ethanol and thoroughly washed with distilled water. Tissue residues were then burned using a 700^{o} oven. Scaffolds were sanded and polished using sand papers and distilled water. Finally, scaffolds were autoclaved in closed glass plates and inserted into well-plates under sterile conditions (Ehrig 2017).

3.1.3 Cell and tissue culture with magnetic beads

MC3T3-E1, pre-osteoblast (Ludwig Boltzmann Institute of Osteology, Vienna, Austria) cells were seeded inside a rectangular well plate (Thermo Fisher Scientific, Waltham, MA) at a density of $10^5 \frac{\text{cells}}{\text{cm}^2}$ for 3D experiments (Fig. 9), or at a ratio of $6 * 10^3 \frac{\text{cells}}{\text{cm}^2}$ for 2D experiments. Cells and tissues were kept in an incubator throughout the experiments, to maintain constant temperature (37 degrees) and CO_2 levels (5%) and were taken out of the incubator only for media change and imaging (Manjubala, Woesz et al. 2005, Bidan, Kommareddy et al. 2010).

Pre-osteoblast cells, were grown in α-MEM (Sigma-Aldrich, St. Louis, MO), containing 10% fetal bovine serum (PAA laboratories, Linz, Austria), 0.1% ascorbic acid (Sigma-Aldrich, St. Louis, MO) and 0.1% gentamicin (Sigma-Aldrich, Steinheim, Germany) (prepared in collaboration with the cell culture lab technician Christine Pilz). Tissue was cultured for 24 days during which growth medium together with magnetic beads were replaced twice a week.

After tissue started to appear in the pores of the scaffold, well plates were filled with cell culture medium containing sterilized Dynabeads M450 (section 3.1.1)(Thermo Fisher

Scientific, Waltham, MA), superparamagnetic beads solution, every time growth medium was replaces. The ratio of MBs introduced with medium was 0.1% of MBs per medium volume and was chosen together with Alan West (a master student in John Dunlop's group I helped supervise) to enable sufficient concentration of MBs for incorporation in tissue while trying to keep MBs sufficiently separated from each other.

3.2 The magnet actuator setup

A 2 cm^3 Neodymium magnet of the highest grade, N52, with 1.43 T remanence magnetization was used for actuating tissues in tissue growth experiments. Following a magnetic force bioreactor designed by Dobson et al. (Dobson, Cartmell et al. 2006), a magnet actuator was built in the MPICI mechanical workshop (Fig. 9a), which rotated with a frequency of 1 Hz with a displacement amplitude of 0.015 m. The rod was fixed to an axial surface parallel to the well plate with the scaffold (Fig. 9a). The resulting back-and-forth motion of the magnet is a simple harmonic oscillation. Given the relation between magnet position and force applied (calculated in section 3.3.3) and following the inverse square law, a pulse form of the variation of the force on the magnetic beads was determined (Fig. 9b) (more information about force variation in scaffolds can be found in section 4.1.3).

In total, 18 scaffolds consisting of 80 pores each were incubated with MC3T3-E1 cells for 24 days, imaged and analyzed (see Table 1 for an overview). 9 of the scaffolds were subjected to 1 Hz oscillatory forces using the magnet actuator for 1 hour, 5 times a week. Of this 9 scaffolds 5 were grown with epoxy MBs and 4 of them with RGD MBs. 3 scaffolds were grown with epoxy beads and subjected to static forces by growing them with a static permanent magnet located in the same location as the oscillating magnet when closest to the scaffold (Fig. 9a is an image of the scaffold with the adjacent magnet). The static magnet was removed only for media change. In all the experiments forces were applied 24 hours after media change and beads introduction to allow beads to adhere to and to be incorporated in cells (sections 4.1.1 and 4.1.2). The number of scaffolds imaged in each case depends on the number of scaffolds which reached 24 days of incubation without getting contaminated.

6 control scaffolds were incubated with cells for 24 days. 4 of the control scaffolds examined were grown with magnetic beads but no force was applied to them, 1 were grown without MBs but with an oscillating magnet applied to them. One control was grown without beads or forces and was placed in the inner part of well plate.

Table 1. Scaffolds incubated with MC3T3-E1 cells for 24 days for mechanical stimulation of *in-vitro* tissue growth experiments

Applied magnetic force	Magnetic beads' functionalization	Number of scaffolds (total of 18 scaffolds)
oscillatory	epoxy MBs	5
oscillatory	RGD MBs	4
static	epoxy MBs	3
no magnet	epoxy MBs	4 (control)
oscillatory	no MBs	1 (control)
no magnet	no MBs	1 (control)*

(a)

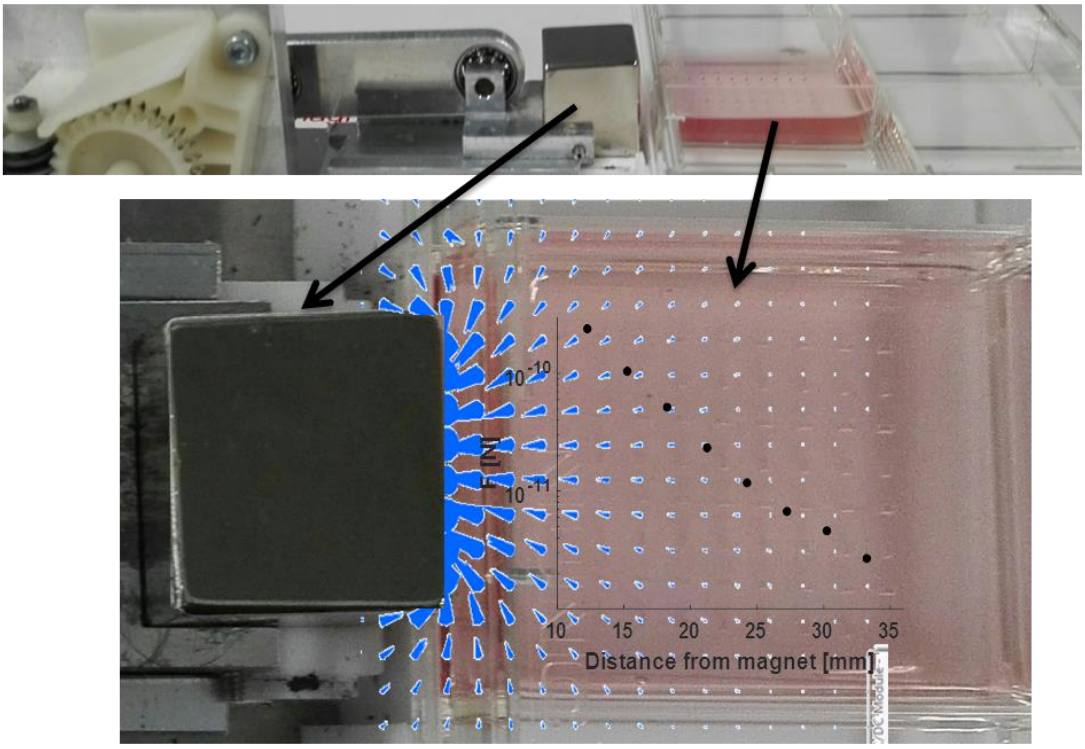

(b)

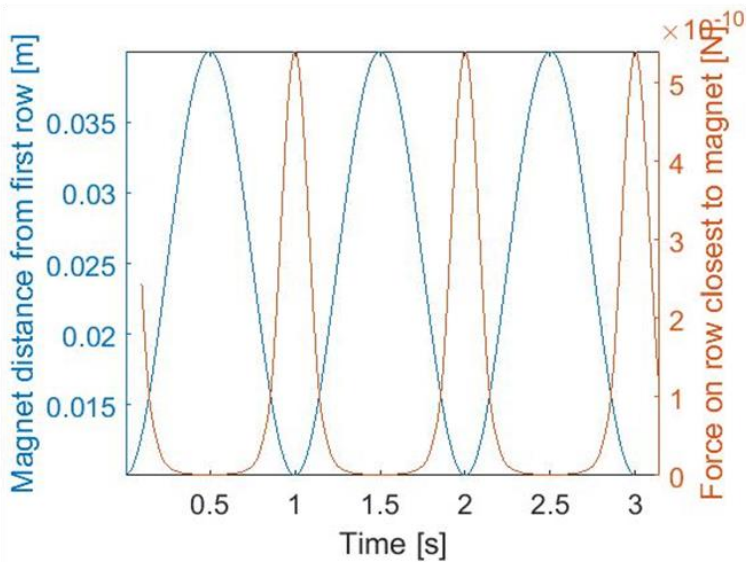

9. Forces exerted on pores in the scaffold as a function of distance from the magnet and time: (a) On top, photo (side view) of the magnet actuator setup. Below, a top view of the experimental setup with simulation results of the magnetic flux density lines overlaid (blue arrows). The size of the arrows indicates the relative magnitude of the magnetic field at the arrow's location and the directions to which the arrows are pointing are the magnetic field's directions. The graph in black shows the calculation of the magnetic force felt by magnetic beads in the center of rows, as a function of distance from the center of the magnet. The graph in the figure is placed on top of approximately the right location on an image of the

scaffold (pink in the background). (b) The magnet performs a simple harmonic oscillation with a frequency of 1 Hz and an amplitude of 1.5 cm (blue). The red line shows the calculated force pulses form the magnet on the MBs.

3.3 Methods used for preparatory investigations

3.3.1 Verifying beads' attachment to cells

To ensure MBs anchoring to or within the cells, a preparatory investigation of beads' attachment to cells was performed. A setup allowing the approach and retraction of a 7x7x3 cm N40 neodymium permanent bar magnet to varying distances from a cell culture plate with MBs, while imaging it using a bright field inverted microscope (Nikon Eclipse TS100, Japan) was built by the MPICI mechanical workshop, resembling a setup previously designed by Hughes et al. (Hughes, Dobson et al. 2007). A cell culture dish with a confluent cell monolayer was placed on the microscope's stage within the calculated "measurement area" of the magnet, in a location next to the magnet where forces on MBs in the well plate are relatively homogenous (more explanation and calculation of forces in the "measurement area" for the smaller magnet used in the tissue culture experiments are in section 4.1.3). The scaffold was then approached with the magnet at different distances and after varying incubation times of beads with cells.

Using this setup a magnetic force of different magnitudes was applied to magnetic beads with different surface functionalizations at several time points: 0.5 hour, 2 hours, 4 hours and 24 hours after introducing the beads to the cells. The magnet was placed at distances of 300, 97, 67, 37 and 7 mm from the sample exerting forces of ~aN, femto-Newton (fN), 50 fN, pN and 0.5nN respectively on MBs. Magnetic fields from a 7x7x3 cm N40 Neodymium magnet were simulated and calculated as described in section 3.3.3. Forces at every magnet-sample distance were applied for 5 minutes on sample before imaging which allowed relaxation and steady number of beads left in frame. The number of beads per frame was detected using FIJI software and figures 13e-f were plotted using Matlab.

The magnetic beads were either functionalized with epoxy by Thermo Fisher Scientific, with arginylglycylaspartic acid (RGD) or with bovine serum albumin (BSA), a protein standard (details about bead functionalization are in section 3.1.1). Results of this preparatory investigation are in section 4.1.1.

3.3.2 Observing beads' locations within cells and tissues

To determine whether MBs were incorporated inside cells, MBs incubated with MC3T3-E1 cells for 24 hours were observed using an optical microscope (Zeiss Axioobserver) with a 40x phase contrast and with a Achroplay objective lens (0.6 numerical aperture) in collaboration with Dr. Vasil Georgiev (Department of theory and bio-systems, MPICI)(Fig. 14 in section 4.1.2).

To determine the percentage of MBs incorporated inside cells, Matlab protocols were used. First, cell membrane was detected and outlined (Fig. 14e) using an image segmentation technique where the gradient of the image is calculated and the edges of the cells are determined where the gradient is maximal. Then, the circular beads were detected and sorted to outside and inside the boundaries of cells (Fig. 14f) and their ratio was calculated (Matlab protocols).

The incorporation of MBs into cells was further investigated by incubating MC3T3-E1 cells with MBs for 24 hours and staining actin stress fibers as described below. Stained cells and MBs were then imaged with confocal microscopy (Leica-TCS-SP8) in collaboration with Dr. Carmen Remde (Department of Theory and Bio-Systems, MPICI) and Christine Pilz (Department of Biomaterials) (Fig. 15 in section 4.1.2).

To determine how MBs are incorporated in tissues, PDMS scaffold cultured with MC3T3-E1 cells and MBs was imaged after 24 days in culture. The integrations of magnetic beads in growing tissue was first imaged using bright field microscopy (Fig. 16 in section 4.1.2). The tissue was then stained for actin stress fibers and nuclei and imaged using fluorescent confocal microscope combined with bright field microscopy (Leica) in collaboration with Dr. Carmen Remde (Theory and Bio-systems department) (Fig. 17 in section 4.1.2).

Actin and nuclei staining was performed as follows: tissue samples were first washed to remove media and fixed in 4% paraformaldehyde for 5 to 10 minutes followed by another wash with phosphate buffer saline (PBS), then permeabilised with 1% Triton X-100 (Sigma Aldrich) in PBS and left in the refrigerator for 15 minutes if only a cell layer and overnight if a whole tissue sample was stained; samples were then washed thoroughly with PBS. If actin staining was required, samples were incubated in a dark place with Alexa Fluor 488 phalloidin (Invitrogen) with a 1:20 dilution, 45 minutes for cell layers and for 90 minutes for scaffolds and then washed with PBS. If nuclei staining was required, samples were incubated in a dark place with TO-PRO-3 692-661 (Invitrogen) with a 1:300 dilution in PBS for 5 minutes and washed thoroughly with PBS (Bidan, Kommareddy et al. 2013).

3.3.3 Simulating and calculating magnetic forces on beads

An estimation of the magnitude of the magnetic field produced by the magnet in the experimental set-up along its axis of symmetry z (Fig 10a is a sketch of the cubic magnet and the definition of the z-axis) was performed using the equation for magnetic field, B_Z, of a cubical bar magnet along its axis of symmetry, z:

$$B_z = \frac{B_r}{\pi}\left[\arctan\left(\frac{a^2}{2z\sqrt{4z^2+2a^2}}\right) - \arctan\left(\frac{a^2}{2(a+z)\sqrt{4(a+z)^2+2a^2}}\right)\right]$$, (Camacho and Sosa 2013)

where a denotes the magnetic cube's side length and B_r is the remanence magnetization of N52 neodymium magnet, B_r = 1.43T. This analytical calculation describes the magnetic field around the center line of the tissue culture scaffold along the bar magnet's axis of symmetry (Fig. 10a).

However, a spatial map of forces on magnetic beads in all areas of the tissue culture scaffold is required. Therefore a Comsol simulation of the magnetic flux density emerging from the magnet in a three dimensional box was performed followed by a Matlab calculation of the forces applied on MBs in the scaffold's area.

In performing the Comsol simulation, a current-free space is assumed. Therefore, a scalar magnetic potential V_m can be defined, $\vec{H} = -\nabla V_m$, were $\vec{H}$ is the H-magnetic field. With $\vec{B} = \mu_0(\vec{H} + \vec{M})$, where μ_0 is the vacuum permeability and $\vec{M}$ the magnet's

magnetization, and since $\vec{B}$ is a solenoidal vector field, i.e., $\nabla * \vec{B} = 0$, the scalar potential can be calculated by solving the equation $-\nabla * (\nabla V_m - \vec{M}) = 0$ (Comsol protocols).

Magnetic flux density from a 2 cm^3 N52 Neodymium magnet was simulated using the magnetostatic module with no currents from Comsol Multyphysics 3.5a. First, a magnet cube with the dimensions 2x2x2 cm was drawn and assigned with residual magnetization of 1.43T corresponding to the properties of an N52 Neodymium magnet (Fig. 10b). To have as little influence as possible on the calculated magnetic field from boundary conditions a large airbox was drawn around the magnet cube with the dimensions of 10x10x10 cm. The magnetic field was tangential to the airbox boundaries and the magnetic insulation boundary condition was assigned: $\hat{n} * \vec{B} = 0$. The simulation mesh was chosen to be fine free tetrahedral. The resulting 3D magnetic field vector data was exported for further calculations.

Magnetic forces acting on superparamagnetic beads in the presence of the obtained magnetic field were calculated using Matlab (Fig. 10c red stars). Due to their small volume resulting in a low energy barrier that is highly sensitive to external perturbations such as thermal fluctuations or external magnetic fields, superparamagnetic beads align their magnetization direction entirely in the direction of the magnetic field. The force on superparamagnetic beads with magnetic moment $\vec{\mathrm{m}}$ is given by $\vec{\mathrm{F}} = (\vec{\mathrm{m}} * \nabla)\vec{\mathrm{B}}$. Neglecting the interaction forces between the beads and taking into account the beads' dimensions and susceptibility, the force is then

$$\vec{\mathrm{F}} = \frac{\mathrm{V}\chi}{\mu_0}(\vec{\mathrm{B}} * \nabla)\vec{\mathrm{B}} = \frac{\mathrm{V}\chi}{\mu_0}\begin{bmatrix} B_x\frac{\partial B_x}{\partial x} + B_y\frac{\partial B_x}{\partial y} + B_z\frac{\partial B_x}{\partial z} \\ B_x\frac{\partial B_y}{\partial x} + B_y\frac{\partial B_y}{\partial y} + B_z\frac{\partial B_y}{\partial z} \\ B_x\frac{\partial B_z}{\partial x} + B_y\frac{\partial B_z}{\partial y} + B_z\frac{\partial B_z}{\partial z} \end{bmatrix}$$

where V is the volume of the bead and χ is its magnetic susceptibility (Dobson, Cartmell et al. 2006)(Shevkoplyas, Siegel et al. 2007).

The result of the simulation using Comsol followed by the calculation using Matlab was compared to the analytical calculation along the magnet's axes of symmetry suggested by Camacho and Sosa in 2013 (Camacho and Sosa 2013). Calculation and analytical solution are not identical, but the order of magnitude and trend of force change versus distance from

magnet along the axes of symmetry were approved (Fig. 10c).

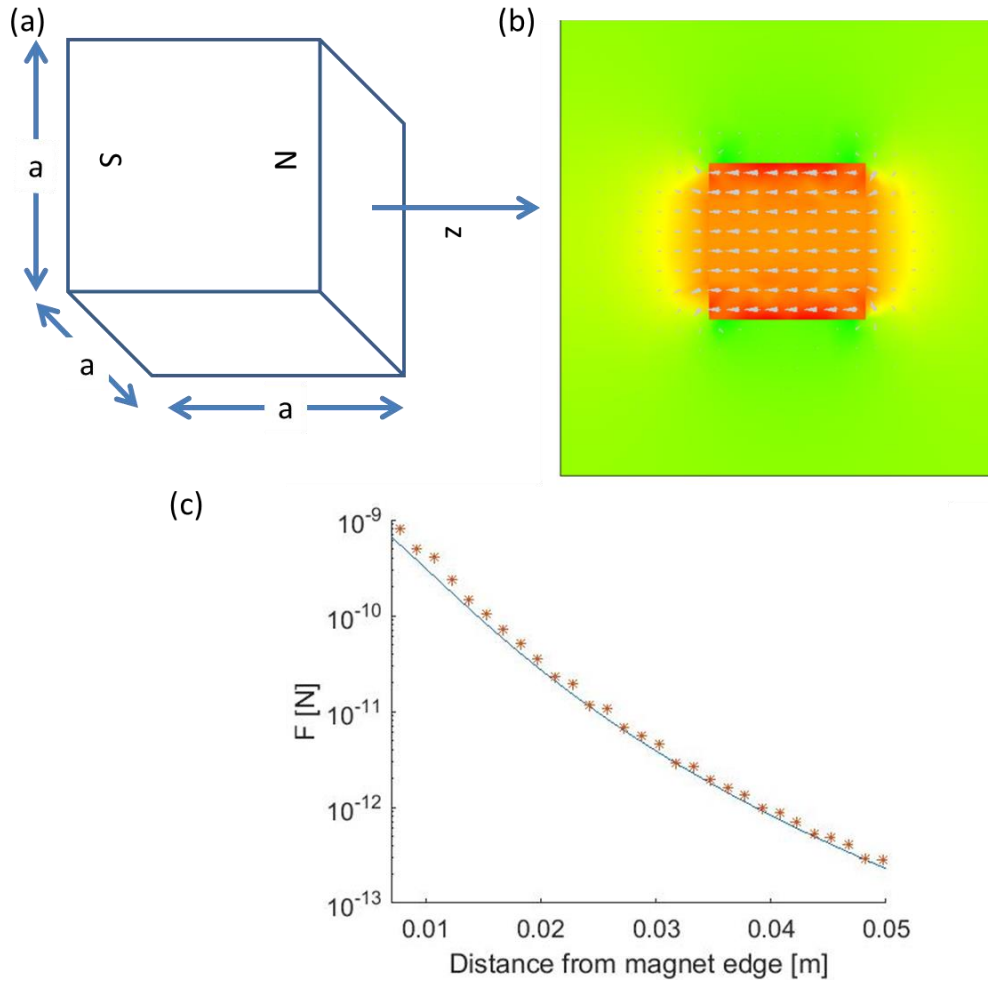

10. Calculation of magnetic forces exerted by the magnet on the magnetic beads in the experimental setup: (a) Sketch of the cubic Neodymium magnet (b) A Comsol plot of a slice of the magnetic field from a 2 cm^3 N52 Neodymium magnet (c) Comparison of the resulting magnetic forces acting on superparamagnetic beads in the presence of the calculated magnetic field using Comsol and Matlab (red stars) with the analytical solution along the magnet's axes of symmetry using the equation by Camacho and Sosa (Camacho and Sosa 2013) (blue line).

3.3.4 Tracking magnetic beads' movement in tissue due to magnetic force

To understand where inside tissues the magnetic beads are located and how they respond to the pulse force applied to them in the magnet actuator setup, a rough estimation of the velocity and displacement of the beads inside viscous fluid due to the force applied was performed and compared to experimental observation of MBs movements when forces were applied in MC3T3-E1 tissues.

3.3.4.1 Theoretical calculation

The velocity of MBs in viscous fluid due to the applied forces was calculated using Stoke's law. The frictional force (Stoke's drag) is given by $\mathrm{F_{drag}} = 6\pi\mu\mathrm{Rv}$, where μ is the viscosity, R is the radius of the beads and v is their velocity. The frictional force $\mathrm{F_{drag}}$ is the response to a magnetic force F_{mag} acting on the beads. Using Newton's second law this results in an ordinary differential equation $\frac{\mathrm{dv}}{\mathrm{dt}} = \frac{1}{\mathrm{m}}\left(\mathrm{F_{mag}} - \mathrm{F_{drag}}\right) = \frac{1}{\mathrm{m}}\left(\mathrm{F_{mag}} - 6\pi\mu\mathrm{Rv}\right)$. The solution of this equation, under the initial condition $\mathrm{v_{t=0}} = 0$, is $\mathrm{v} = \frac{\mathrm{F_{mag}}}{6\pi\mu\mathrm{R}}\left(1 - \mathrm{e}^{-\frac{6\pi\mu\mathrm{R}}{\mathrm{m}}\mathrm{t}}\right)$, where m is the mass of the MBs. Because of the particles' small mass, the velocity quickly reaches a steady-state value and was, therefore, considered as constant (Stokes 1851, Fonnum, Johansson et al. 2005).

Previous studies estimated soft tissue's viscosity to be on the order of magnitude of 0.5Pa*s (Girnyk, Barannik et al. 2006) and cells' viscosity to be around 10^3 Pa*s (Lim, Zhou et al. 2006). The displacement of the MBs in fluids with viscosity of 0.5 Pa*s and $5*10^3$ Pa*s were calculated numerically using the results from the previous section about magnetic forces acting on the MBs.

3.3.4.2 Experimental observation

To test the calculated displacement of MBs by observing actual movement of the beads due to the magnetic forces applied, MC3T3-E1 cells were seeded inside a rectangular Nonclun

well plate (Thermo Fisher Scientific, Waltham, MA) with recycled triangular HA scaffolds (section 3.1.2.2) and incubated together with MBs . Cells were allowed to proliferate and form tissues inside the pores of the scaffold. The well plate was covered with a custom-made glass slide (made by the MPICI glass workshop) that allowed the insertion of a magnet to the adjacent well while the well plate was inside an on-stage incubator (Okolab, NA, Italy).

The tissue in the pores was imaged using time lapse microscopy at an imaging rate of one image every 5 minutes. Our experimental protocol started with an imaging of the tissue for 1 hour without magnetic forces. Then a 2 cm^3 N52 magnet was inserted into the well adjacent to the well with the scaffold exerting a magnetic force on the order of 0.5nN and the time-lapse measurement continued for another 18 hours.

Video analysis using a Matlab code tracked the trajectories of the beads within the tissue (Fig. 19e). The code first finds all dark circles in each frame with a diameter of ~5µm, then connects beads' locations to form trajectories using a code written by Dr. Peter Vach (Biomaterials department); the code connects beads' entries between adjacent frames by finding minimum distances between beads' location in adjacent frames that are smaller than a defined maximum distance (Lefèvre, Bennet et al. 2014). Maximum distance was chosen to be 5µm per 5 minutes, yielding a maximum possible velocity of 60µm/hour which is ~50% more than the maximal velocity found for cells at the front line in collective cell migration (~40µm/hour) (Vedula, Leong et al. 2012). Trajectories were plotted on top of first frame of the video for further evaluation if they described bead motion for a time longer than 5 frames (25 minutes) and if the mean velocity was greater than 10µm/hour (to dismiss noise effects in the beads' trajectories).

3.4 Methods used for mechanical stimulation of *in-vitro tissue* growth experiments

3.4.1 Imaging and analyzing the amount of tissue formed

After 24 days in culture, tissues in scaffolds were imaged using bright field inverted microscopy (Nikon Eclipse TS100, Japan). To assess tissue volume, the microscope's focal

plane was first adjusted to display the area within the pore where the tissue is thickest and thus its cross-sectional area is largest. This area is referred to as the maximum projected tissue area (PTA) within the pore (black arrows in Fig. 4e) (Bidan, Kommareddy et al. 2012). This procedure was repeated for all the 80 pores in the scaffolds while also recording the position of the pore in the pore array within the scaffold.

A binary mask was created to measure the tissue area by using a polygon drawn around the tissue-medium interface, finding the area inside the polygon, and subtracting it from the pore's area (Bidan, Kommareddy et al. 2012) (Fig. 11a-b). The polygon was drawn manually using a Matlab interface to render as close as possible the shape of the tissue-medium interface imaged. Tissue area values were than organized in a form of a matrix corresponding to the right location of tissues in the array within the scaffold. In case where a pore was blocked and tissue could not be found, blocked pore in tissues array was approximated with the average value of tissue areas in the same row of the blocked pore.

To evaluate the relative change in tissue growth in proportion to the relative change in the magnitude of force, a power law fit was performed. Linear regression analysis of the logarithm of the PTA as a function of the logarithm of the magnitude of force applied on MBs was determined using Matlab (Fig. 11c). The logarithm was taken to fit the power law to the data and to correct the skewed distribution of the magnitude of force, since linear regression analysis required its variables to be normally distributed. A quantity obtained from the fit is the exponent of the power law fit of PTA as a function of force (Fig. 11c).

The position of the pore in the scaffold does not only result in a different magnetic force, but also in possible variations of cell concentration, nutrient supply, and CO_2 level. To take into account these hard to control effects, control cell cultures were used to establish a baseline (details about the controls used are in section 4.3). 5 control scaffolds were considered to set the baseline. One control scaffold, which was not taken into account when calculating the baseline, was placed in a reversed order inside the well plate, in a way that pores were farther away from the edge on the well plate. This "reversed control" experiment was performed to further examine how the geometry of the experimental setup itself effects tissue growth.

The baseline was defined by, first, by performing a linear regression analysis of the logarithm of the PTA as a function of the logarithm of the magnitude of force, if forces were applied, for each control scaffold. Then the mean values of the slopes and the intercepts were calculated, resulting in a baseline given by

$\log(PTA_{control}) = \overline{intercepts} + \overline{slopes} * \log(F_{correspondent})$

where $F_{correspondent}$ is the force in the non-control case corresponding to the row number on the scaffold.

A regression analysis of $\log(\frac{PTA}{PTA_{control}})$ as a function of $\log(F)$ is then performed for all scaffolds where forces were applied (example in Fig. 11d). The standard error of regression (S) reported is the average distance of $\log\left(\frac{PTA}{PTA_{control}}\right)$ values from the regression lines. This yields exponents y of a power law fit: $\frac{PTA}{PTA_{control}} = k * F^{y}$. P-values of the y exponents were calculated for each scaffold relative to the control base line.

Another way to evaluate trends in tissue growth as a function of the magnitude of force was to take the Spearman's correlation of PTA [µm] with force [N] (using Matlab R2016a). Here correlation coefficients and p-values were calculated relative to no change of PTA as a function of force (and not relative to control).

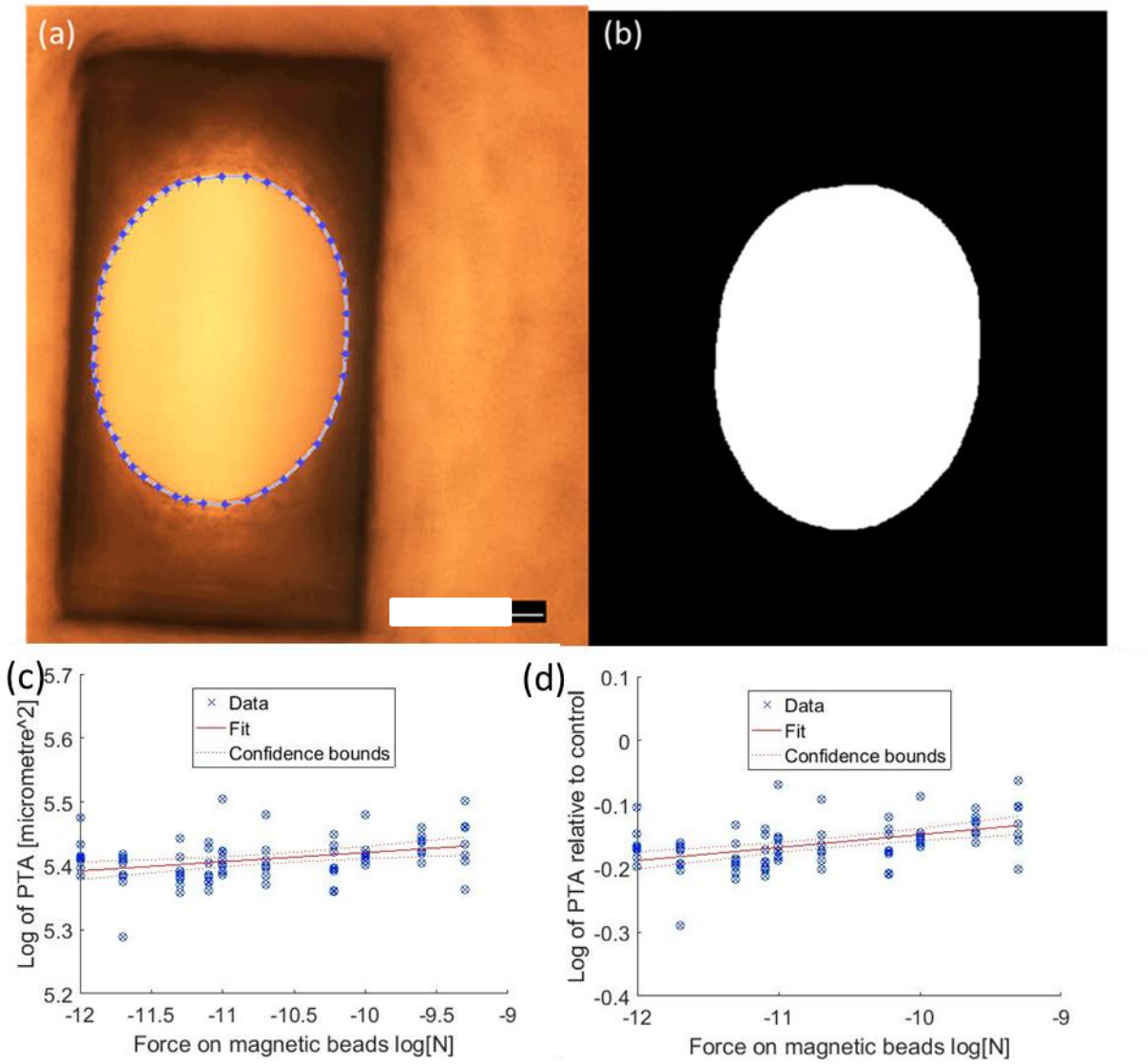

11. Measurement and analysis of the maximum projected tissue area (PTA), the area within the pore where the tissue is thickest and thus its cross-sectional area is largest, as a function of the magnetic force acting on MBs within the tissue: a) Phase contrast image of the PTA (dark area) of tissue grown by MC3T3-E1 cells in a rectangular pore in a PDMS scaffold containing an array of such pores. Area boundaries marked manually (blue dots) are connected to yield a polygon and (b) resulting in a binary mask. The white scale bar denotes 250 nm. (c) Example of the evaluation of data acquired from one scaffold consisting of 80 tissues with magnetic beads and subjected to magnetic forces. Tissues' PTA (blue circles) were plotted as a function of the maximum magnetic force applied to them. Linear regression analysis was performed on a double-logarithmic plot of PTA vs. force (red line)

and the p-value was determined relative to the null hypothesis of a constant PTA independent of the applied force. (d) Example of a data evaluation after correction taking into account control experiments (as described in the text). The straight line in red denotes a linear regression of the data.

3.4.2 Measurement and evaluation of Alkaline phosphatase (ALP) expression

Alkaline phosphatase is a known indicator of cell differentiation towards osteogenic lineage (Quarles, Yohay et al. 1992, Fratzl-Zelman, Hörandner et al. 1997). To get insight on the cell state as a function of the applied type and magnitude of force, 2 fixed scaffolds from each force type were stained together for ALP expression after all the tissue culture experiments were over. Scaffolds were fixed with 4% Paraformaldehyde solution (Boster Biological Technology, Valley Ave, CA) in PBS, washed and stained for ALP expression using, 2.5mg Naphtolphosphate diluted with 1mL 0.9% NaCl solution with 750µL Borax 5%, 40µL $MgS0_4$ 10% and 10mg Fast Blue RR salt (Sigma-Aldrich, Steinheim, Germany) (Fratzl-Zelman, Hörandner et al. 1997, Rumpler, Woesz et al. 2007). Stained scaffold areas at 10 different distances from the magnet were imaged using phase contrast microscope (Nikon Eclipse TS100, Japan) (Fig. 12a). The imaged areas were of the cell layer between tissue pores in the center of each row in the scaffold (Fig 4e in section 2.2.2 is an illustration of a cross section of cell layer grown on top of scaffold and around tissue pores).

To examine how the blue stains indicating ALP expression vary as a function of the applied force, color brightness intensities in images of stained cells were plotted as a function of the logarithm of the magnitude of force (Fig. 12b). Red, green and blue conventional color intensities (RGB channels ranging between 0-255) of each image were normalized across all images by dividing the intensity value in each image by the sum of intensities in the same image, as was previously performed for analyzes of different colors in confocal microscopy (Bidan, Kollmannsberger et al. 2016). Normalized color intensities were then plotted as a function of the logarithm of force applied (Fig. 12c). Normalized ALP stain intensities were analyzed using Spearman's correlation with force [N], and by taking mean values and standard deviations (SDs) of the intensities for each scaffold.

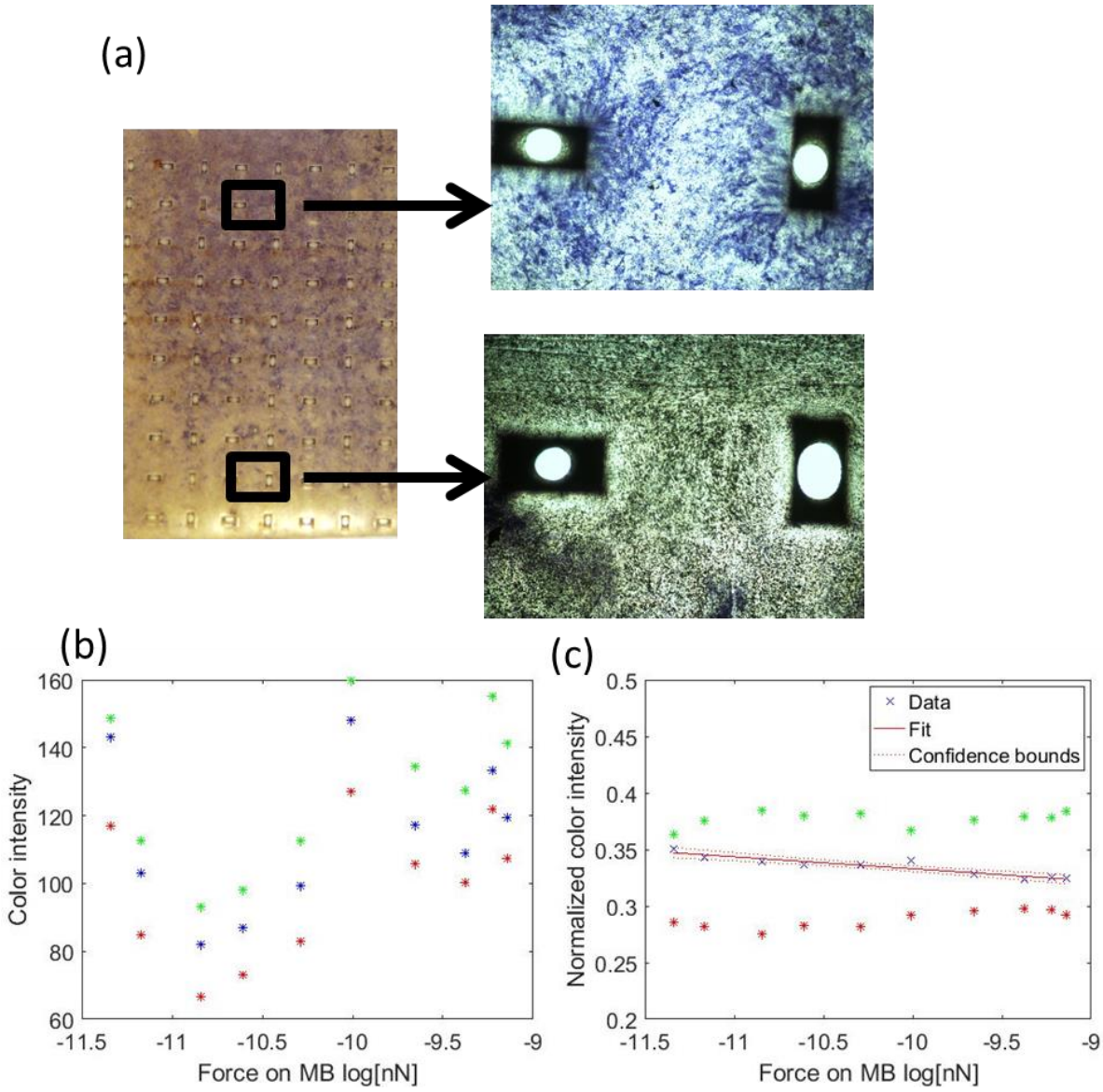

12. Alkaline phosphatase (ALP) expression as a function of the applied force on MBs and consequent analysis: (a) PDMS scaffold cultured with MC3T3-E1 cells and MBs for 24 days while oscillating magnetic fields were applied and stained for ALP (left side). Examples of 2 out of 10 phase contrast images of pores and cell layer in different rows of the scaffold (right side). A stained layer of tissue on top of PDMS scaffolds area can be seen around the pores with 3D tissues, which appear black (Fig 4e in section 2.2.2 is an illustration of a cross section of cell layer grown on top of scaffold and around tissue pores). Blue stain is visible in the upper image on the right side of (a) corresponding to tissue grown farther away from the oscillating magnet. (b) RGB brightness intensities of images at 10 different distances from the magnet corresponding to different forces. Color of data point represents the color of

which the average brightness intensity was calculated. (c) Normalized red, blue and green brightness intensities as a function of the applied force on the MB. Linear regression analysis was performed for the blue stain intensity level using Matlab (fit as a red straight line and confidence bounds as dotted lines).

3.4.3 Statistical analysis

Results were analyzed first on a scaffold-by-scaffold basis, whereby each scaffold (containing 80 pores) was treated as its own experiment, and statistically evaluated on its own. Subsequently, all experiments (scaffolds) were grouped according to the type of force applied to them (static, oscillating on epoxy beads or on RGD beads) and mean slopes and errors from regression analysis of all scaffolds in each group were taken.

Two-sample Z-test for comparing two means was used to compare mean values acquired for each type of force. First the Z score was calculated, $Z = \frac{\overline{x_1} - \overline{x_2}}{\sqrt{\frac{\sigma_1^2}{n_1} + \frac{\sigma_2^2}{n_2}}}$, where $\overline{x_1}$ and $\overline{x_2}$ are the values of the means compared, σ_1 and σ_2 are the mean SDs acquired from all the scaffolds in each type of force and n_1 and n_2 are the number of scaffolds studied for each type of force. Then, the p-value was acquired from the Z-score by calculating the cumulative distribution function at the value of Z.

Group p-values were determined using Fisher's method. Fisher's combined probability test combines p-values from several independent experiments relating to the same hypothesis. First, a two tailed test statistics $\boldsymbol{\chi}^2$, combining p-values from all related experiments is calculated, $\chi^2 = -2\sum_{i=1}^{k} \ln(p_i)$, where k is the number of experiments combined and p_i are the independent p-values. The distribution of $\boldsymbol{\chi}^2$ is the chi-squared distribution. Group p-value is then obtained by calculating the chi-square cumulative distribution of $\boldsymbol{\chi}$ with 2k degrees of freedom (Matlab code adapted from the Mathworks user Dmitry Smirnov https://stats.stackexchange.com/users/75214/dmitry-smirnov). Results were considered statistically significant for $p<0.05$. P values less than 0.05 were marked by one asterisk, less than 0.01 by two asterisks, and less than 0.0001 by three asterisks.

Tissue growth in rectangular pores in two different orientations relative to the force vector were compared by preforming linear regression analysis of PTA of each kind of pore orientation separately as a function of force, and using two-sample t-test (Matlab).

4 Results

4.1 Preparatory investigations

4.1.1 The attachment of the magnetic beads to cells

To assess whether magnetic beads (MBs) firmly attach to cells or the application of force in the magnetic setup would result in detachment of beads from cells, adhesion tests were performed as described in section 3.3.1. Epoxy beads, beads with RGD functionalization and beads with BSA functionalization were tested for adhesion to cells grown on a flat petri dish under magnetic forces ranging between aN and nN and after different incubation times (30m, 120m, 240m, and 24h are presented here, other incubation times showed similar trends and are not presented in this thesis) (Fig. 13f). While after 30 minutes or 120 minutes of incubation time many beads got detached from the cells and migrated toward the magnet upon magnetic force application (Fig. 13a-b), in most cases 24 hours of incubation were sufficient so that even the strongest forces tested on the samples – on the order of magnitude of nN – produced no detectable macroscopic movement of MBs under force application (Fig. 13c-d). The beads were therefore assessed to be strongly anchored in or on the cells 24 hours after the beads' introduction to the tissue. Hence in all subsequent tissue culture experiments, cells were incubated with MBs for 24 hours before application of forces on tissues thereby ensuring that beads pull on the tissue rather than detach from it.

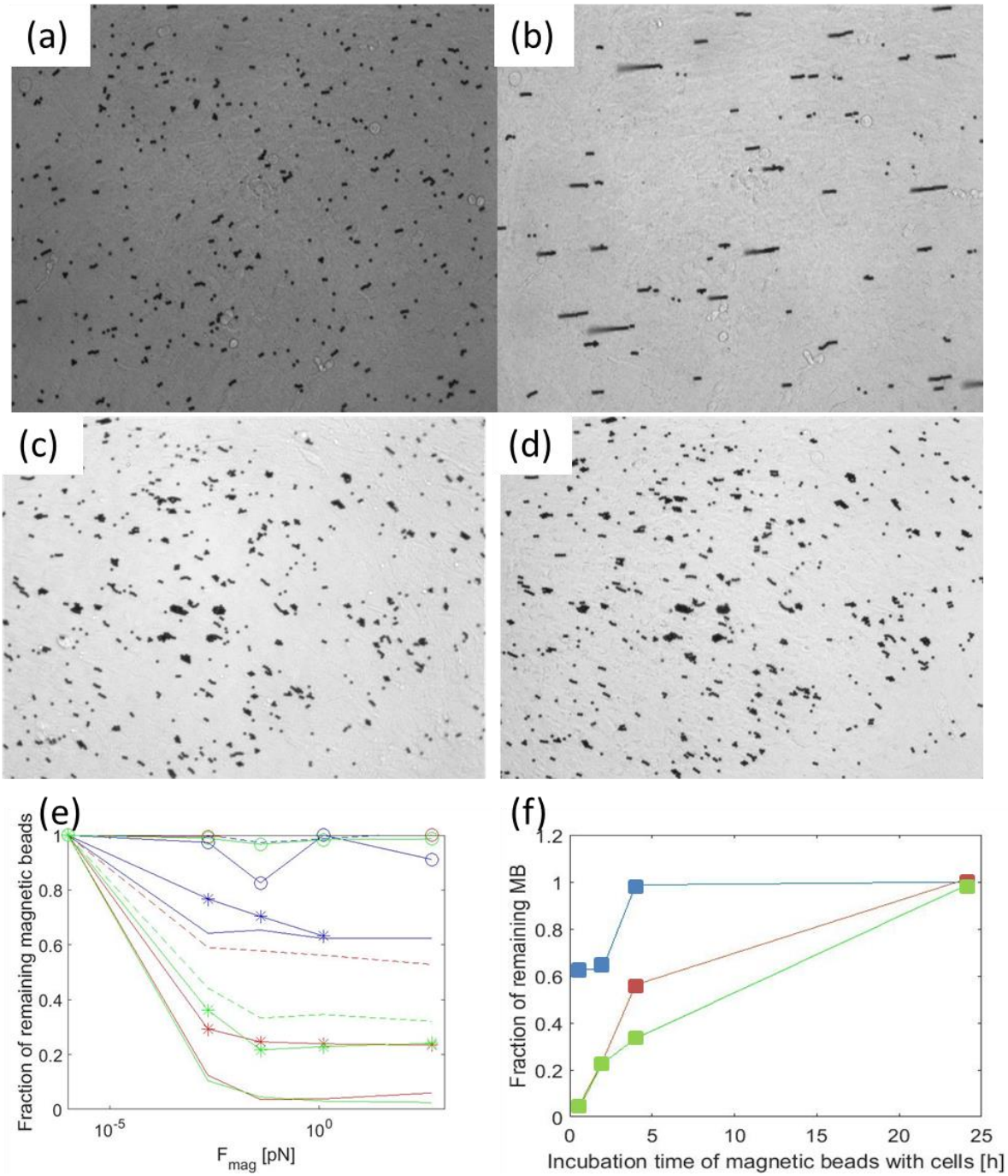

13. Magnetic bead (MBs) attachment to cells upon force application: Each image, a-d, is a bright field image (Nikon Eclipse TS100) of magnetic beads (darker spots) incubated with MC3T3-E1 cell monolayer (lighter area). (a) MBs functionalized with RGD peptides and incubated with cells for 30 minutes. (b) Beads detached from cells when magnetic force was applied. Chains of beads formed while MBs got detached from cells and pulled towards the magnet can be seen in the image. Only one end of the chain of MBs is still anchored to cells while the rest of the beads of each chain are connected to each other, floating in the media, and therefore out of focus. (c) Bright field image of RGD functionalized MB seeded on cell

monolayer 24 hour before image was taken. Image (d) was taken 5 minutes after an approximately nN force was applied to the cell layer. The force application did not result in a detectable movement of the MBs. (e) Fraction of magnetic beads attached to the cell layer upon force application. Magnetic beads functionalized with BSA (red), epoxy groups (blue) and RGD (green) were incubated with a cell monolayer for 30 minutes (-) 120 minutes (*) 240 minutes (--) and 24 hours (o) and pulled using magnetic forces in the aN-nN range. (f) Longer incubation times resulted in better adhesion of beads to cells. Fraction of remaining magnetic beads after a force in the pN order of magnitude was applied vs. incubation time of magnetic beads with cell monolayer (color code like in (e)).

4.1.2 Magnetic beads incorporation in cells and in growing tissues

To localize the MBs within the tissue culture and, consequently, to better understand how they pull on cells upon magnetic force application, MBs location relative to single cells was examined after 24 hours of incubation using a phase contrast microscope (section 3.3.2). Most beads were seen within cell membrane boundaries (about 70%), and around the nucleus of the cells (Fig. 14).

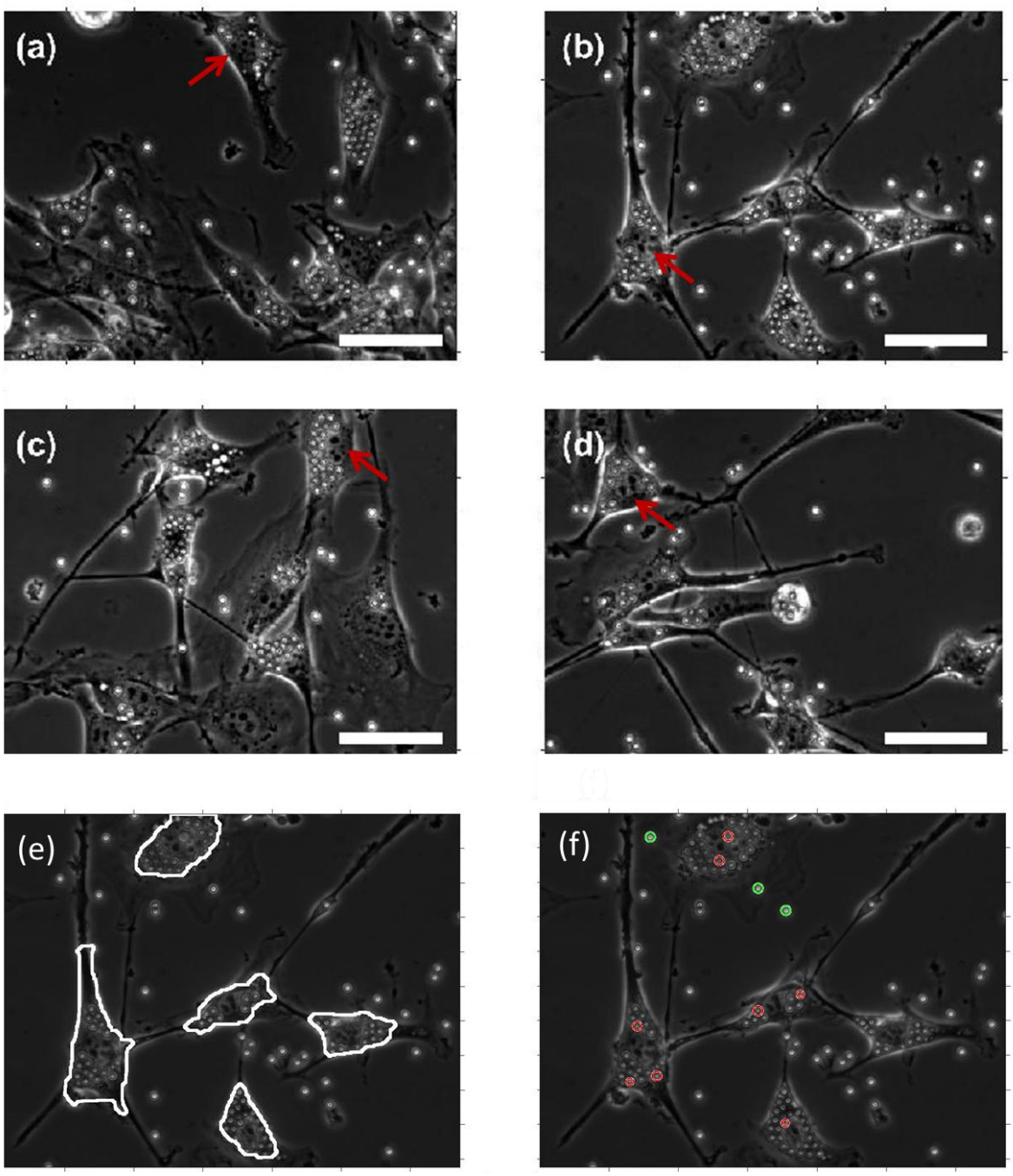

14. Phase contrast images of MC3T3-E1 cells incubated with magnetic beads for 24 hours: (a)-(d) MBs (round and white) are confined by cells' membrane and clustered around cells' nuclei (some of the nuclei highlighted by red arrows). Scale bar in all images is 50 µm. (e) Cells in image b were segmented and outlined using Matlab. (f) Beads were located outside the cells (some examples circled in green) and preferentially inside cells (examples circled in red) using Matlab object recognition. The ratio of incorporated beads to overall beads was approximated to be ~70%.

The incorporation of MBs inside cells was additionally studied using confocal microscopy (section 3.3.2). Again cells were incubated with MBs for 24 hours. Beads (round and black) can be observed using inverted confocal microscopy above the cell cytoskeleton (Fig. 15a), in the same focal plane as the cell cytoskeleton (Fig. 15b-c), and as the beads are opaque to the focused laser beam of the confocal microscope, their shadow becomes apparent when imaging the cytoskeleton above them (Fig. 15d). These observations with different microscopy techniques lead to the conclusion that the majority of MBs in long-term (i.e., >24h) studies have been taken up by the cells, and thus magnetic forces exerted at them pull the tissue from within the cells.

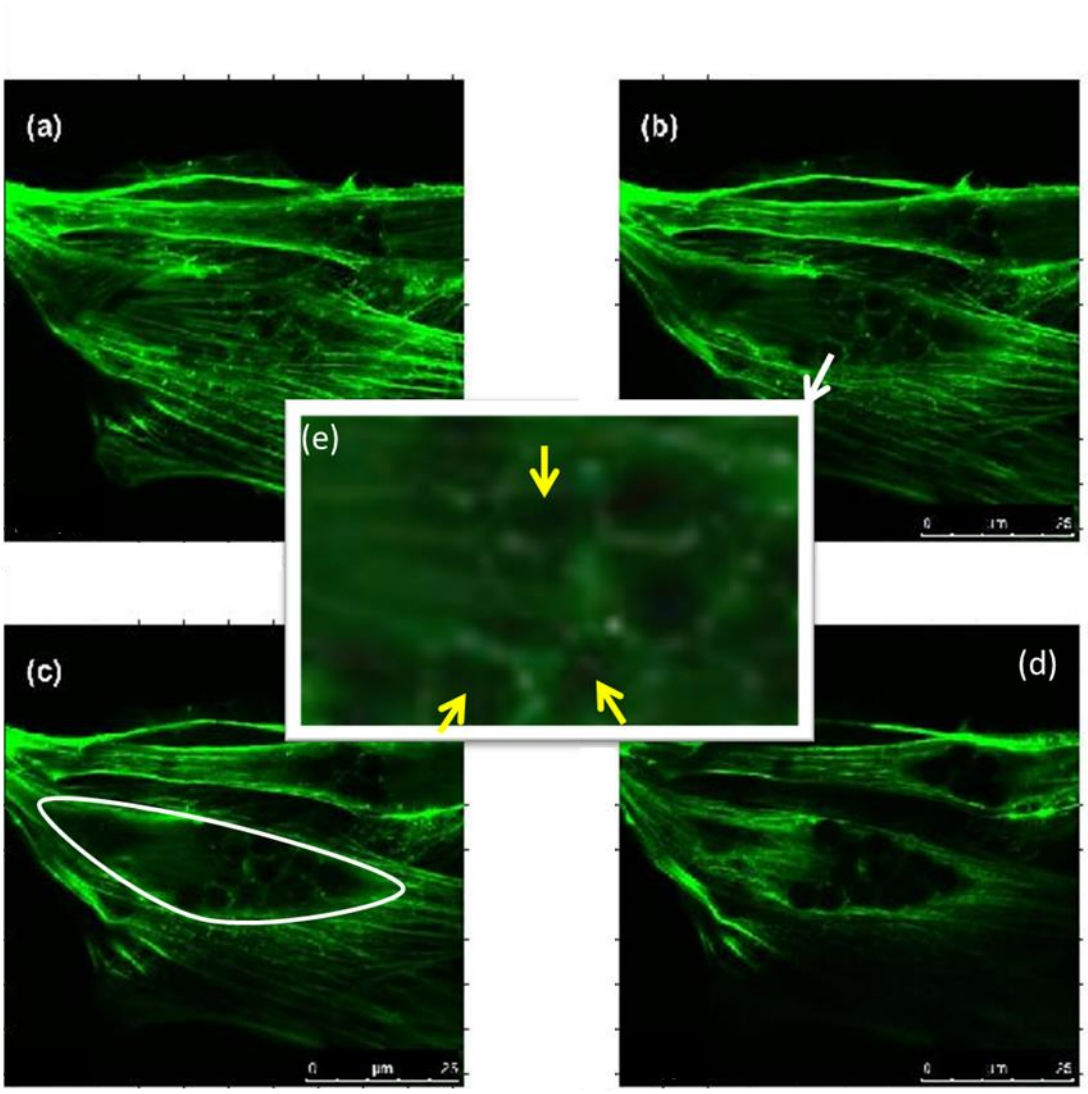

15. Fluorescent confocal images of MC3T3-E1 cells incubated with magnetic beads for 24 hours. Cell cytoskeleton's actin fiber bundles are green and MBs are round and black. Actin

fibers can be observed below MBs (a), in the same focal plane as MBs (b & c) and above MBs where the shadow of MBs can still be observed (d). White scale bars are 25µm. A contour of one cell (out of two visible in the frame) is marked in white in (c). In (b) and (c) some of the beads are surrounded by a thin fluorescent green layer. A zoom into the area of (b) marked by a white arrow is shown in (e); some of the MBs visible inside the cell (with actin fibers below and above them) are marked by yellow arrows.

The incorporation of MBs was also studied in the experimental setting of tissue growth in pores. The tissue grown for 24 days with MBs was imaged with bright field microscopy measurement (Nikon Eclipse TS100, Japan) by stepping through the tissue incrementally using a focal drive. Beads were observed in different focal planes within the tissue. They can be mainly seen in younger and more transparent parts of tissue. MBs aggregations in tissues tend to align in the direction of the longest axis of stretched cells that form the tissue, i.e. parallel to the medium-tissue interface (Fig. 16).

In observing the incorporation of MBs in tissues studied using confocal microscopy combined with bright field microscopy (Fig. 17) MBs were again more apparent in younger, more transparent parts of tissue. Cells' nuclei can be seen throughout the tissue, in younger and older parts of tissue.

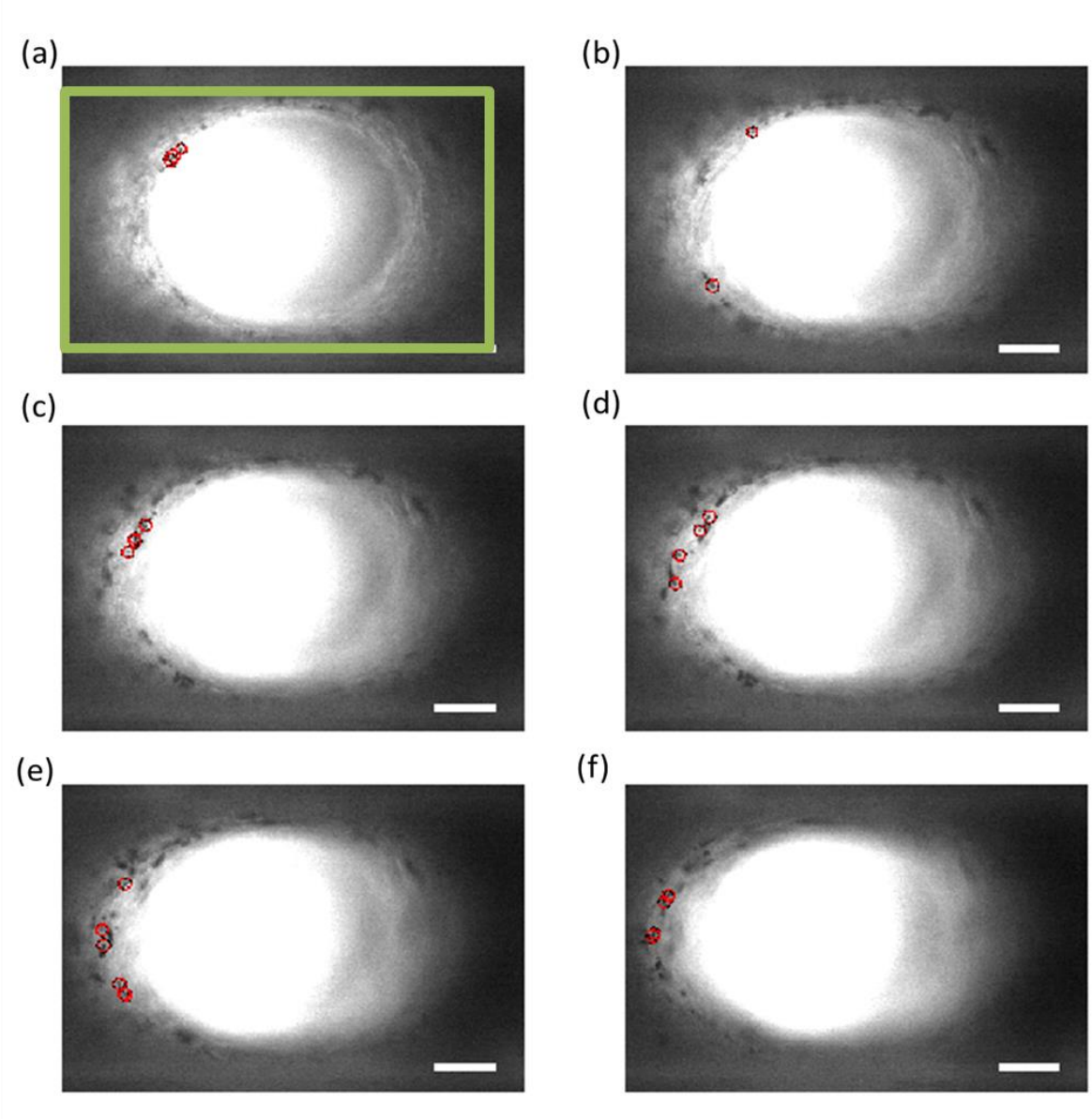

16. Incorporation of magnetic beads in different focal planes of 3D tissue: Stack bright field microscopy measurement of 24 days old MC3T3-E1 with RGD functionalized MBs. (a) shows an image of the tissue in the focal plane where tissue area is maximal. The green frame marks the tissue–scaffold interface. Each of the following pictures (b-f) shows an image taken with a slightly altered focal plane, where tissue is thinner than in (a). MBs (black and round) can be seen in different focal planes of the tissue. Some examples of MBs in each image are circled in red. MBs, incorporated inside cells, may aggregate and reflect the elongated shape of cells within tissue with an alignment in the direction parallel to the medium-tissue interface. Scale bars are 100µm. A sketch to clarify the three dimensional shape of the tissue can be found in Fig. 4e.

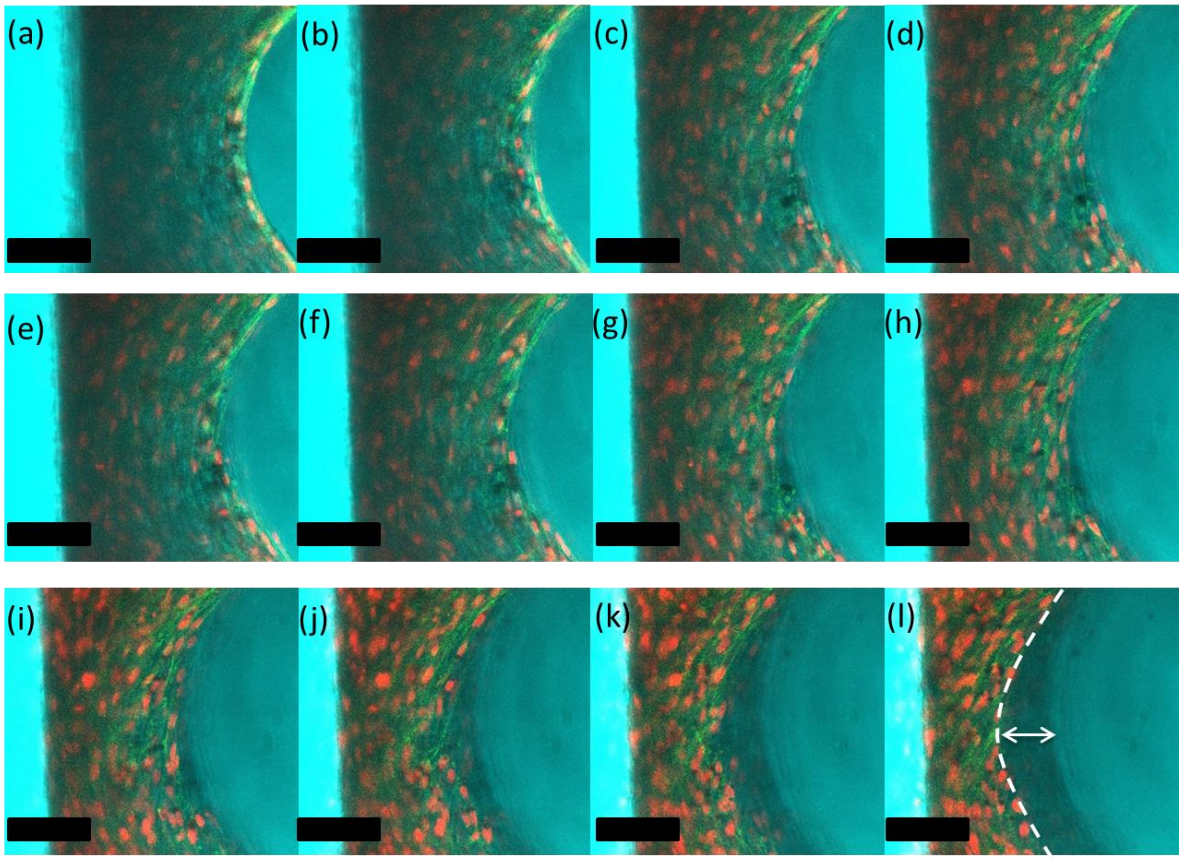

17. Confocal microscope images of tissue grown in pores with magnetic beads: (a)-(l) Combined fluorescent confocal microscope and bright field images at different focal planes within a 24 day old MC3T3-E1 tissue grown in a PDMS scaffold. MBs (black spots) are found around actin filaments (green) and next to nuclei (red). The tissue – medium interface is marked by a white dashed line in (l). The white arrow indicates the shadow of tissue out of focal plane visible in darker blue. Scale bars are 75µm.

4.1.3 Force variation in different locations in tissue growth scaffold

To have an approximation of how force varies between tissues in the array of tissues in the scaffold, also termed "the measurement area", magnetic forces exerted by the magnet on single MBs were simulated and calculated in scaffold's area as described in section 3.3.3.

When calculating the force applied to MBs in each row of the scaffold (see Fig. 8a for scaffold position relative to magnet and an example of the term “row in tissues array”) as a function of distance from the magnet, the values of the force in the middle of the row are taken into account. However, magnetic force varies within each row as well. A calculation of the force in different area points on the scaffolds was required. To create a map of forces on the scaffold used in this study, first magnetic flux density exerted by the N52 cube magnet was simulated using Comsol. Then magnetic force applied by the magnetic flux density gradient on superparamagnetic beads was calculated (section 3.3.3) (Dobson, Cartmell et al. 2006)(Shevkoplyas, Siegel et al. 2007). Magnetic force calculations are presented in Fig. 18 and show a decrease in force as a function of distance from the center of the row in the scaffold’s area (Fig. 18b). However, in each row within the scaffold’s area there is an entirely distinct force range (Fig. 18c).

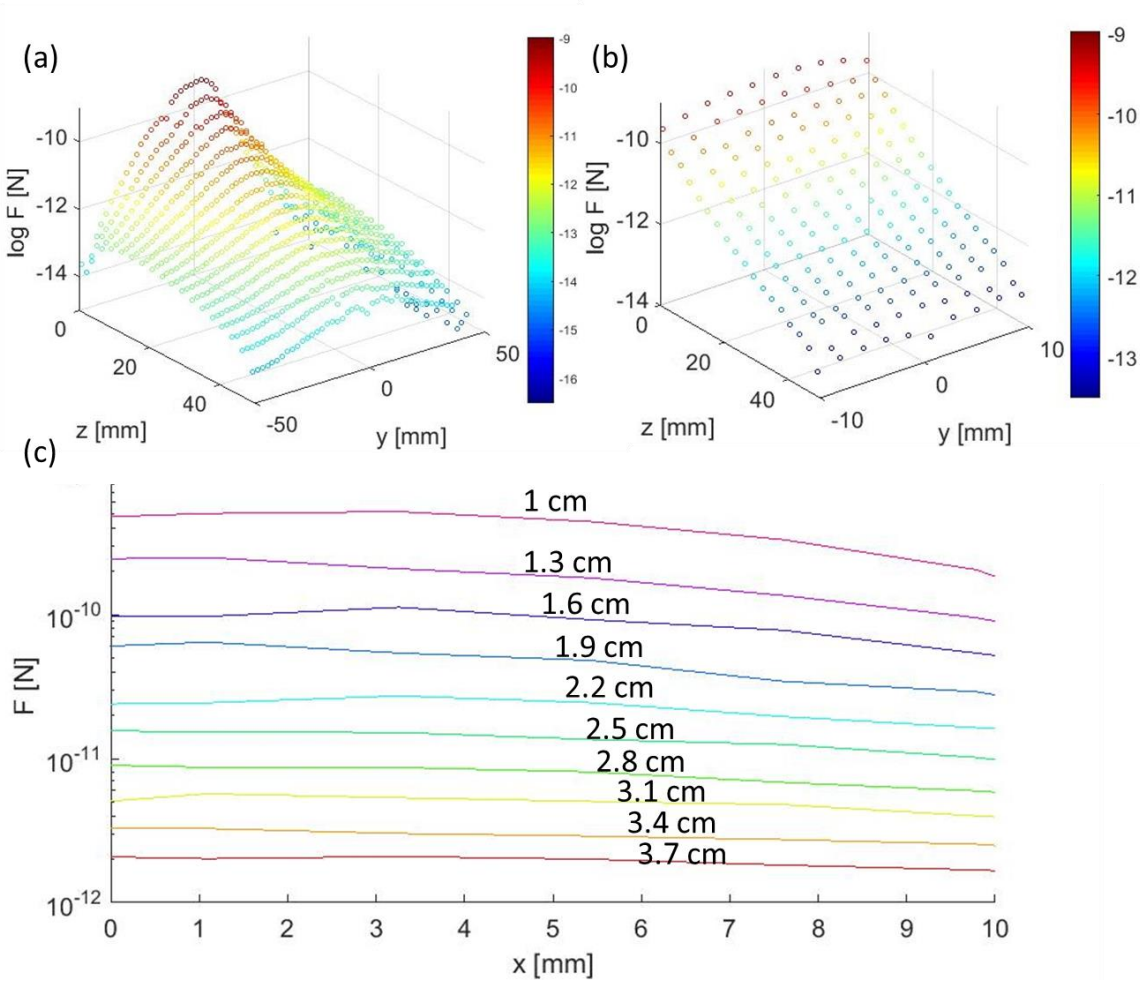

18. Magnetic force variation in the "measurement area", where forces in the direction parallel to the edge of the magnet are relatively homogenous and where the tissue culture scaffold is placed: a) in a 50x50 mm box around the scaffold. b) in the area of the scaffold only. (c) Magnetic force in each row of the scaffolds as a function of location in row. The middle of the right edge of the magnet is at [0,0]. Distances from the magnet, marked on top of each lines are locations along the z-axis.

4.1.4 Magnetic beads movement within tissue due to force

To examine whether tissues studied can be seen as viscous fluid with regards to MBs movement within them when magnetic forces are applied, velocities of magnetic beads in tissue when forces were applied, were evaluated using time lapse microscopy videos. These velocities were compared with a calculation of movement of these beads in viscous fluid. In calculating magnetic beads' displacement due to oscillating force in magnetic setup (Fig.

19a), bead movement of about 9µm after an hour of applied force, visible using a light microscope was calculated when viscosity was taken to be in the order of magnitude of cells' viscosity, $5*10^3$ Pa*s (Lim, Zhou et al. 2006)(Fig. 19b) and 90mm per hour when viscosity known for soft tissues, 0.5 Pa*s (Girnyk, Barannik et al. 2006), was taken into account.

To assess thermal fluctuations, Einstein's relation for stochastic Brownian motion of spherical particles in viscous fluid was calculated: $\overline{x^2}(\Delta t) = \frac{k_B T}{3\pi\mu R}\Delta t$ (Einstein 1905), where $\overline{x^2}$ denotes the particle's mean square displacement, k_B is the Boltzmann constant; the temperature T was set to room temperature, and R is the radius of the MBs. The calculation resulted in an average absolute velocity of ~10 nm per hour at room temperature, when viscosity was taken to be $\mu=5*10^3$ Pa*s and ~100µm per hour when tissue viscosity was taken to be µ=0.5 Pa*s . In both cases, calculated velocities were about 3 orders of magnitude smaller than the experimentally measured velocities due to applied force. Therefore thermal fluctuations were neglected.

In testing whether MBs will move through tissue as calculated, triangular tissue grown with MBs on a hydroxyapatite scaffold was time lapse imaged while exerting magnetic forces on it as described in section 3.3.4. Imaged beads were mostly observed moving in the filaments' direction as was previously demonstrated for cells' movement within tissue (Ma, Wang et al. 2015, Ehrig 2017) instead of to the magnet's direction.

Video analysis of this time lapse measurement showed that while most trajectories were in a direction parallel to the tissue-medium interface, some trajectories of very slow movement of few micro-meters over the 18 hours measured, especially in inner, older parts of tissue were in the direction of the magnetic field (Fig. 19e).

Other time-lapse measurements of tissues with MBs were performed as well to probe mechanical properties of these tissues. However, since MBs were incorporated inside cells and therefore moved with cells instead of to the magnetic field's direction, these experiments are described in the inconclusive experiments chapter in section 5.1.

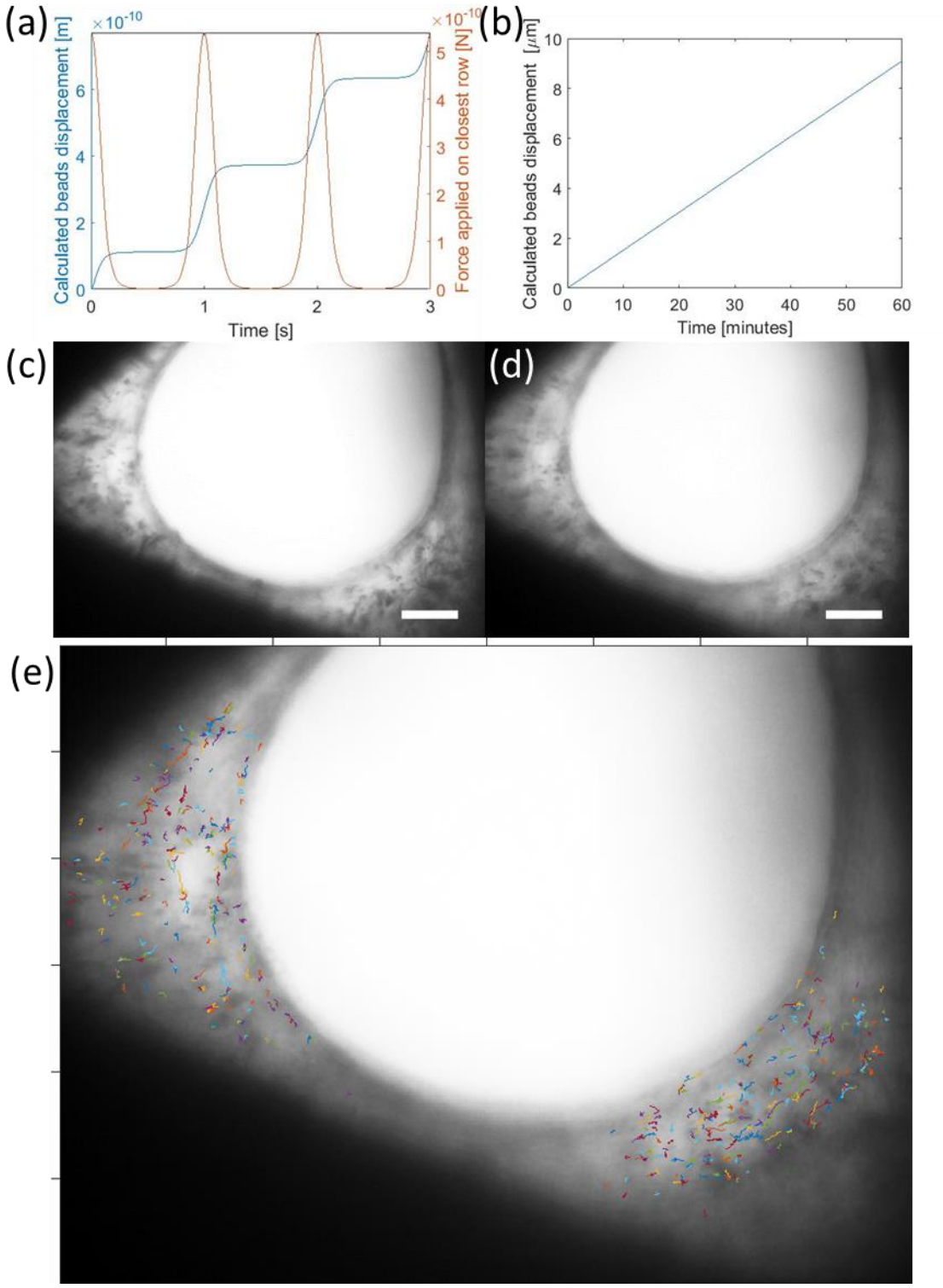

19. Movement of magnetic beads in tissue subjected to magnetic gradient. a-b) Calculation of beads' movement in fluid with viscosity of $5*10^3$ Pa*s, and forces applied to tissue by the magnet actuator setup. c) Time lapse microscopy was used to observe MBs movement in tissue subjected to magnetic forces from a 2 cm^3 N52 Neodymium magnet. MC3T3-E1 tissue (gray area) grown with MB (black dots) in a triangular pore in an hydroxyapatite (HA)

scaffold (black area) was images every 5 minutes for 18 hours while a magnetic force was applied to it to the right direction. c) Time lapse microscopy photo taken immediately after magnet was applied. d) Time lapse microscopy photo taken 18 hours after magnet was applied. Scale bar (white) is 50 µm. (e) Particle tracking analysis of beads' motion within the tissue. Trajectories that lasted more than 25 minutes and had a velocity greater than $10\frac{\mu m}{h}$ were plotted on top of the first frame of the video.

4.2 No influence of pore orientation on tissue growth

The influence of pore orientation relative to the magnetic force direction, on tissue growth in the scaffolds was investigated. To do so, the scaffolds were designed such that the long face of half of the rectangular pores in each row align with the direction of the magnetic force (parallel pores) and half in the perpendicular direction (perpendicular pores) (Fig. 8 in section 3.1.2.1). In the pores the amount of newly formed tissue is evaluated as projected tissue area (PTA) (section 3.4.1). Examples of PTAs of scaffolds of each type as a function of distance from the magnet can be found in Fig. 20 (data from all experiment scaffolds are in Appendix A).

Linear regression lines of parallel pores and perpendicular pores presented on top of raw data are mostly within the confidence bounds of one another (Fig. 20). Two sample t-test showed that in 16 out of 17 scaffolds there was no significant difference between PTAs of parallel and perpendicular pores.

Table 2 presents p-values based on the null hypothesis of no difference between the two pore orientations for each scaffold together with group p-values calculated using Fisher's method (section 3.4.3) for each type of force and control scaffolds. In all cases group p-values were non-significant and the null hypothesis of no difference between parallel and perpendicular pores cannot be rejected. Therefore, in the following evaluations no distinction is made between parallel and perpendicular pores and the formed tissues will be evaluated by their location in rows of scaffold regardless of their orientation.

Table 2. P-values of two-sample t-tests performed to check the null hypothesis that the PTAs of tissues grown in parallel and perpendicular pores are with equal means. Group p-values for all types of scaffolds are insignificant.

Type of force applied to scaffolds and MBs functionalization	p-values	Group p-values
Oscillating forces on epoxy MBs	0.67, 0.65, 0.38, 0.04, 0.43	0.1
Oscillating forces on RGD MBs	0.64, 0.5, 0.47, 0.9	0.86
Static forces on epoxy MBs	0.49, 0.99, 0.66	0.89
Control	0.63, 0.09, 0.41, 0.14, 0.09	0.09

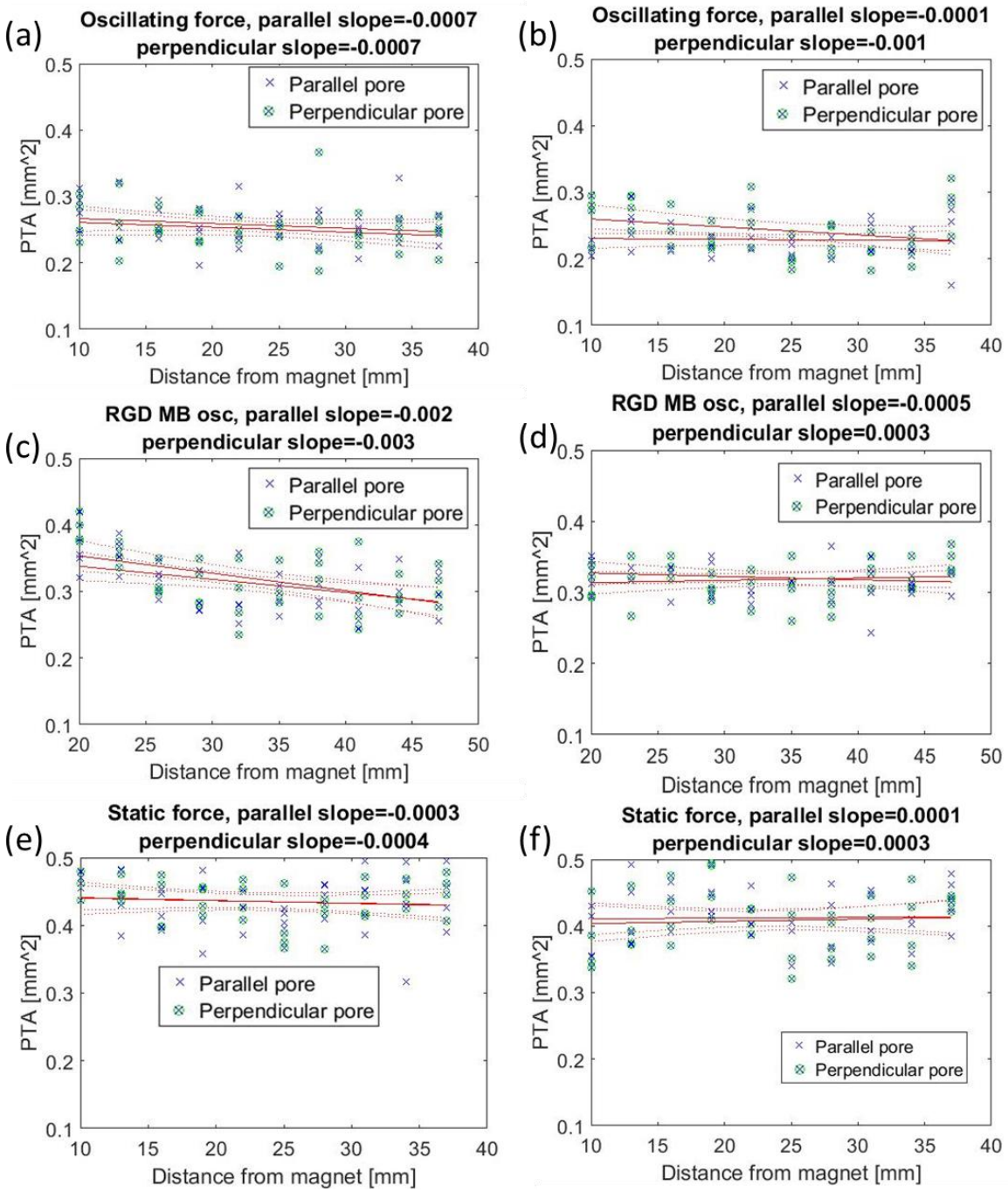

20. Examples of data obtained from single scaffolds after 24 days of tissue culture. Projected tissue areas (PTAs) are plotted as a function of distance from the magnet for tissues grown in pores, which are aligned parallel (green spots) and perpendicular to the magnetic field (blue x marks) The scaffolds were incubated with osteoblast cells and subjected to oscillating magnetic forces on epoxy MBs incorporated inside cells (a-b), oscillating forces on RGD MBs

(c-d), and static forces on epoxy MBs (e-f) separately along with their linear regression analysis lines (red lines). Slopes of linear regression analysis lines are indicated on top of each plot for tissues in parallel and perpendicular pores.

4.3 Control scaffolds

Five control scaffolds #1-5 in Table 3 (Fig. 21a-e) were used to generate the mean control regression analysis line used as a baseline compared to which all results were plotted (controls 1-5 in Table 3). Control #6 (Fig. 21f) was placed in an inverted position inside the well plate, to examine how the geometry of the scaffold relative to the well plate affects tissue growth. The mean value of the slope of the regression analysis of PTAs [μm^2] of control scaffolds as a function of distance from the magnet [µm] in the non-control case is 0.5 µm.

To use the control scaffolds as a base line relative to which regression analysis lines of all scaffolds were evaluated, the mean value of regression analysis lines of the logarithm of PTA [μm^2] as a function of the logarithm of the force [N] corresponding to location in scaffold was determined. Measuring the PTA in μm^2 and the force corresponding to the location of the tissues in the control scaffolds in N, the numerical average values (section 3.4.1) are: $\log(PTA) = 5.434 - 0.006 * \log(F)$.

When imaging scaffold #5 in Table 3 there was the data was not saved correctly and tissues were fixed and imaged again 4 days after the end of the experiment. This is the only control scaffold that has a significant negative slope as a function of distance from the position of magnet corresponding to a positive slope as a function of magnetic force magnitude if forces were applied. All other scaffolds, (1-4) and (6) had a positive slope or non-significant slope as a function of distance from position of magnet.

Table 3. Slopes, standard errors of regression (S) and p-values of linear regression analysis of PTAs as a function of distance from magnet location in the non-control case or when there were no MBs in tissues (control #1). Controls #1-5 were used to generate the mean values and group p-value. Control #6 was with pores located farther from well plate edge and in inner part of well plate.

#	Type of control	Slope	S	p-value
1	Oscillations only	0.02	0.0004	<0.001
2	MBs only	0.0006	0.0006	0.3
3	MBs only	$-9*10^{-5}$	0.0004	0.8
4	MBs only	0.01	0.0005	0.4
5	MBs only, tissues imaged after fixing	-0.02	0.0005	<0.001
6	"Reversed control", pores in inner part of well plate.	0.02	0.003	<0.001
Mean values and group p-value of controls 1-5		0.0005	$4*10^{-4}$	<0.001

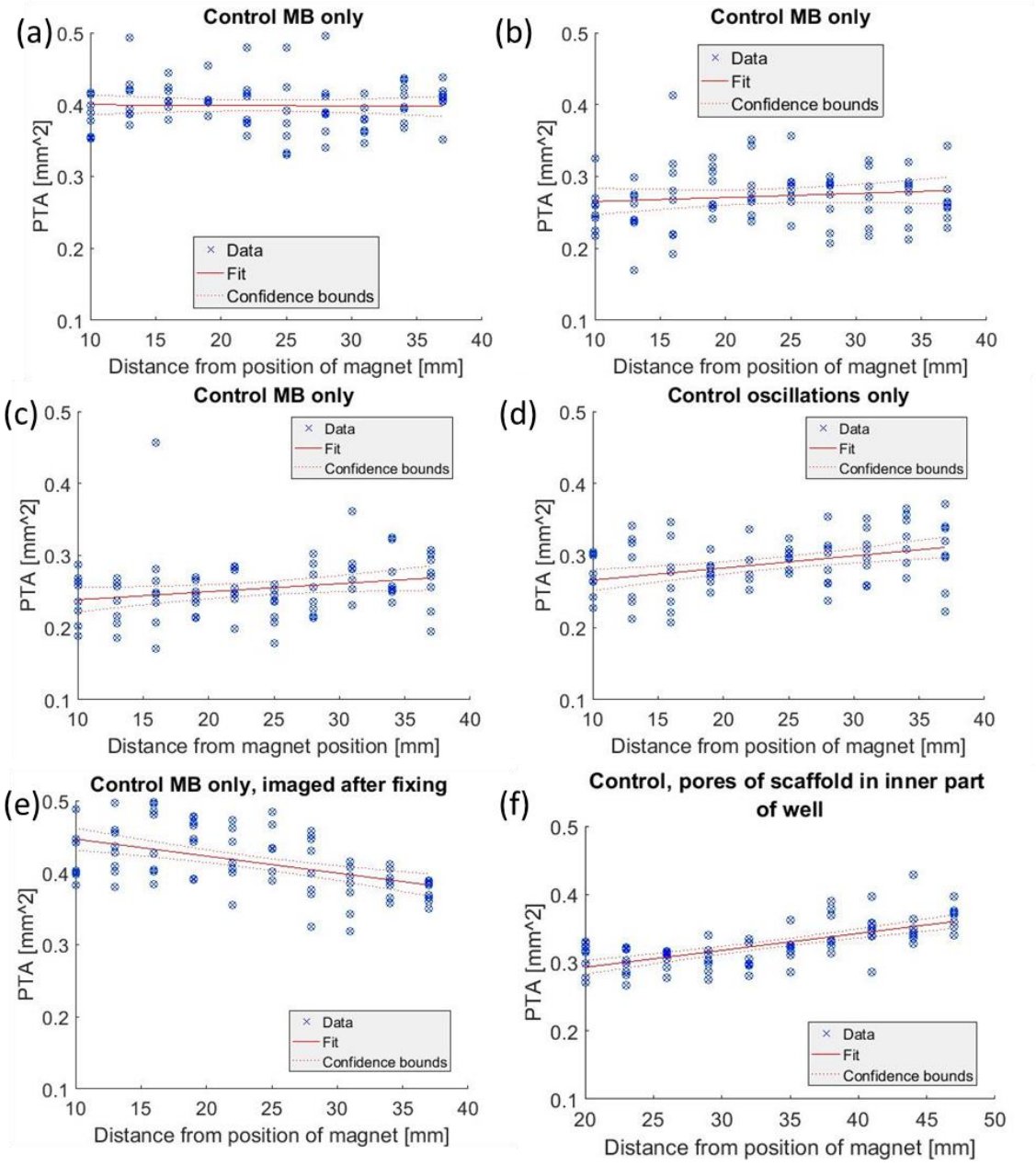

21. Data and regression analysis lines (red lined) of tissues grown in control scaffolds without magnetic forces. In each scaffold 80 tissues were imaged and their projected tissue area (PTA) was measured (blue marks). Scaffolds (a-c) and (e) were cultured with MC3T3-E1 cells and MBs, but magnetic forces were not applied on them. Scaffold (d) was cultured with cells only (no MBs) and was subjected to oscillating magnetic fields. The slope of the regression analysis line of the logarithms of PTAs as a function of the magnitude of forces corresponding to positions of tissues in scaffolds, of scaffolds (a-e) were averaged and used as a baseline for the experiments. Scaffold (f) was not taken into account since its pores were located farther away from the position of the magnet than all other scaffolds.

4.4 The effect of the force on tissue growth

4.4.1 The influence of the type of the force on projected tissue area (PTA)

Table 4 presents the mean values and standard deviations (SDs) of PTAs over the 80 pores in each scaffold studied. Fig. 22 shows the meta-analysis of mean values of PTAs from experiments using either static or oscillating forces and either epoxy or RGD MBs. Applying static forces on epoxy MBs resulted in an increase of mean value of PTA by 25% relative to control with a p-value of 0.002. Oscillating forces decreased mean tissue area by 23% relative to control with a p-value smaller than 0.001. Oscillating forces on RGD MBs did not change mean tissue area relative to control. Comparing tissue growth under application of oscillating forces but different MBs, RGD MBs resulted in a significantly higher PTA than epoxy MBs with a p-value smaller than 0.001. P-values were determined using two-sample Z-test (section 3.4.3).

Table 4. Mean PTAs and SDs of individual scaffolds studies grouped by the type of the force applied on MBs (static, oscillating, oscillating on RGD MBs, no force).

Type of force applied on MBs	Mean PTAs of individual scaffolds [mm^2]	SDs of individual scaffolds
Static forces	0.377,0.41, 0.435	0.038,0.042,0.035
Oscillating forces	0.258,0.276,0.236,0.254, 0.226	0.021,0.029, 0.032,0.032, 0.037
Oscillating forces on RGD MBs	0.351,0.315,0.326,0.319	0.032,0.042,0.037,0.027
No force	0.254,0.273,0.289,0.415,0.399	0.042,0.045,0.038, 0.042,0.033

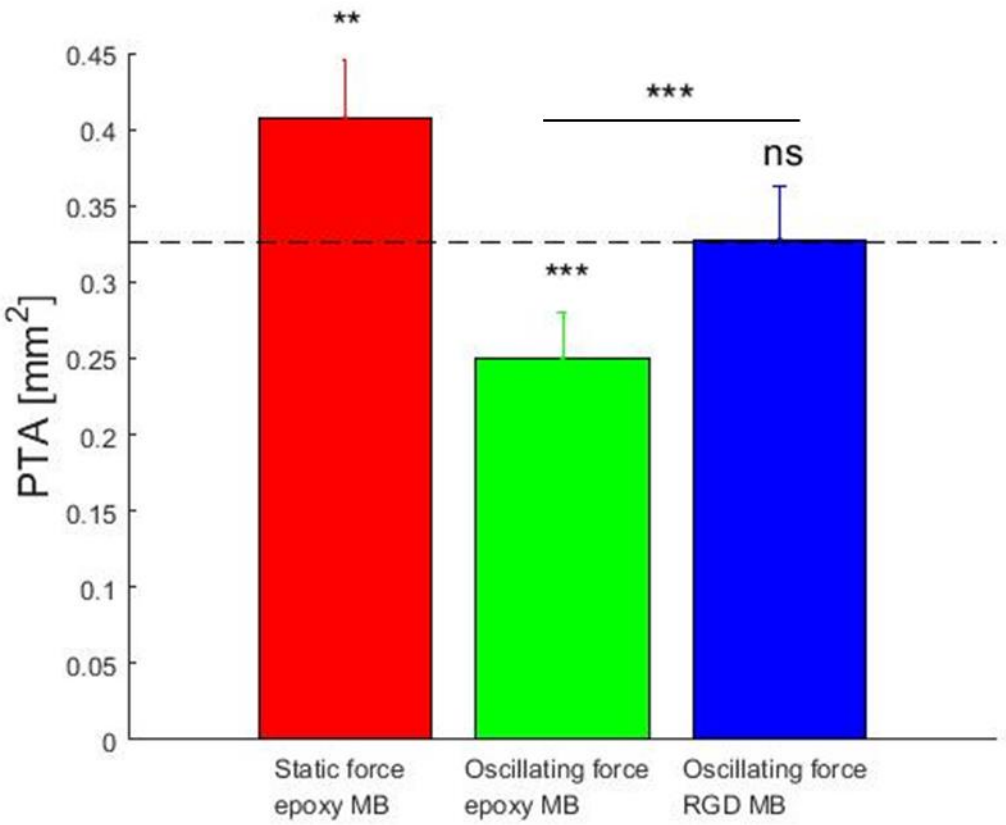

22. Meta-analysis of mean PTAs [mm^2] with their mean SDs for the different types of forces studied. Black dashed line mark the mean value of mean PTAs of control scaffolds. Static forces applied on epoxy MBs resulted in an increase of tissue area with group p-value of 0.002 (red bar) in comparison to the control. Oscillating forces applied on epoxy MBs (green bar) reduced mean PTA relative to control with p-value smaller than 0.001. Oscillating forces applied on RGD MBs did not change the mean PTA values significantly relative to control (blue bar). P-values were determined using Two-sample Z-test for comparing two means for every type of force applied relative to control. Significance is denoted by asterisks (*p<0.05,**p<0.01 and ***p<0.001).

4.4.2 The influence of the magnitude of force on PTA

In 11 out of 12 scaffolds where forces were applied, a regression analysis of the scatter plot of $\frac{PTA}{PTA_{control}}$ as a function of the applied force F, shows a moderate positive exponent y when fitted with a power law $\frac{PTA}{PTA_{control}} = k * F^y$ (Fig. 23e). Figure 23a-d shows the fitted exponents y for all the performed experiments along with their standard errors of regression

(S). When MBs were functionalized with epoxy MBs and subjected to static forces, 2 out of 3 y exponents were significantly positive (Fig. 23a) and a mean exponent value was 0.012 (Fig. 23d). When oscillating forces were applied on epoxy MBs, 4 out of 5 scaffolds had a significantly positive exponent value (Fig. 23b) with a mean exponent of 0.018, maximum value of exponent 0.02 and minimum value of 0.014 (Fig. 23b). When oscillating forces were applied on RGD functionalize MBs, 2 out of 4 scaffolds had a significantly positive y exponent (Fig. 23c) and the mean exponent value was 0.014. Group p-values, calculated using Fisher's method (section 3.4.3) was smaller than 0.001 in all cases of force application (oscillating force on epoxy functionalized MBs, oscillating force on RGD functionalized MBs, and static force on epoxy functionalized MBs) (Fig. 23d).

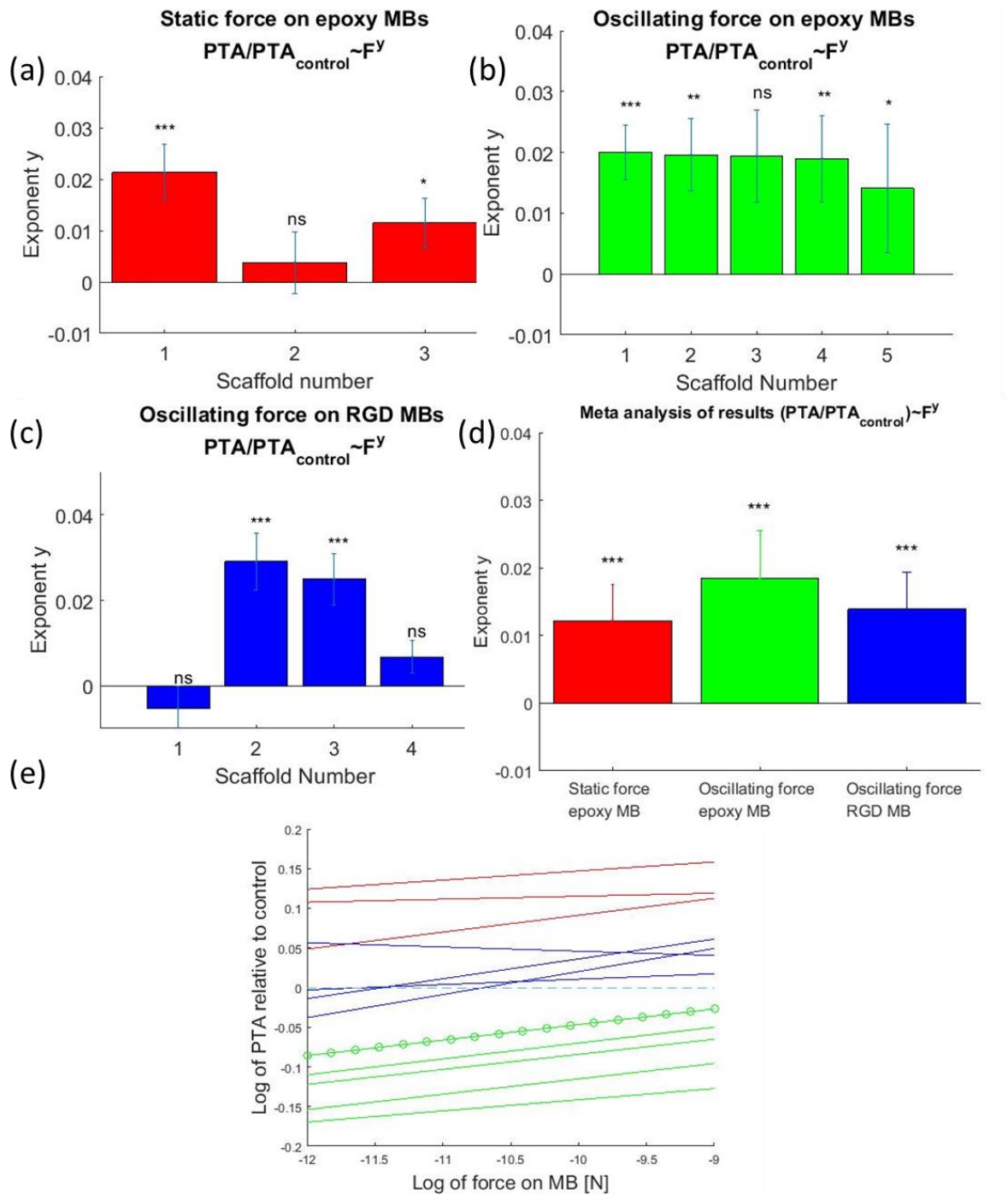

23. a-d) Exponents y of PTA relative to control as a function of applied force when fitted by a power law, $\frac{\mathbf{PTA}}{\mathbf{PTA_{control}}} = \mathbf{k}\,\mathbf{F^{y}}$, error bars denote standard errors of regression (S). Where the tissue was grown under the influence of: a) static forces on epoxy functionalized MBs b) oscillating forces on epoxy functionalized MBs. In bar b2, between oscillating force sessions, a static force was applied. c) oscillating forces on RGD functionalized MBs. d) meta-analysis

of y exponents of each type of force applied: red bar is the mean value of y exponents of scaffolds subjected to static force on epoxy MBs, green bar is for oscillating force on epoxy MBs and blue bar is for oscillating forces for RGD functionalized MBs. P-values with respect to the null hypothesis of no influence of forces on the PTA were calculated for each scaffold and their significance is indicated above each bar with asterisks. Group p-values were calculated using Fisher's method and their significance is denoted by asterisks (*p<0.05,**p<0.01 and ***p<0.001). e) Linear regression analysis lines $\log\left(\frac{\mathrm{PTA}}{\mathrm{PTA}_{\mathrm{control}}}\right)$ as a function of the logarithm of force. Lines are red in case of continuous forces applied on tissue with epoxy MBs; blue for oscillating forces applied on tissue with RGD MBs; green for oscillating forces applied on epoxy MBs; the green line marked with circles is the scaffold where both static and oscillating forces were applied; dashed line marking control.

Spearman's correlation coefficients of PTA values [µm] with force [N] were calculated for each scaffold along with their SDs. In calculating mean values of coefficients and SDs for each experimental setting, a positive correlation was found when oscillating forces were applied (on epoxy or RGD MBs). A non-significant positive correlation was found when static forces were applied (Fig. 24). Correlation values are summarized in Table. 5.

Table 5. Spearman's correlation coefficients of PTA [µm] with force [N] for individual scaffolds. P-values were calculated relative to the NULL hypothesis of no change of PTA with the magnitude of force.

Type of force	Correlation coefficients	P-values
Control	-0.29, -0.1, -0.36, 0.49, 0	0.009, 0.35, 0.001, $4*10^{-6}$, 1
Static force on epoxy MBs	0.28, -0.06, 0.09	0.01, 0.62, 0.43
Oscillating force on epoxy MBs	0.35, 0.25, 0.001, 0.2, 0.17	0.001, 0.03, 0.99, 0.08, 0.13
Oscillating force on RGD MBs	-0.12, 0.45, 0.39, 0.03	0.27, $2*10^{-5}$, 0.0003, 0.81

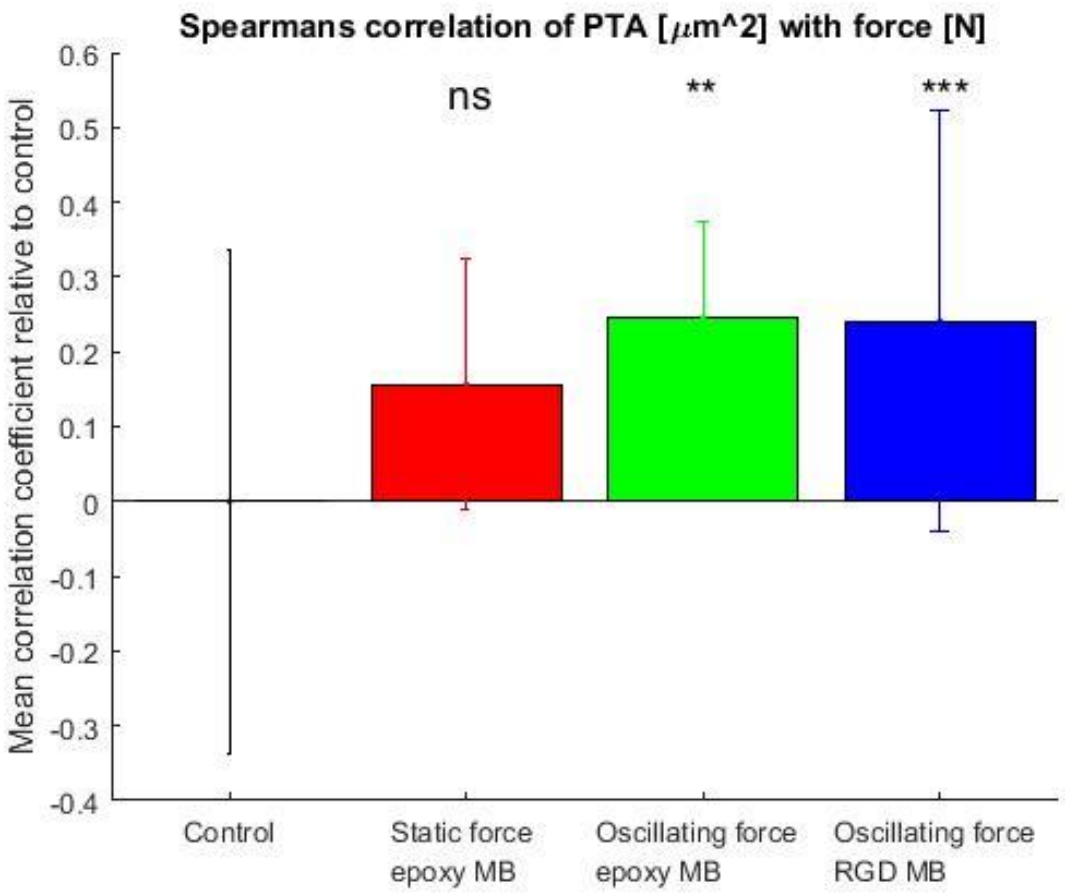

24. Mean Spearman's correlation coefficients relative to control of PTA [μm^2] with force [N] for the different types of forces studied. Static force on epoxy MBs resulted in a non-significant Spearman correlation with group p-value of 0.078 (red bar). Oscillating force on epoxy MBs resulted in a positive correlation with a group p-value of 0.001 (green bar). Oscillating forces applied on RGD MBs resulted in a positive correlation with group p-values smaller than 0.001 (blue bar).

4.5 The effect of the force on cell differentiation

To study the effect of the applied forces on cell differentiation, alkaline phosphatase (ALP) expression, a known indicator of cell maturation into the osteoblast lineage (Quarles, Yohay et al. 1992), was measured in the MC3T3-E1 cell layers grown on top of PDMS scaffolds (Fig. 4e) and subjected to the types and magnitudes of forces described above. At the end of

tissue growth experiments, 2 scaffolds from each force type were stained for ALP expression. Stained cell layer from areas in scaffolds was imaged at 10 different distances from the magnet, in the center of each row in scaffold (data in Appendix B) and analyzed.

A negative correlation of ALP expression with the magnitude of force was found both when static forces and oscillating forces were applied on epoxy MBs (Fig. 25), indicating an increasing delay in cell maturation when stronger forces were applied. When RGD MBs were used, a non-significant negative correlation of ALP expression with the magnitude of force was found. Control scaffolds had no significant correlation with respect to location in the scaffold (Table 6).

Table 6. Spearman's correlation coefficient of normalized ALP stain intensity with the magnitude of force applied on MBs [N] for individual scaffolds studies. The different experimental settings were: no force, static force on epoxy MBs, oscillating force applied to epoxy MBs, and oscillating force applied to RGD functionalized MBs.

Type of force	Spearman's correlation coefficients	Spearman's correlation p-values	Group p-values using Fisher's method
No force	0.43,-0.2	0.22, 0.58	0.39
Static force on epoxy MBs	-0.95,-0.53	<0.001, 0.12	<0.001
Oscillating force on epoxy MBs	-0.89, 0.13	0.001, 0.73	0.008
Oscillating force on RGD MBs	0.26 -0.65	0.47, 0.049	0.11

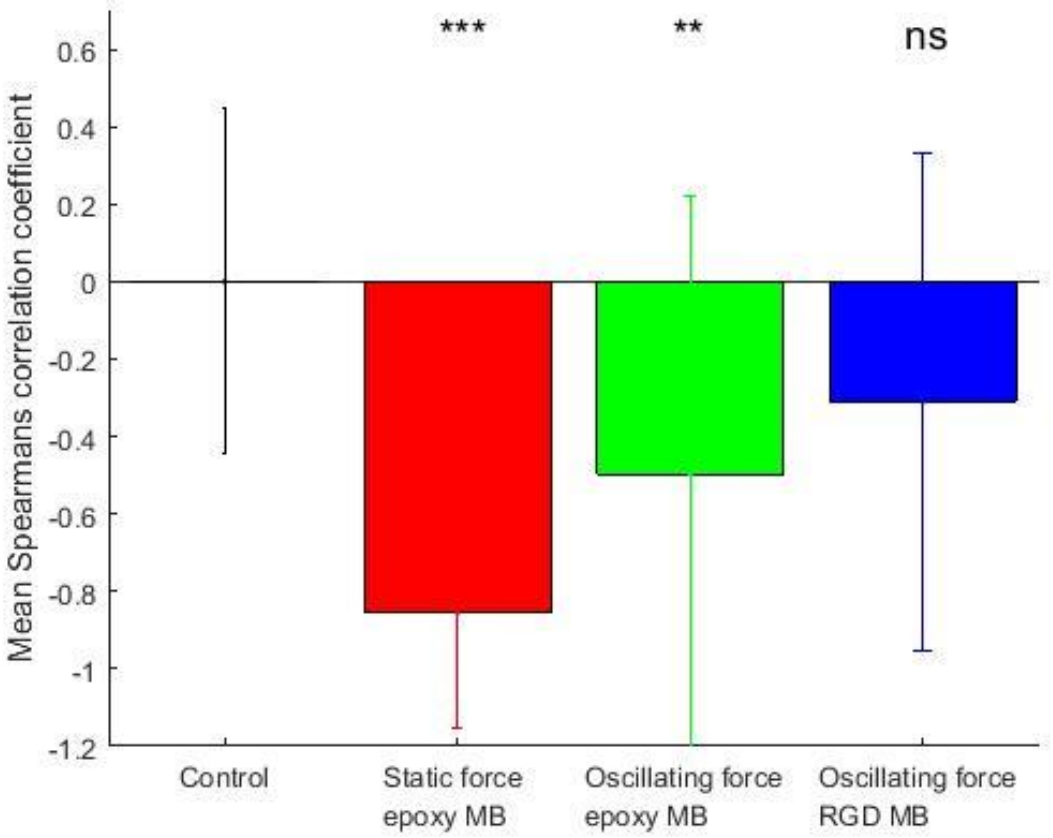

25. Mean Spearman's correlation coefficient with their SDs of normalized ALP stain intensity and magnitude of force applied [N]. Control cases had non-significant positive correlation (black bar), static forces on epoxy MBs resulted in a negative correlation with group p-value smaller than 0.001 (red bar), oscillating forces applied to epoxy MBs resulted in a significant negative correlation with group p-value of 0.008 (green bar), and oscillating force applied to RGD functionalized MBs had a non-significant negative correlation (blue bar). Group p-values were determined using Fisher's method.

Fig. 26 depicts the results of a meta-analysis of mean values of normalized ALP stain color intensity, from the different experimental settings. In scaffolds where static forces were applied, ALP stain intensity did not change significantly relative to control. When oscillating forces were applied on epoxy MBs, ALP stain intensity decreased by 10% relative to control with a p-value smaller than 0.001. When oscillating forces were applied on RGD MBs, mean ALP stain intensity was decreased by 25.5% relative to control (which did not include RGD

MBs) with a p-value smaller than 0.001. RGD MBs had a lower ALP stain intensity than epoxy MBs when oscillating forces were applied with a p-value smaller than 0.001. P-values were determined using two-sample Z-tests for comparing two means (section 3.4.3).

Table 6. Mean normalized blue ALP stain color intensity and standard deviations (SDs) of individual scaffolds grouped by the type of the force applied on MBs incubated in each of them (static, oscillating, oscillating on RGD MBs, no force).

Type of force applied on MBs	Mean normalized blue color intensity of individual scaffolds	SDs of individual scaffolds
Static forces	0.33, 0.38	0.015, 0.015
Oscillating forces	0.33, 0.31	0.009, 0.005
Oscillating forces on RGD MBs	0.26, 0.29	0.016, 0.015
No force	0.38, 0.34	0.02, 0.004

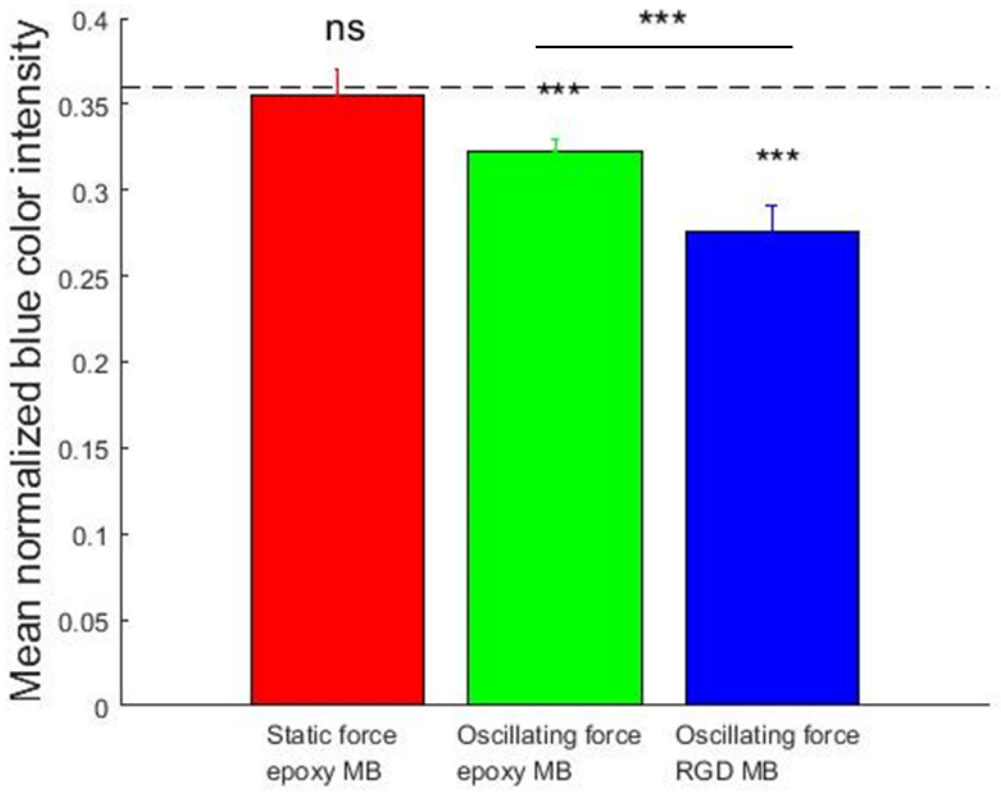

26. Mean normalized color intensity values with mean SDs for the different types of forces. Black dashed line mark the mean value of mean values of normalized blue stain color of control scaffolds. Static forces applied on epoxy MBs resulted in a non-significant change in ALP expression level (red bar). Oscillating forces applied on epoxy MBs (green bar) or RGD MBs (blue bar), reduced ALP expression level relative to control with p-values smaller than 0.001. Using RGD MBs when oscillating forces were applied resulted in a significantly lower ALP expression than using epoxy MBs with p-value smaller than 0.001. P-values were determined using two-Sample Z-test for comparing two means.

5 Inconclusive experiments

5.1 An attempt to probe mechanical properties of tissues using magnetic beads

Following a study by Galy and colleagues (Galy, Latour-Lambert et al. 2012) where mechanical properties of bacterial biofilms were investigated by integrating MBs in growing biofilms and applying forces on them using magnetic tweezers, an attempt was made to study mechanical properties of tissues using a similar method.

By probing three-dimensional physical properties of growing tissues in defined geometries at high spatial resolutions and generating forces within them, the hope was to gain insight into the mechano-regulation of tissue formation. The plan was to measure physical properties of the growing tissues by growing them in the presence of magnetic particles that are dispersed throughout the tissue, and then actuating the particles using magnetic forces while observing their movement. Analyzing the particles' trajectories was assumed to provide insight into the material's viscoelasticity at high spatial resolution and how these vary as a function of the direction of the applied magnetic forces relative to the tissue-substrate interface. An estimation of tissue viscosity to be around 10^3 Pa*s allowed to calculate that applying a constant force of ~0.5 nN for several hours should result in significant movement of MBs in the direction of applied force which could be observed using a simple phase contrast time lapse microscopy (section 3.3.4). However, time lapse videos of MC3T3-E1 tissues grown in hydroxyapatite (HA) scaffolds showed little migration of magnetic beads in the magnet's direction. Instead, beads mainly moved in the direction of the tissue's stress fibers, parallel to tissue-medium interface.

The suggested explanation for this failure is to be found in the incorporation of beads inside cells in this experiment (sections 4.1.2 and 6.2). In the bacterial biofilms studied by Galy et al., the bacteria studied are significantly smaller than the beads' size and hence could not incorporate them. This is likely to account for the difference in outcomes. An equivalent experiment might have utilized beads an order of magnitude larger than those used in this study and beads would then have been found between cells and in the ECM. However,

superparamagnetic beads of these sizes with good force to volume ratios could not be easily acquired or manufactured.

5.2 An attempt to validate magnetic forces calculated using the viscous drag test

The magnetic field simulations performed for this study's setup were first subjected to validation by using the viscous drag test, i.e. testing the magnetic setup in a viscous fluid with a known viscosity as was previously described (Alenghat, Fabry et al. 2000). Magnetic beads were introduced to 99% Glycerol (Sigma Eldrich) and approached with a 7x7x3 cm N40 Neodymium magnet at different distances. Videos of the beads' movement were taken using bright field microscope and their trajectories and velocities were analyzed using Matlab. The protocol used first found particles in each image by subtracting the background, enhancing the contrasts, transforming the image to a binary image, removing noise and dilating the connected objects found (Fig. 27). It then saved all objects in all images in an array and formed trajectories by connecting closest objects between frames that are closer than a given threshold using a code written by De. Peter Vach (Crocker and Grier 1996, Lefèvre, Bennet et al. 2014). Mean velocities and standard errors were calculated for all trajectories giving a weight to the length of trajectory found.
Surprisingly, beads migrated away from the magnet, rather than towards it as would be expected from superparamagnetic beads. Then it was observed that the viscous fluid glycerol flows away from the magnet. As glycerol is diamagnetic and the fluid volume is significantly larger than the beads' volume, and as the magnetic gradient exerted by the permanent magnet cube's effective area was much larger than the magnetic beads and affected the entire viscous fluid area, fluid diamagnetic properties were more prominent than beads' superparamagnetic properties and beads were carried, together with the flow of fluid, away from magnet, as was previously demonstrated (Ueno and Iwasaka 1994). Other fluids with known viscosities such as PDMS and mineral oil with viscosities of 0.1 Pa*s and 1 Pa*s were also tested but in all cases the magnet created a stream within the fluids due to the magnetic field, that had the effect of pushing the magnetic beads away from the magnet instead of pulling them towards it. Instead, the Comsol simulation was validated by

comparing it to an analytical calculation for magnetic forces emerging from a cube magnet along its axes of symmetry (sections 3.3.3 and 4.1.3).

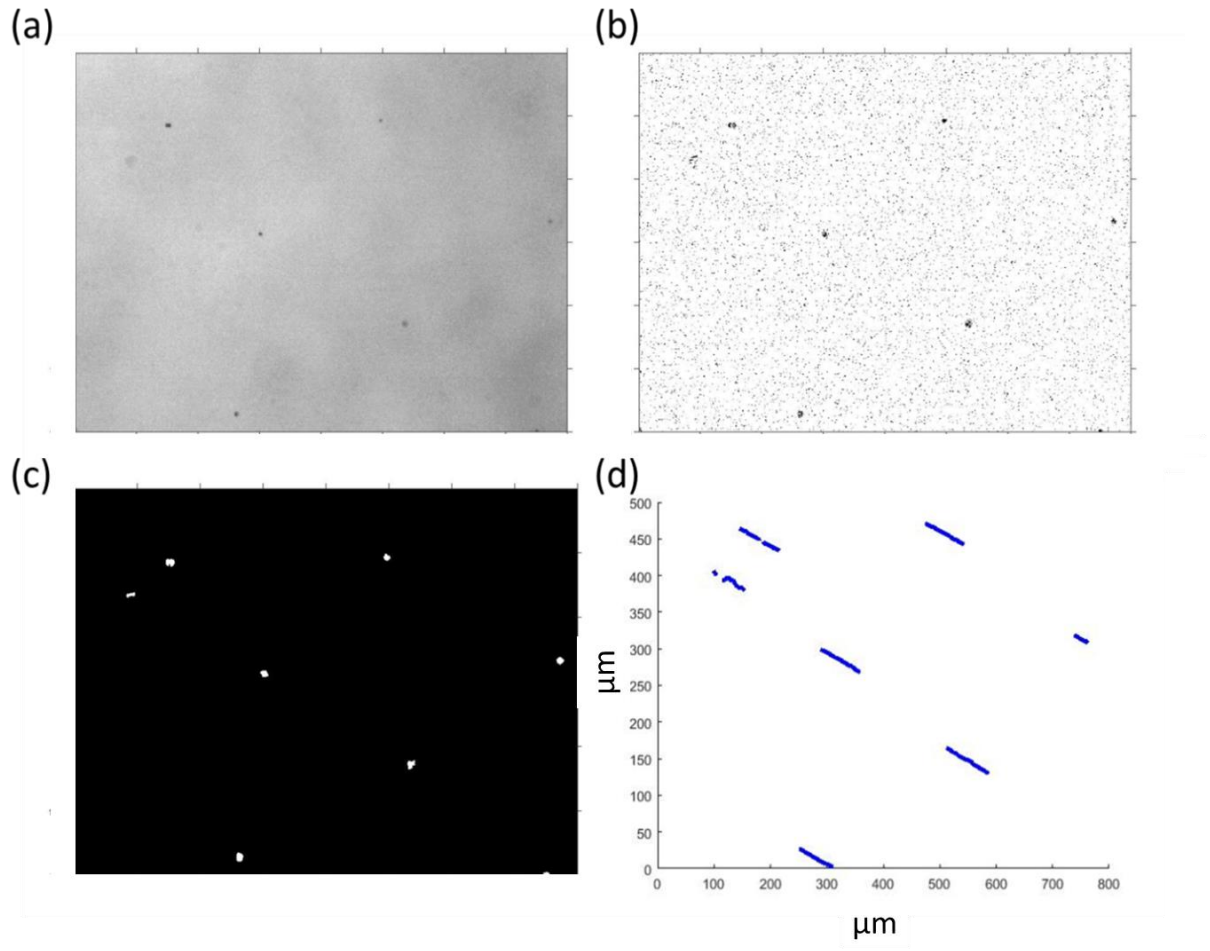

27. Particle tracking performed to detect beads' movement in glycerol due to magnetic forces. Each image (a) was processed using Matlab by removing its background (b), removing noise, dilating the particles found and converting to a binary image (c). Connecting beads' locations in adjacent frames that have the minimum distance between them that is below a pre-determined threshold resulted in particles' trajectories (d) (Crocker and Grier 1996, Lefèvre, Bennet et al. 2014).

5.3 Gap closure between cell layers while static mechanical force was applied

To examine whether MC3T3-E1 cell migration symmetry could be altered by attaching MBs to cells and applying magnetic forces on them, a cell migration assay in the dedicated magnetic system was performed.

A silicone insert, composed of two wells with a well-defined gap suitable for wound healing assays and cell migration studies (Culture insert for self-insertion, Ibidi, Inc.) with a width of a cell free gap of 500 µm +-100µm, was placed in the bottom of a rectangular well plate next to its edge and seeded according to the company's protocol with MC3T3-E1 cells in culture media containing 0.25% magnetic beads. The well was covered by a glass slide that allowed an easy insertion of a bar magnet to the adjacent well and placed in an onstage incubator (Okolab, NA, Italy). It was then imaged (Fig. 28) using time-lapse microscopy with a 5 minute gap between images for one hour, after which an N52 Neodymium magnet was introduced and gap closure was imaged overnight. No asymmetry in gap closure could be observed.

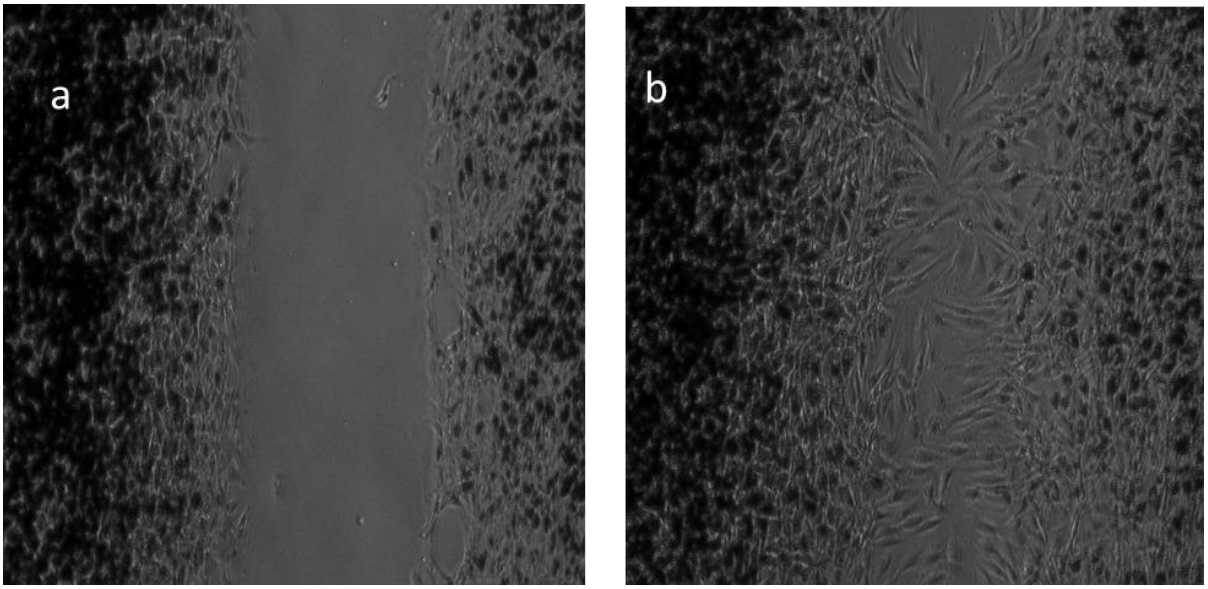

28. Gap closure between cell monolayers under the influence of magnetic force. MC3T3-E1 cell layer with magnetic beads (black spots) under the influence of magnetic force emerging from a 2x2x2 cm N52 neodymium magnet placed to the right side of the microscope and exerting a force of ~0.5 nN. Before gap closure (a) and after (b).

5.4 Cell migration pattern upon force application

Investigation of how magneto-mechanical stimulation in the same order of magnitude as the maximum force exerted on tissues in this study affects collective cell migration in MC3T3-E1 cells was performed. In particular, the question whether cells change their migration pattern due to applied force was examined.

MC3T3-E1 cells were seeded on Nonclun rectangular well plates (Thermo Fisher Scientific, Waltham, MA) and introduced to Dynabeads M-450 MB (Thermo Fisher Scientific, Waltham, MA) a day before the measurement. On the day of the measurement, a well with cells and beads was covered with a dedicated glass slide (made by the MPICI glass workshop), covering the well where the beads were seeded while enabling an insertion of a rectangular magnet to the adjacent well. An onstage incubator was used, maintaining a cell-friendly environment of 37^{o} and 5% CO_2 (Okolab, NA, Italy) (Fig. 29c).

Cell migration was monitored by time-lapse microscopy with a 20x objective using a Nikon inverted microscope (Nikon Eclipse TS100, Japan). Bright field images of the magnetic beads were acquired every 5 minutes. Cells were imaged for one hour before magnetic force was applied; then a force of ~0.5 nN was applied continuously while imaging of cells continued. Videos were analyzed using PIVlab 1.41 written by W. Thielicke and E.J. Stamhuis (Thielicke and Stamhuis 2014, Chepizhko, Giampietro et al. 2016). Average velocity components and standard errors were plotted as a function of time before and after the magnet was applied (Fig. 29e) using Matlab. Results were compared to cells without MBs subjected to the same magnetic gradient (Fig. 29g) and cells with MB where a brass cube with similar weight and dimensions as the magnet (Fig. 29d) was placed instead of a magnet (Fig. 29f).

Imaging cells with MBs using bright field microscopy allows for a good contrast between cells and beads. After application of magnetic force, beads form chains and align over time with the field's direction while staying in most cases within cell wall limits (Fig. 29a and b). In all cases where single cells were monitored, whether the magnet was applied on cells with MBs, or the control brass cube was used (Fig. 29d), a slight shift in migration direction was observed upon perturbation application that lasted 10 to 15 minutes, after which cell

migration was the same as before the perturbation was applied (Fig. 29e-g). This is an indication that the perturbation found was not due to the magnetic forces applied on the cells but rather due to a general perturbation in the system due to the insertion of the cubes. Other investigations with a more confluent cell layer yielded diverse results, perhaps due to a detachment of the cell layer from the well plate due to the perturbation.

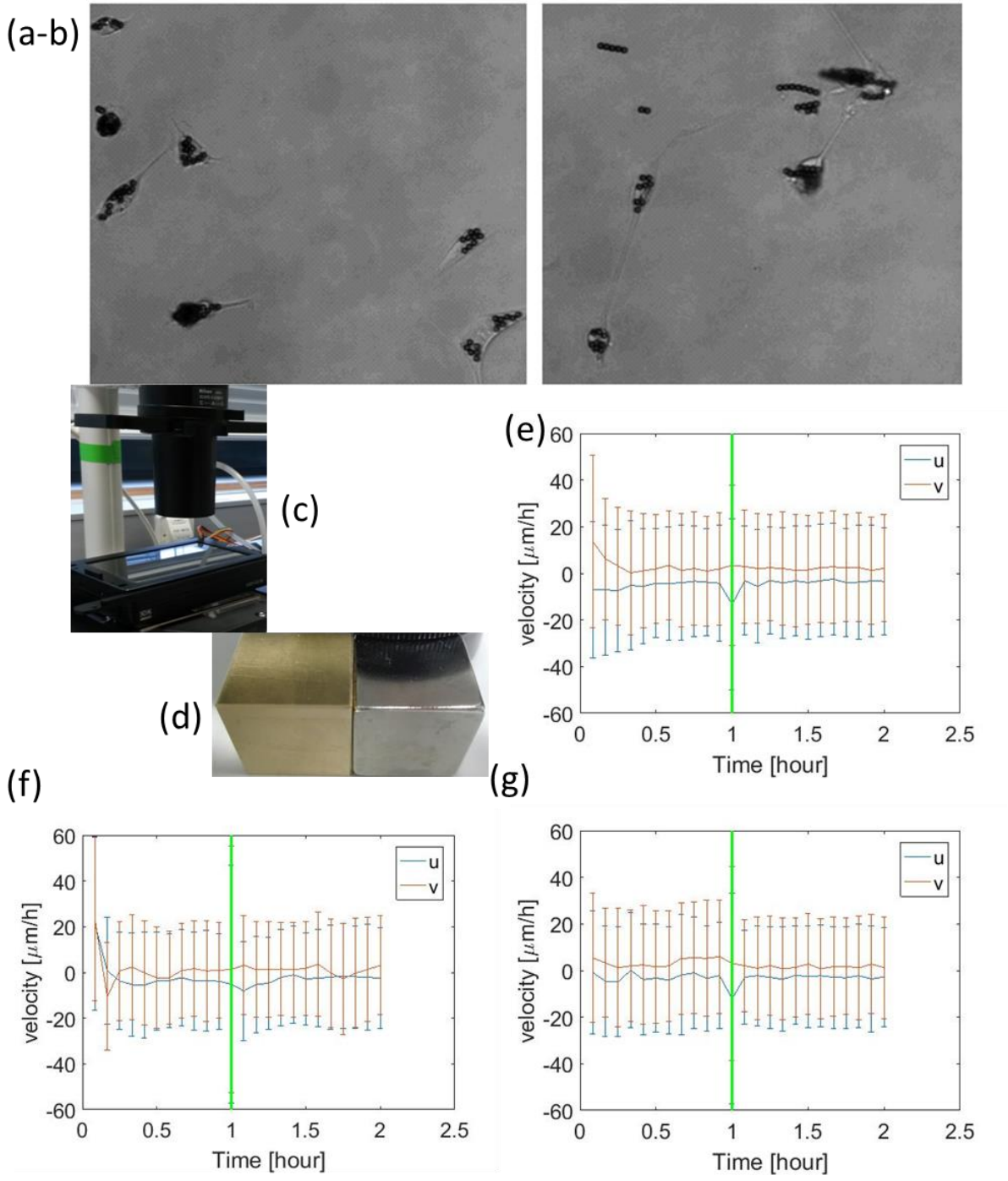

29. Cell migration pattern with and without magnetic force: Time lapse microscopy of cells with MBs under a magnetic force. Bright field image of MC3T3-E1 cells seeded on a Nunclon

surface well plate. MBs (round and black) were introduced to the cell culture the day before the measurement. a) Before magnetic force was applied. b) 1 hour after magnetic force was applied. e-f) Cells' migration observed in time lapse microscopy inside an onstage incubator (c): u is the horizontal velocity component and v is the vertical one. Average velocity values imaged are plotted together with their standard deviation. Green vertical lines indicate the time when magnet was inserted. Cells migration without magnetic forces was observed for one hour, after which a 2x2x2 cm N52 neodymium magnet applying a force of ~0.5 nN was applied for 1 hour (e). The same experiment was repeated with two controls: (f) A brass cube with similar dimensions (d, left) as the neodymium magnet (d, right) was applied instead of the magnet; (g) Neodymium magnet was applied to cell culture with no MBs.

6 Discussion and conclusion

6.1 Tissue growth measurements and analyses

It is well known that cells and tissues are sensitive to mechanical forces applied to them, however how exactly tissue formation and maturation depends on the type and magnitude of these forces is still under debate. The system developed in this study allows comparing the mechanoresponsiveness of tissues to forces ranging over 3 orders of magnitude, in a single well plate, and allows studying different parameters of force application over an array of tissues growing in pores.

While static forces in this study resulted in an increase of tissue growth, oscillating forces resulted in a decrease of tissue growth. In a scaffold where both static and oscillating forces were applied, tissue area decreased relative to control and was not significantly larger than scaffolds upon which only oscillating forces were applied. Mean normalized ALP stain intensity was lower than control when oscillating forces were applied and did not change significantly relative to control when static forces were applied.

A positive correlation of tissue growth with the magnitude of force applied was found both when static forces and oscillating forces were applied. However, the correlation was significant relative to no change in tissue growth as a function of force only when oscillating forces were applied. Regression analysis of tissue growth relative to control as a function of the magnitude of force resulted in a positive exponent of the power law fit both when static forces and oscillating forces were applied. Thus newly formed tissue area increased as a function of increasing force relative to control. Correlation of ALP expression, marking cell differentiation into the osteoblast lineage, with the magnitude of force was negative both when oscillating forces and static forces were applied on epoxy MBs in cell layer between tissues. ALP stain intensity was lower than control for oscillating forces and did not change relative to control when static forces were applied to cell layer.

Functionalizing the MBs with RGD peptides and applying oscillating forces resulted in an increased tissue area relative to tissues incubated with “plain” epoxy MBs and a decrease in ALP expression in cell layer relative to cell layer incubated with “plain” epoxy MBs. No

dependency of tissue growth on the orientation of the rectangular pore relative to the force vector was found.

The increase in tissue growth relative to control when static forces were applied, in addition to the increase in tissue growth as a function of the magnitude of force is an indication that a combination of cell proliferation and matrix production was enhanced due to static forces applied in the range of forces studied. An increase in cell proliferation and collagen type I synthesis (related to matrix production) was found in a previous study of another progenitor cell line differentiating into the osteoblast lineage, when moderate static stretch forces were applied to the cells' substrate. However, when more prominent forces were applied, cell apoptosis was measured (Kim, Song et al. 2009). The different trend of the combination of cell proliferation and matrix production as a function of force strength between these studies could be attributed to many factors such as: the exact cell line used, the exact location relative to the cells upon which the forces were applied or the magnitude of force applied. Nevertheless, in the system described in this thesis, it is also likely that above a certain magnitude, forces will damage tissues and will cause growth arrest. Therefore the analysis of the logarithm of PTA dependency on the logarithm of force cannot remain linear as for higher and higher forces and the power law applied can only fit in part of the force ranges possible.

When oscillating forces were applied in this study, tissue growth was arrested or slowed down relative to control but increased as a function of the magnitude of force. Cell proliferation and collagen synthesis, related to matrix production, were found in previous studies to respond to forces in an opposite manner to later markers of osteoblast differentiation such as ALP expression (Neidlinger-Wilke, Wilke et al. 1994, Kaspar, Seidl et al. 2000). In addition, the proliferative stage and mature, ready to mineralize state of these cells where proposed to be sequential (Quarles, Yohay et al. 1992, Golub and Boesze-Battaglia 2007). Previous experiments found an increase in later markers of osteoblast differentiation when 1 Hz oscillating forces were applied to cells via MBs (Cartmell, Dobson et al. 2002, Dobson, Cartmell et al. 2006, Kanczler, Sura et al. 2010, Henstock, Rotherham et al. 2014). Based on these previous experiments, it can be speculated that in this work as well, applying 1Hz oscillating forces on tissues via MBs, accelerate differentiation and therefore cause growth arrest in tissues.

However, contrary to previous studies, mean ALP stain intensity found in cell layer was reduced relative to control. In addition, this reduction in ALP expression does not fit well to the tissue growth reduction found when oscillating forces were applied in this study, which may implicate differentiation was accelerated. This reduction in stain intensity may have occurred due to variations of the time scaffolds were stored fixed before they were stained which could affect overall stain intensity in each scaffold. Other factors, including the dimensionality of the growth substrate, 3-dimensional for tissues and 2-dimensional for cell layer, should also be considered. To better understand this, it may be necessary to refine the ALP staining procedure for these scaffolds, and to include the amount and structure of extracellular matrix as well as other factors that were not monitored in the experiment and which may influence tissue growth and maturation.

While the type of force applied in the oscillating forces case reduced tissue growth relative to control the magnitude of the force applied had a positive correlation with tissue growth. However, tissue growth was lower than control in all the force range studies. As oscillating forces became smaller, the difference found between PTA values of tissues subjected to smaller and smaller oscillatory forces and control without force increased instead of converging. Therefore, in the oscillating forces case as well, the analysis of the logarithm of PTA dependency on the logarithm of force could not remain linear as the magnitude of force goes to zero. In previous comparative studies, higher oscillating strain values of cells' substrate resulted in an increase in cell proliferation and collagen type I expression (Koike, Shimokawa et al. 2005, Song, Ju et al. 2007, Kim, Song et al. 2010). However, in another study, higher relative strains resulted in a decrease in cell proliferation (Neidlinger-Wilke, Wilke et al. 1994) and yet in another study, higher relative forces increased cell differentiation (Haasper, Jagodzinski et al. 2008). While strains on cell substrate in most of these studies were about 2-8% and therefore forces applied are assumed to be similar, the type of cells used varied. Most of these studies used MSC cells and the Neidlinger-Wilke study used human osteoblast cells. The different cell type used could be one explanation of this discrepancy and the discrepancy between the Neidlinger-Wilke study and this thesis. Other explanations could be rooted in the different ways and exact locations forces were applied (externally to cell substrate in the Neidlinger-Wilke study or on MBs in cells in this study); in the different magnitudes of forces applied in these studies and may be attributed to the non-linear trend of cell response to different magnitude of forces.

ALP expression in cell layer decreased as a function of force magnitude within single scaffolds, while tissue growth increased for higher and higher forces. The reduction in this marker of cell differentiation as a function of the magnitude of force could be explained by the prolongation of the proliferative stage when higher forces were applied which may cause a delay in cell maturation. The suggested prolongation of the proliferative stage when higher forces were applied may explain the tissue growth increase as a function of the magnitude of force. A decrease in cell maturation accompanied by an increase in cell proliferation and collagen synthesis when higher strains were applied relative to lower strains was also found in a previous study where oscillating forces were applied to cells' substrate (Koike, Shimokawa et al. 2005).

In this study, functionalizing MBs with RGD peptides, increased the average tissue growth and decreased ALP stain intensity in cell layer relative to tissues incubated with "plain" epoxy beads. The addition of RGD peptides may prolong the proliferative stage of these cells and delay cell differentiation. One possible explanation of this effect of RGD MBs may be that the availability of RGD peptides, which are abundant in ECM, in the culture medium, increases due to the introduction of the MBs and enhance matrix formation. In a previous study it was found that the availability of ECM components enhance tissue growth in pores (Herklotz, Prewitz et al. 2015). Although, MBs were found to be incorporated in the cells studied (section 6.2) as well as in other studies (Cartmell, Dobson et al. 2002), it remains possible that some MBs were attached externally to cell integrins via the RGD peptides and stimulated integrin signaling as was previously suggested (Kanczler, Sura et al. 2010, Henstock, Rotherham et al. 2014).

6.2 Location of magnetic beads in the cells and tissues studied

To better understand where the forces are applied in the tissues studied, the results of the sections 4.1.1, 4.1.2 and 4.1.4 will be discussed. It was previously demonstrated that MBs of the same size as used here are internalized into cells (Hughes, Dobson et al. 2007). However, since in different studies MBs of similar sizes were considered to be attached to the cell membrane in long term cell cultures rather than being internalized in cells (Dobson, Cartmell

et al. 2006, Kanczler, Sura et al. 2010, Henstock, Rotherham et al. 2014), beads incubated with cells were also investigated here. When testing the adhesion of MBs to cells, 24 hours after beads were introduced to cells, beads were firmly attached to cells and did not detach when magnetic forces pulled on them (section 4.1.1). This could be either due to the incorporation of beads in cells or due to strong adhesion of the beads to the membrane of the cells.

To further investigate this point, MBs incubated with MC3T3-E1 cells were also imaged using light and confocal microscopy. Using the phase contrast microscope, beads could be seen inside the region of the cells' membrane (section 4.1.2). This could mean that MBs are either beneath cells, inside cells, or on top of cells. However, since beads were mostly seen around cells' nuclei, it was speculated that beads were incorporated inside cells and migrated towards the nucleus as would be expected from endosomes.

This assessment was bolstered by moving the focus along the z-axis using a confocal microscope imaging of single cells with MBs. Here, actin cytoskeleton could be seen around, below and above magnetic beads (section 4.1.2). In addition, a thin layer of green stain, marking the existence of actin filaments, could be seen around beads as would be expected from endosomes where the cytoskeleton around them help to keep them in place, around the nucleus.

Thus, since MBs were found to be incorporated inside cells, it was assumed that beads were located as well inside cells in the tissues studied. To examine it, magnetic beads were incubated with growing tissues and imaged using both bright field and confocal microscopy. MBs could be seen in younger, thinner and more transparent parts of tissues. However, since magnetic beads were introduced continuously throughout the tissue growth time, it is likely that magnetic beads exist in all areas of tissues where there are cells. In some cases MBs formed groups that were aligned in the direction of tissue-medium interface. Since cells align in this direction, this is also an indication that beads are indeed incorporated inside cells and therefore, since cells stretch within tissues, beads aggregations also aligned in this direction.

Finally, imaging of beads in tissue located in an on-stage incubator showed movement of beads mainly in the direction of the tissue filaments, i.e. parallel to the tissue – medium

interface (section 4.1.4), as is expected from migrating cells within tissue (Ma, Wang et al. 2015, Ehrig 2017) – and not in the direction of the force. This is another indication that the MBs were incorporated inside the cells.

Thus, indications that the MBs were indeed incorporated inside cells were acquired as was also previously demonstrated for MBs of similar sizes (Hughes, Dobson et al. 2007). The tissue – MB system studied cannot be seen as a viscous fluid with particles (as was seen when similar MBs were used to study mechanical forces in biofilms (Galy, Latour-Lambert et al. 2012)). Rather tissues can be seen as having a network structure where the MBs are confined to the nodes of the network (Regul 1988). Thus, it would appear that the effect of these forces on tissue size and cell layer differentiation state occurs not through tissue deformation but either due to the local forces cells exert on each other; or possibly via oscillations or pressure on the nucleus as was previously suggested (Bacabac, Smit et al. 2006).

6.3 Strengths and weaknesses of the setup

The experimental setup designed and studied can produce a wide range of long term magneto-mechanical forces, static or oscillating, on an array of tissues in a single well plate. All pores are incubated in the same well, followed by one seeding process, with same media, and same conditions inside the incubator (Kommareddy, Lange et al. 2010). The decay in the magnitude of force along the rows of tissues in scaffold enables a comparative study in one batch. Thus, the setup could shed light not only on how the different forces affect tissue growth but also on the slope of the curve of the magnitude of force vs. tissue state, in a wide range of forces.

One weakness of the system lies in the geometry of the scaffold and the way different pore locations within cell culture well can interact with tissue growth due to differences in air diffusion within the well. This was corrected for by a comparison to control experiments without applied forces; however, a better design could include a smaller scaffold relative to well dimensions to provide more homogenous cell culture conditions.

One difficulty that was encountered during initial experiments was cell culture contamination. The large dimensions of the dedicated cell culture scaffold relative to the cell culture well rendered the amount of media usually inserted in the well too big for this experiment. This resulted in small spills of media which caused contamination. To overcome this difficulty, the scaffold's dimensions were adjusted so the scaffold is thinner and therefore takes less space in cell culture well that should be occupied by media. Other reasons for contamination in this long term experiment, lasting 24 days, should be taken into account such as contamination in culture media, inserted MBs etc.

It is hard to explain the variation between ALP expression values found in different scaffolds subjected to the same forces and beads' functionalization (which persists in all ALP experiments). While some scaffolds showed very significant changes in cell maturation stage as a function of the magnitude of applied forces on them, other scaffolds showed no significant change. Even though when combining p-values using Fisher's method for each case, ALP stain as a function of force tests significant, it would still be important in future experiments to refine the protocols to understand this variation. One possible alteration that should be made is defining a time period after fixing the scaffolds after 24 days of culture in which the staining should be performed.

While MBs were introduced to growing tissue in a fixed manner by first stirring them in fresh medium and then introducing them to cell culture well, variations in bead distribution within and between tissues were observed. In addition, since MBs are incorporated inside cells they tend to aggregate along the cell within the tissue structure. This may influence the total force applied on each cell and tissue and the experiments' standard errors.

When calculating magnetic forces on magnetic beads, the magnetic interactions between magnetic beads were neglected. They were neglected since in superparamagnetic beads, superparamagnetic nucleations in the polystyrene sphere should be dispersed and sufficiently far away from each other to not have an effect on each other. This diluted colloid structure should be a fundamental property of the superparamagnetic spheres. If the nucleations were dispersed enough to have negligible effect on each other in a single bead, they would also not significantly influence magnetic nucleations in adjacent spheres. However, when observing the results of the imaging it was apparent that magnetic beads do interact with each other and form chains in the direction of the external magnetic field,

especially when they were outside cells and could move freely in the cell culture medium. Hence, in future experiments, other magnetic beads with better superparamagnetic qualities should be considered, or alternatively the concentration of MBs should be reduced in order to support sufficient separation between them.

The average force applied on 1 μm^2 area within focal adhesions by surrounding cells ranges from 1 to 8 nN (Schoen, Pruitt et al. 2013), on the same scale as the higher forces applied on cells during this work. This motivated the design of this setup as a way to understand the biological mechanisms behind – and ultimately to influence – tissue growth *in-vitro* in conditions closer to those in nature. However, during the course of the preparatory investigations, it was concluded that beads were incorporated inside cells and did not apply external forces directly on cells' focal adhesion. Rather MBs were found to be close to the nucleus and apply forces on cells and tissues from within the cells.

6.4 Outlook

The reported system is suggested as a tool to continue investigating how forces affect cells and tissues in defined confining geometries, and how this effect depends on the magnitude of force.

Most interesting would be to extend the force range of this study to include tissue state dependency on weaker forces. Specifically to examine how smaller forces, ranging between fN-pN, would affect tissue growth and differentiation curves. Studying the effect of smaller forces could shed light on questions that emerged during this study like that the regression analysis line of PTA as a function of the magnitude of oscillating force did not converge with control at the limit of small forces. This raised the possibility that much smaller forces then studied could have an effect on tissue growth. Extending the force range can shed light on the tissue growth curve as a function of the magnitude of force at lower forces and how it corresponds with other comparative studies (as discussed is section 6.1). In addition it would provide an indication to the extent to which forces should be small to not have any detectable effect on tissue growth in pores. This could be easily done by adjusting the magnetic system so scaffolds are farther away from the force source while increasing the

magnet's dimensions so the forces remain relatively homogenous along the rows of the scaffold.

Another parameter to investigate would be the number of oscillating force cycles applied on tissues each time (Kaspar, Seidl et al. 2002, Song, Ju et al. 2007). In this study static forces resulted in an increase of tissues growth relative to control and 1 Hz oscillating forces for 1 hour a day resulted in a decrease of tissue area. Changing the time of oscillations applied on different scaffolds from 1 hour to 1 minute can shed light on the contribution of the number of oscillations in addition to force magnitude.

Assessing cell proliferation while keeping the sample alive and growing is possible using the tissue area imaging technique (Bidan, Kommareddy et al. 2012) used in this study. As it was previously suggested that the effect of force application on cells may be dependent on cell differentiation stage (Weyts, Bosmans et al. 2003), imaging tissue projected tissues area in different days of tissue growth can enable studying tissue growth dependency on force application in different stages of tissue maturation on an ongoing growing sample.

In this study, the effect of the existence of RGD peptides on the effectivity of different kind of forces on cell growth and differentiation was measured. This system could also be used to see how different parameters affecting tissue growth, such as the growth factor BMP2 (Kopf, Petersen et al. 2012), influence the curve of tissue growth vs. force magnitude.

Geometrical constraints studied here consisted in one particular rectangular dimension with different orientation of the rectangular pore's long edge relative to the force vector. It would be interesting to adjust the design of the mold for PDMS casting to enable the study of how different geometrical constraints and pore sizes can affect tissue growth under the forces studied.

Acknowledgements

I would like to thank all those at the Max Planck Institute of Colloids and Interfaces who helped and supported completing my PhD. I am very grateful to my PhD supervisor Prof. Dr. Dr.h.c. Peter Fratzl without whom, this PhD could not have been completed. His guidance, insightful discussions, scientific instructions, and the accepting providing environment and facilities he enables in the Biomaterials department, were invaluable to my study and the scientific process. I would like to thank my group leader Prof. Dr. John Dunlop, for his support throughout my PhD project, giving me the opportunity and freedom to study various interesting aspect of tissue mechanics in his lab, for being full of new ideas and available to my many questions.

I am very grateful to Dr. Richard Weinkamer for his comments on the content and structure of this thesis. His help in the writing and data evaluation process was invaluable while finalizing this thesis far away from Golm.

Many thanks to my Potsdam University mentor, Prof. Dr. Carsten Beta, for insightful discussions during IMPRS workshops and personal meetings and for guiding me towards the right path to complete my PhD.

My great gratitude to the cell culture laboratory manager, Christine Pilz for supervising my work in the lab and helping me conduct my research. The opportunity she provided to have access to many research facilities and learn new techniques was of great value to this research.

Many thanks to all the past and present members of the Dunlop group for their support and enjoyable working atmosphere. Special thanks to Dr. Sebastian Ehrig for introducing me to the tissue lab expertise and the mold manufacturing process including the Rhinoceros software and the mechanical workshop; to Alan West, a master student in John Dunlop's group I helped supervise, for his kind help with the experiments defining the protocol for MBs introduction into growing tissues in pores; to Dr. Lorenzo Guiducci for his help with simulations and feedback on presentations; and to Cornelius Mueller for his help around the lab whenever a good advice was needed. I would also like to thank other Dunlop group

members for making working in the group a pleasant experience: Rafael Sera, Hubert Taieb and Karen Lam.

Many thanks to Dr. Peter Vach for helpful discussions on magnetic forces simulations and calculations as well as practical advice on understanding MBs behavior inside medium; to Dr. Mathieu Bennet for useful microscopy instructions and advice; to Susann Weichold for filling in for me in the lab when needed and helping me learn German by talking German with me; and all other department members for kind chats and discussions and an excellent working atmosphere.

My gratitude to Dr. Carmen Remde and Dr. Vasil Georgiev from Theory and Bio-systems departments for their kind help with obtaining data with fluorescent confocal microscopy and phase contrast microscopy.

The MPIKG technical support was essential to this project. I would like to thank Jan von Szada-Borryszkowski from the mechanical workshop for manufacturing the aluminum mold used for PDMS casting in this experiment. Many thanks to Klaus Bienert from the electronic workshop for producing the magnet actuator used in this thesis. My thanks to Cliff Janiszewski from the glass workshop for manufacturing the dedicated glass covers for the cell culture plates. Many thanks to the outstanding MPIKG IT technical support for making sure all ran smoothly and for enabling our work. Special thanks to René Genz and Paul Meißner for being available and always coming up with a good solution when needed. Thanks to Silke Niehaus from the Bibliothek for providing with access to papers and aiding in finding requested books.

My warm gratitude to Kerstin Gabbe for her kind help and guidance through bureaucracy and for enabling the essential meetings with Prof. Peter Fratzl.

Thank you Katrin Edery for translating the abstract to German and for being such a good friend.

Finally and most importantly, I would like to thank my family for encouraging and supporting me and for making this possible.

References

Alenghat, F. J., B. Fabry, K. Y. Tsai, W. H. Goldmann and D. E. Ingber (2000). "Analysis of cell mechanics in single vinculin-deficient cells using a magnetic tweezer." Biochemical and biophysical research communications **277**(1): 93-99.

Assanah, F. and Y. Khan (2018). "Cell responses to physical forces, and how they inform the design of tissue-engineered constructs for bone repair: a review." Journal of Materials Science **53**(8): 5618-5640.

Bacabac, R. G., T. H. Smit, J. J. Van Loon, B. Z. Doulabi, M. Helder and J. Klein-Nulend (2006). "Bone cell responses to high-frequency vibration stress: does the nucleus oscillate within the cytoplasm?" The FASEB journal **20**(7): 858-864.

Bao, G. and S. Suresh (2003). "Cell and molecular mechanics of biological materials." Nature materials **2**(11): 715-725.

Bausch, A. R., F. Ziemann, A. A. Boulbitch, K. Jacobson and E. Sackmann (1998). "Local measurements of viscoelastic parameters of adherent cell surfaces by magnetic bead microrheometry." Biophysical journal **75**(4): 2038-2049.

Bidan, C., K. Kommareddy, I. Manjubala, M. Rumpler, P. Fratzl and J. Dunlop (2010). "Geometric Control of Tissue Growth." Bone(46): S47-S48.

Bidan, C. M., P. Kollmannsberger, V. Gering, S. Ehrig, P. Joly, A. Petersen, V. Vogel, P. Fratzl and J. W. Dunlop (2016). "Gradual conversion of cellular stress patterns into pre-stressed matrix architecture during in vitro tissue growth." Journal of The Royal Society Interface **13**(118): 20160136.

Bidan, C. M., K. P. Kommareddy, M. Rumpler, P. Kollmannsberger, Y. J. Bréchet, P. Fratzl and J. W. Dunlop (2012). "How linear tension converts to curvature: geometric control of bone tissue growth." PloS one **7**(5): e36336.

Bidan, C. M., K. P. Kommareddy, M. Rumpler, P. Kollmannsberger, P. Fratzl and J. W. Dunlop (2013). "Geometry as a factor for tissue growth: towards shape optimization of tissue engineering scaffolds." Advanced healthcare materials **2**(1): 186-194.

Bidan, C. M., K. P. Kommareddy, M. Rumpler, P. Kollmannsberger, P. Fratzl and J. W. C. Dunlop (2013). "Geometry as a Factor for Tissue Growth: Towards Shape Optimization of Tissue Engineering Scaffolds." Advanced Healthcare Materials **2**(1): 186-194.

Bonnet, N. and S. L. Ferrari (2010). "Exercise and the skeleton: how it works and what it really does." IBMS BoneKEy **7**(7): 235-248.

Burger, E. H. and J. Klein-Nulend (1999). "Mechanotransduction in bone—role of the lacuno-canalicular network." The FASEB Journal **13**(9001): S101-S112.

Camacho, J. and V. Sosa (2013). "Alternative method to calculate the magnetic field of permanent magnets with azimuthal symmetry." Revista mexicana de física E **59**(1): 8-17.

Cartmell, S. H., J. Dobson, S. B. Verschueren and A. J. El Haj (2002). "Development of magnetic particle techniques for long-term culture of bone cells with intermittent mechanical activation." IEEE Transactions on NanoBioscience **99**(2): 92-97.

Chen, J., B. Fabry, E. L. Schiffrin and N. Wang (2001). "Twisting integrin receptors increases endothelin-1 gene expression in endothelial cells." American Journal of Physiology-Cell Physiology **280**(6): C1475-C1484.

Chepizhko, O., C. Giampietro, E. Mastrapasqua, M. Nourazar, M. Ascagni, M. Sugni, U. Fascio, L. Leggio, C. Malinverno and G. Scita (2016). "Bursts of activity in collective cell migration." Proceedings of the National Academy of Sciences: 201600503.

Coey, J. M. (2010). Magnetism and magnetic materials, Cambridge University Press.

Crocker, J. C. and D. G. Grier (1996). "Methods of digital video microscopy for colloidal studies." Journal of colloid and interface science **179**(1): 298-310.

Dobson, J. (2008). "Remote control of cellular behaviour with magnetic nanoparticles." Nat Nano **3**(3): 139-143.

Dobson, J., S. H. Cartmell, A. Keramane and A. J. El Haj (2006). "Principles and design of a novel magnetic force mechanical conditioning bioreactor for tissue engineering, stem cell conditioning, and dynamic in vitro screening." IEEE transactions on nanobioscience **5**(3): 173-177.
Drury, J. L. and D. J. Mooney (2003). "Hydrogels for tissue engineering: scaffold design variables and applications." Biomaterials **24**(24): 4337-4351.
Ehrig, S. (2017). 3D Curvature and its role on tissue organization. PhD Thesis, Potsdam University.
Einstein, A. (1905). "On the motion of small particles suspended in liquids at rest required by the molecular-kinetic theory of heat." Annalen der physik **17**: 549-560.
Fedarko, N. S., P. Bianco, U. Vetter and P. G. Robey (1990). "Human bone cell enzyme expression and cellular heterogeneity: correlation of alkaline phosphatase enzyme activity with cell cycle." Journal of cellular physiology **144**(1): 115-121.
Fonnum, G., C. Johansson, A. Molteberg, S. Mørup and E. Aksnes (2005). "Characterisation of Dynabeads® by magnetization measurements and Mössbauer spectroscopy." Journal of Magnetism and Magnetic Materials **293**(1): 41-47.
Fratzl-Zelman, N., H. Hörandner, E. Luegmayr, F. Varga, A. Ellinger, M. Erlee and K. Klaushofer (1997). "Effects of triiodothyronine on the morphology of cells and matrix, the localization of alkaline phosphatase, and the frequency of apoptosis in long-term cultures of MC3T3-E1 cells." Bone **20**(3): 225-236.
Galy, O., P. Latour-Lambert, K. Zrelli, J.-M. Ghigo, C. Beloin and N. Henry (2012). "Mapping of bacterial biofilm local mechanics by magnetic microparticle actuation." Biophysical journal **103**(6): 1400-1408.
Gieré, R. (2016). "Magnetite in the human body: Biogenic vs. anthropogenic." Proceedings of the National Academy of Sciences **113**(43): 11986-11987.
Girnyk, S., A. Barannik, E. Barannik, V. Tovstiak, A. Marusenko and V. Volokhov (2006). "The estimation of elasticity and viscosity of soft tissues in vitro using the data of remote acoustic palpation." Ultrasound in medicine & biology **32**(2): 211-219.
Golub, E. E. and K. Boesze-Battaglia (2007). "The role of alkaline phosphatase in mineralization." Current opinion in Orthopaedics **18**(5): 444-448.
Haasper, C., M. Jagodzinski, M. Drescher, R. Meller, M. Wehmeier, C. Krettek and E. Hesse (2008). "Cyclic strain induces FosB and initiates osteogenic differentiation of mesenchymal cells." Experimental and Toxicologic Pathology **59**(6): 355-363.
Heinemann, D., C. Lohmann, H. Siggelkow, F. Alves, I. Engel and G. Köster (2000). "Human osteoblast-like cells phagocytose metal particles and express the macrophage marker CD68 in vitro." Bone & Joint Journal **82**(2): 283-289.
Henstock, J. R., M. Rotherham, H. Rashidi, K. M. Shakesheff and A. J. El Haj (2014). "Remotely Activated Mechanotransduction via Magnetic Nanoparticles Promotes Mineralization Synergistically With Bone Morphogenetic Protein 2: Applications for Injectable Cell Therapy." STEM CELLS Translational Medicine **3**(11): 1363-1374.
Herklotz, M., M. C. Prewitz, C. M. Bidan, J. W. Dunlop, P. Fratzl and C. Werner (2015). "Availability of extracellular matrix biopolymers and differentiation state of human mesenchymal stem cells determine tissue-like growth in vitro." Biomaterials **60**: 121-129.
Huang, C. H., M. H. Chen, T. H. Young, J. H. Jeng and Y. J. Chen (2009). "Interactive effects of mechanical stretching and extracellular matrix proteins on initiating osteogenic differentiation of human mesenchymal stem cells." Journal of cellular biochemistry **108**(6): 1263-1273.
Huang, H., C. Y. Dong, H.-S. Kwon, J. D. Sutin, R. D. Kamm and P. T. So (2002). "Three-dimensional cellular deformation analysis with a two-photon magnetic manipulator workstation." Biophysical journal **82**(4): 2211-2223.
Huang, H., R. Y. Kwon and C. Jacobs (2012). Introduction to cell mechanics and mechanobiology, Garland Science.
Hughes, S., J. Dobson and A. J. El Haj (2007). "Magnetic targeting of mechanosensors in bone cells for tissue engineering applications." Journal of biomechanics **40**: S96-S104.

Ignatius, A., H. Blessing, A. Liedert, D. Kaspar, L. Kreja, B. Friemert and L. Claes (2004). "Effects of mechanical strain on human osteoblastic precursor cells in type I collagen matrices." Der Orthopade **33**(12): 1386-1393.
Kanczler, J. M., H. S. Sura, J. Magnay, D. Green, R. O. Oreffo, J. P. Dobson and A. J. El Haj (2010). "Controlled differentiation of human bone marrow stromal cells using magnetic nanoparticle technology." Tissue engineering Part A **16**(10): 3241-3250.
Kaspar, D., W. Seidl, C. Neidlinger-Wilke, A. Beck, L. Claes and A. Ignatius (2002). "Proliferation of human-derived osteoblast-like cells depends on the cycle number and frequency of uniaxial strain." Journal of biomechanics **35**(7): 873-880.
Kaspar, D., W. Seidl, C. Neidlinger-Wilke, A. Ignatius and L. Claes (2000). "Dynamic cell stretching increases human osteoblast proliferation and CICP synthesis but decreases osteocalcin synthesis and alkaline phosphatase activity." Journal of Biomechanics **33**(1): 45-51.
Kim, I., Y. Song and S. Hwang (2010). "Osteogenic responses of human mesenchymal stromal cells to static stretch." Journal of dental research **89**(10): 1129-1134.
Kim, I. S., Y. M. Song, T. H. Cho, J. Y. Kim, F. E. Weber and S. J. Hwang (2009). "Synergistic action of static stretching and BMP-2 stimulation in the osteoblast differentiation of C2C12 myoblasts." Journal of biomechanics **42**(16): 2721-2727.
Kim, J., A. Ahmad and S. A. Boppart (2013). "Dual-coil magnetomotive optical coherence tomography for contrast enhancement in liquids." Optics express **21**(6): 7139-7147.
Kirschvink, J. L., A. Kobayashi-Kirschvink, J. C. Diaz-Ricci and S. J. Kirschvink (1992). "Magnetite in human tissues: a mechanism for the biological effects of weak ELF magnetic fields." Bioelectromagnetics **13**(S1): 101-113.
Klein-Nulend, J., R. Bacabac and M. Mullender (2005). "Mechanobiology of bone tissue." Pathologie biologie **53**(10): 576-580.
Klein-Nulend, J., A. Van der Plas, C. Semeins, N. Ajubi, J. Frangos, P. Nijweide and E. Burger (1995). "Sensitivity of osteocytes to biomechanical stress in vitro." The FASEB Journal **9**(5): 441-445.
Kodama, H.-a., Y. Amagai, H. Sudo, S. Kasai and S. Yamamoto (1981). "Establishment of a clonal osteogenic cell line from newborn mouse calvaria." 歯科基礎医学会雑誌 **23**(4): 899-901.
Koike, M., H. Shimokawa, Z. Kanno, K. Ohya and K. Soma (2005). "Effects of mechanical strain on proliferation and differentiation of bone marrow stromal cell line ST2." Journal of bone and mineral metabolism **23**(3): 219-225.
Kollmannsberger, P. and B. Fabry (2007). "High-force magnetic tweezers with force feedback for biological applications." Rev Sci Instrum **78**(11): 114301.
Kommareddy, K. P., C. Lange, M. Rumpler, J. W. Dunlop, I. Manjubala, J. Cui, K. Kratz, A. Lendlein and P. Fratzl (2010). "Two stages in three-dimensional in vitro growth of tissue generated by osteoblastlike cells." Biointerphases **5**(2): 45-52.
Kopf, J., A. Petersen, G. N. Duda and P. Knaus (2012). "BMP2 and mechanical loading cooperatively regulate immediate early signalling events in the BMP pathway." BMC biology **10**(1): 37.
Lefèvre, Christopher T., M. Bennet, L. Landau, P. Vach, D. Pignol, Dennis A. Bazylinski, Richard B. Frankel, S. Klumpp and D. Faivre (2014). "Diversity of Magneto-Aerotactic Behaviors and Oxygen Sensing Mechanisms in Cultured Magnetotactic Bacteria." Biophysical Journal **107**(2): 527-538.
Li, Y. J., N. N. Batra, L. You, S. C. Meier, I. A. Coe, C. E. Yellowley and C. R. Jacobs (2004). "Oscillatory fluid flow affects human marrow stromal cell proliferation and differentiation." Journal of Orthopaedic Research **22**(6): 1283-1289.
Lim, C., E. Zhou and S. Quek (2006). "Mechanical models for living cells—a review." Journal of biomechanics **39**(2): 195-216.
Ma, Z., J. Wang, P. Loskill, N. Huebsch, S. Koo, F. L. Svedlund, N. C. Marks, E. W. Hua, C. P. Grigoropoulos and B. R. Conklin (2015). "Self-organizing human cardiac microchambers mediated by geometric confinement." Nature communications **6**.
Mack, P. J., M. R. Kaazempur-Mofrad, H. Karcher, R. T. Lee and R. D. Kamm (2004). "Force-induced focal adhesion translocation: effects of force amplitude and frequency." American journal of physiology-Cell Physiology **287**(4): C954-C962.

Manjubala, I., A. Woesz, C. Pilz, M. Rumpler, N. Fratzl-Zelman, P. Roschger, J. Stampfl and P. Fratzl (2005). "Biomimetic mineral-organic composite scaffolds with controlled internal architecture." Journal of Materials Science: Materials in Medicine **16**(12): 1111-1119.
Mullender, M., A. El Haj, Y. Yang, M. Van Duin, E. Burger and J. Klein-Nulend (2004). "Mechanotransduction of bone cellsin vitro: mechanobiology of bone tissue." Medical and Biological Engineering and Computing **42**(1): 14-21.
Neidlinger-Wilke, C., H. J. Wilke and L. Claes (1994). "Cyclic stretching of human osteoblasts affects proliferation and metabolism: a new experimental method and its application." Journal of Orthopaedic Research **12**(1): 70-78.
Pandey, E., K. Srivastava, S. Gupta, S. Srivastava and N. Mishra (2016). "SOME BIOCOMPATIBLE MATERIALS USED IN MEDICAL PRACTICES-A REVIEW." INTERNATIONAL JOURNAL OF PHARMACEUTICAL SCIENCES AND RESEARCH **7**(7): 2748-2755.
Proff, P. and P. Römer (2009). "The molecular mechanism behind bone remodelling: a review." Clinical oral investigations **13**(4): 355-362.
Quarles, L. D., D. A. Yohay, L. W. Lever, R. Caton and R. J. Wenstrup (1992). "Distinct proliferative and differentiated stages of murine MC3T3-E1 cells in culture: an in vitro model of osteoblast development." Journal of Bone and Mineral Research **7**(6): 683-692.
Rauh, J., F. Milan, K.-P. Guenther and M. Stiehler (2011). "Bioreactor systems for bone tissue engineering." Tissue Engineering Part B: Reviews **17**(4): 263-280.
Regul, N. I. C. G. (1988). "Mechanotransduction across the cell surface and through the cytoskeleton." Nat. Immun. Cell Growth Regul **7**: 95.
Ringer, P., G. Colo, R. Fässler and C. Grashoff (2017). "Sensing the mechano-chemical properties of the extracellular matrix." Matrix Biology.
Rivière, C., S. Marion, N. Guillén, J.-C. Bacri, F. Gazeau and C. Wilhelm (2007). "Signaling through the phosphatidylinositol 3-kinase regulates mechanotaxis induced by local low magnetic forces in Entamoeba histolytica." Journal of biomechanics **40**(1): 64-77.
Rosenberg, N., M. Levy and M. Francis (2002). "Experimental model for stimulation of cultured human osteoblast-like cells by high frequency vibration." Cytotechnology **39**(3): 125-130.
Rotherham, M. and A. J. El Haj (2015). "Remote Activation of the Wnt/β-Catenin Signalling Pathway Using Functionalised Magnetic Particles." PLOS ONE **10**(3): e0121761.
Rumpler, M., A. Woesz, J. W. Dunlop, J. T. van Dongen and P. Fratzl (2008). "The effect of geometry on three-dimensional tissue growth." Journal of the Royal Society Interface **5**(27): 1173-1180.
Rumpler, M., A. Woesz, F. Varga, I. Manjubala, K. Klaushofer and P. Fratzl (2007). "Three-dimensional growth behavior of osteoblasts on biomimetic hydroxylapatite scaffolds." Journal of Biomedical Materials Research Part A **81**(1): 40-50.
Schoen, I., B. L. Pruitt and V. Vogel (2013). "The Yin-Yang of rigidity sensing: how forces and mechanical properties regulate the cellular response to materials." Annual Review of Materials Research **43**: 589-618.
Shevkoplyas, S. S., A. C. Siegel, R. M. Westervelt, M. G. Prentiss and G. M. Whitesides (2007). "The force acting on a superparamagnetic bead due to an applied magnetic field." Lab on a Chip **7**(10): 1294-1302.
Sikavitsas, V. I., G. N. Bancroft, H. L. Holtorf, J. A. Jansen and A. G. Mikos (2003). "Mineralized matrix deposition by marrow stromal osteoblasts in 3D perfusion culture increases with increasing fluid shear forces." Proceedings of the National Academy of Sciences **100**(25): 14683-14688.
Sodipo, B. K. and A. A. Aziz (2016). "Recent advances in synthesis and surface modification of superparamagnetic iron oxide nanoparticles with silica." Journal of Magnetism and Magnetic Materials **416**: 275-291.
Song, G., Y. Ju, X. Shen, Q. Luo, Y. Shi and J. Qin (2007). "Mechanical stretch promotes proliferation of rat bone marrow mesenchymal stem cells." Colloids and Surfaces B: Biointerfaces **58**(2): 271-277.
Stokes, G. G. (1851). On the effect of the internal friction of fluids on the motion of pendulums, Pitt Press Cambridge.

Tan, W. and T. A. Desai (2004). "Layer-by-layer microfluidics for biomimetic three-dimensional structures." Biomaterials **25**(7): 1355-1364.
Tanakaa, S. M., J. Lib, R. L. Duncana, H. Yokotab, D. B. Burr and C. H. Turner (2003). "Effects of broad frequency vibration on cultured osteoblasts." Journal of Biomechanics **36**: 73-80.
Thielicke, W. and E. Stamhuis (2014). "PIVlab–towards user-friendly, affordable and accurate digital particle image velocimetry in MATLAB." Journal of Open Research Software **2**(1).
Ueno, S. and M. Iwasaka (1994). "Properties of diamagnetic fluid in high gradient magnetic fields." Journal of Applied Physics **75**(10): 7177-7179.
van Midwoud, P. M., A. Janse, M. T. Merema, G. M. Groothuis and E. Verpoorte (2012). "Comparison of biocompatibility and adsorption properties of different plastics for advanced microfluidic cell and tissue culture models." Analytical chemistry **84**(9): 3938-3944.
Vedula, S. R. K., M. C. Leong, T. L. Lai, P. Hersen, A. J. Kabla, C. T. Lim and B. Ladoux (2012). "Emerging modes of collective cell migration induced by geometrical constraints." Proceedings of the National Academy of Sciences **109**(32): 12974-12979.
Vogel, V. and M. Sheetz (2006). "Local force and geometry sensing regulate cell functions." Nature reviews Molecular cell biology **7**(4): 265-275.
Wang, J. H.-C. and B. P. Thampatty (2006). "An Introductory Review of Cell Mechanobiology." Biomechanics and Modeling in Mechanobiology **5**(1): 1-16.
Wang, N., J. Butler and D. Ingber (1993). "Mechanotransduction across the cell surface and through the cytoskeleton." Science **260**(5111): 1124-1127.
Ward Jr, D. F., R. M. Salasznyk, R. F. Klees, J. Backiel, P. Agius, K. Bennett, A. Boskey and G. E. Plopper (2007). "Mechanical strain enhances extracellular matrix-induced gene focusing and promotes osteogenic differentiation of human mesenchymal stem cells through an extracellular-related kinase-dependent pathway." Stem cells and development **16**(3): 467-480.
Weyts, F., B. Bosmans, R. Niesing, J. Leeuwen and H. Weinans (2003). "Mechanical control of human osteoblast apoptosis and proliferation in relation to differentiation." Calcified Tissue International **72**(4): 505-512.

Appendices

APPENDIX A: Projected tissue areas (PTAs) of all scaffolds upon which forces were applied as a function of distance from the magnet.

Data points and regression analysis lines of PTA as a function of distance from the magnet (section 3.4.1). The type of force applied and slopes of regression analysis lines for parallel and perpendicular pores (section 4.2) are indicated on top of each graph.

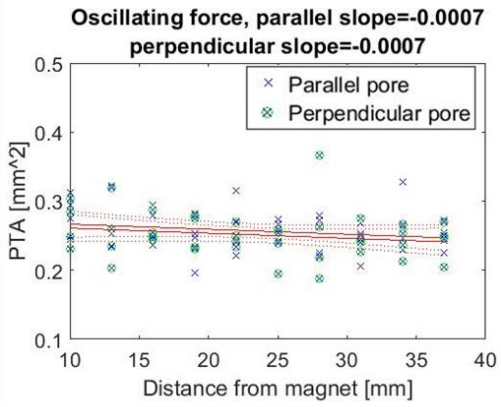

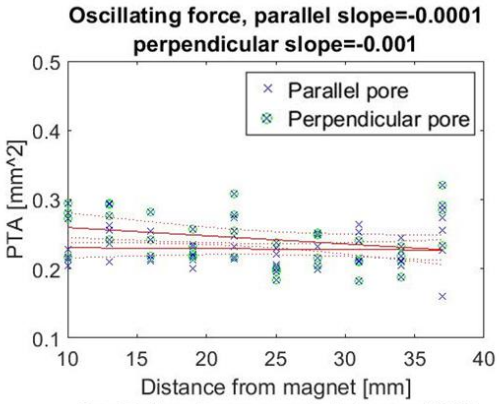

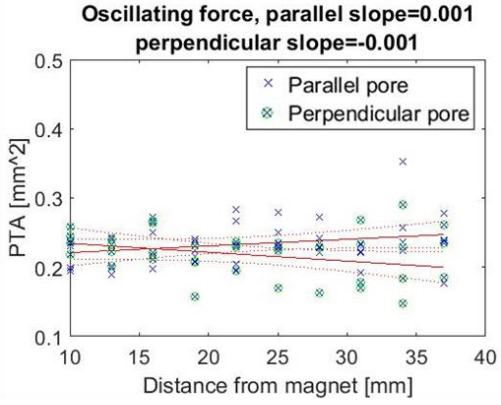

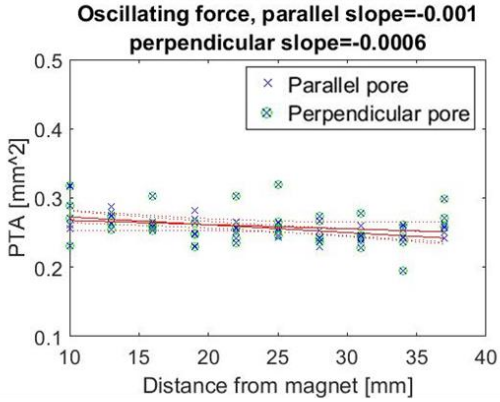

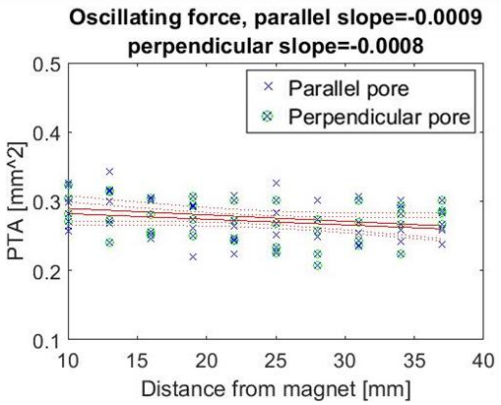

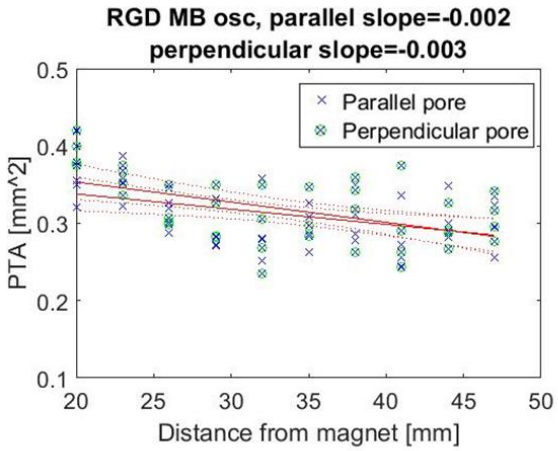
RGD MB osc, parallel slope=-0.002
perpendicular slope=-0.003
Parallel pore
Perpendicular pore
PTA [mm^2]
Distance from magnet [mm]

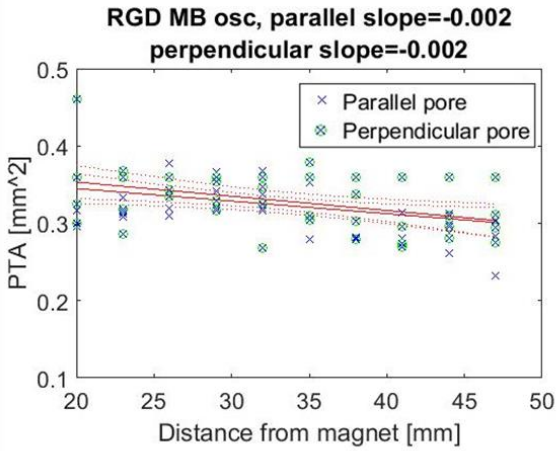
RGD MB osc, parallel slope=-0.002
perpendicular slope=-0.002
Parallel pore
Perpendicular pore
PTA [mm^2]
Distance from magnet [mm]

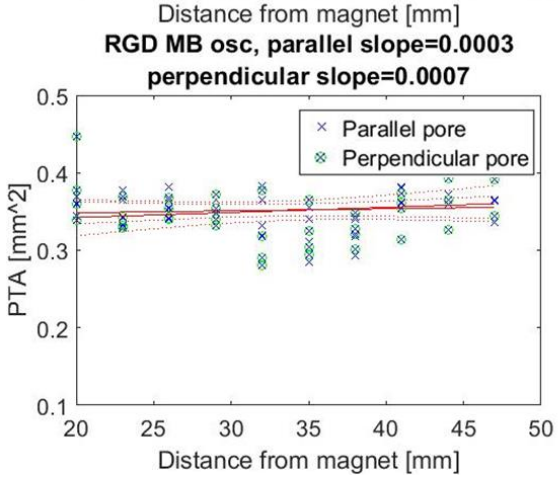
RGD MB osc, parallel slope=0.0003
perpendicular slope=0.0007
Parallel pore
Perpendicular pore
PTA [mm^2]
Distance from magnet [mm]

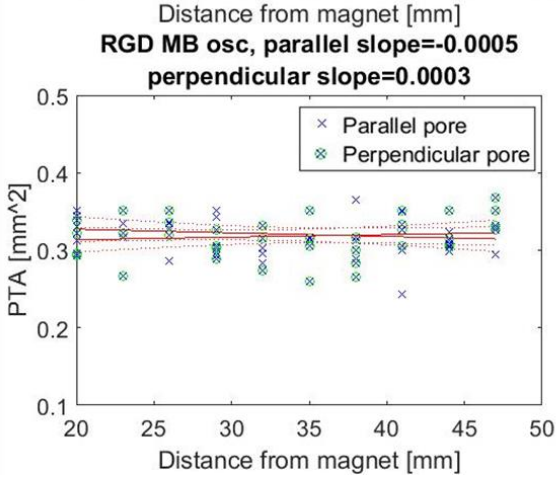
RGD MB osc, parallel slope=-0.0005
perpendicular slope=0.0003
Parallel pore
Perpendicular pore
PTA [mm^2]
Distance from magnet [mm]

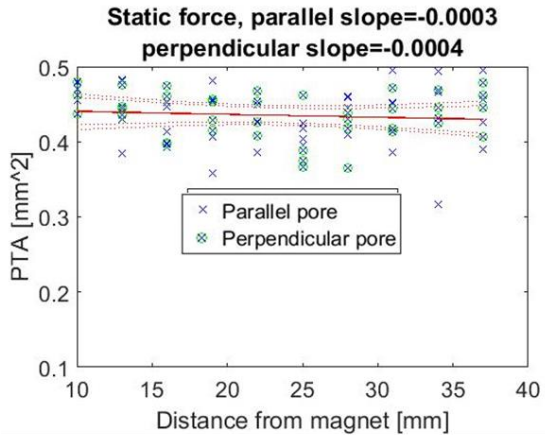

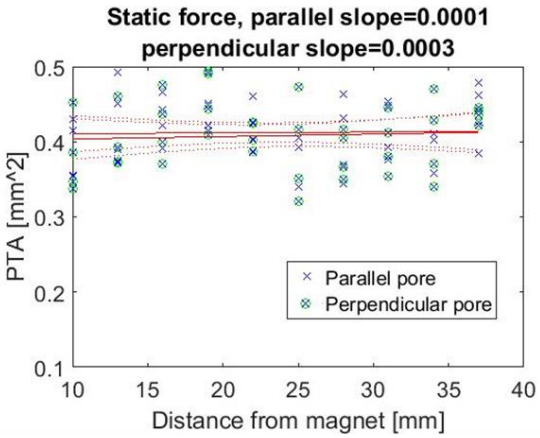

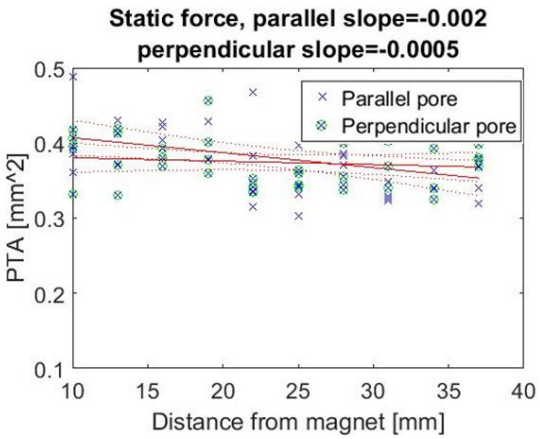

APPENDIX B: Normalized ALP stain intensity as a function of the logarithm of force

Normalized ALP stain color intensity as a function of the logarithm of force applied on MBs in MC3T3-E1 cell layer (section 3.4.2). Data from control scaffolds are denoted by black, from static forces on epoxy MBs by red, for oscillating forces on epoxy MBs by green, for oscillating forces on RGD MBs by blue.

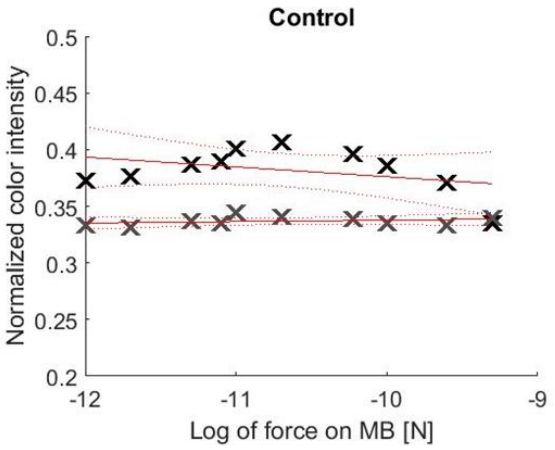
Control
Normalized color intensity
0.5
0.45
0.4
0.35
0.3
0.25
0.2
-12
-11
-10
-9
Log of force on MB [N]

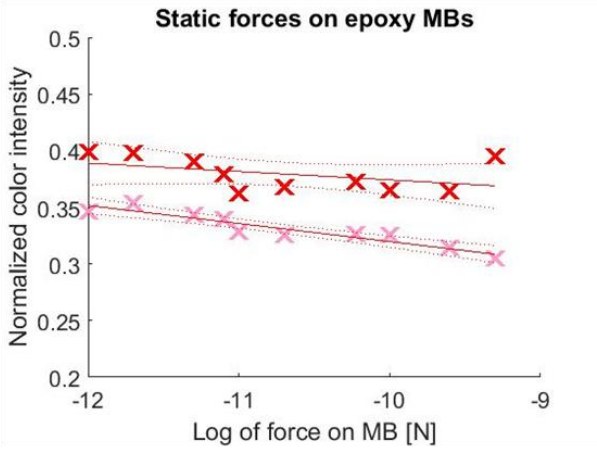
Static forces on epoxy MBs
Normalized color intensity
0.5
0.45
0.4
0.35
0.3
0.25
0.2
-12
-11
-10
-9
Log of force on MB [N]

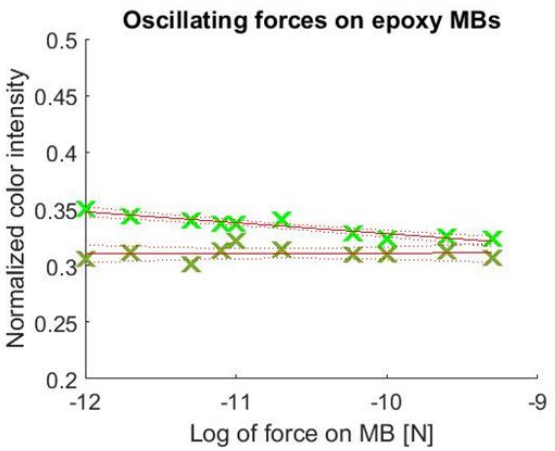
Oscillating forces on epoxy MBs
Normalized color intensity
0.5
0.45
0.4
0.35
0.3
0.25
0.2
-12
-11
-10
-9
Log of force on MB [N]

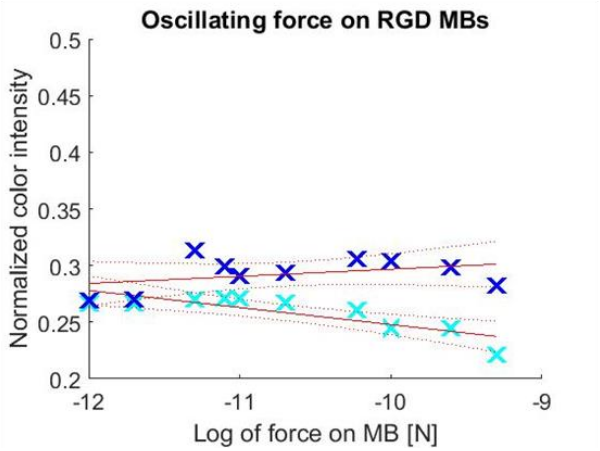
Oscillating force on RGD MBs
Normalized color intensity
0.5
0.45
0.4
0.35
0.3
0.25
0.2
-12
-11
-10
-9
Log of force on MB [N]